8-2014

Impacts of Climate Change on the Evolution of the Electrical Grid

Melissa Ree Allen
University of Tennessee - Knoxville, mallen24@vols.utk.edu

To the Graduate Council:

I am submitting herewith a dissertation written by Melissa Ree Allen entitled "Impacts of Climate Change on the Evolution of the Electrical Grid." I have examined the final electronic copy of this dissertation for form and content and recommend that it be accepted in partial fulfillment of the requirements for the degree of Doctor of Philosophy, with a major in Energy Science and Engineering.

Joshua S. Fu, Major Professor

We have read this dissertation and recommend its acceptance:

Steven J. Fernandez, Hamparsum Bozdogan, Katherine J. Evans, John B. Drake, Thomas J. Wilbanks

Accepted for the Council:
Dixie L. Thompson

Vice Provost and Dean of the Graduate School

(Original signatures are on file with official student records.)

Impacts of Climate Change on the Evolution of the Electrical Grid

A Dissertation Presented for the
Doctor of Philosophy
Degree
The University of Tennessee, Knoxville

Melissa Ree Allen
August 2014

Acknowledgements

I gratefully acknowledge the valuable instruction, encouragement and advocacy of my major professor and mentor, Dr. Joshua Fu, and his guidance throughout the Energy Science and Engineering Doctor of Philosophy degree at the University of Tennessee.

I thank also my Oak Ridge National Laboratory mentor, Dr. Steve Fernandez, for his cultivation of ideas, provision of tools and data and strong scientific, financial and moral support. I've particularly learned from his ability to turn any scientific or social observation into a memorable expression short enough to fit on a bumper sticker.

To Dr. Hamparsum Bozdogan, I give thanks for my introduction to information complexity criteria and to the fundamentals of statistical reasoning from which I am encouraged to seek new development and application. I am grateful to Dr. Thomas Wilbanks for his intuition for characterization of the timely scientific questions of our studies, for his keen leadership in their various branches of investigation and for his confidence in my contribution to them.

My gratitude goes also to Dr. John Drake, whose thorough explanation of atmospheric circulation and climate modelling has deepened my understanding, challenged me computationally and increased my awe of earth system processes; and to Dr. Kate Evans for her scientific, mathematical and personal insight, her life example and role model.

I appreciate the high academic expectation and scientific vision communicated, and the positive learning environment facilitated across the University and the Laboratory by Bredesen Center Director, Dr. Lee Riedinger; Assistant Director, Dr. Mike Simpson and ORNL Graduate Education and University Partnerships Director Dr. Ian Anderson; and the dedication which they, Wanda Davis, Debbie Turner, Ben Allen, Elizabeth Reagan and many other faculty and staff maintain toward the establishment and growth of this leading-edge interdisciplinary scientific and engineering program focused on energy solutions.

Special thanks to University of Tennessee Chancellor Dr. Jimmy Cheek; Oak Ridge National Laboratory Director Dr. Thom Mason; and Tennessee's 48th Governor, Phil Bredesen, for their commitment to excellence in science, education, and policy and for making this program possible.

Abstract

Maintaining interdependent infrastructures exposed to a changing climate requires understanding 1) the local impact on power assets; 2) how the infrastructure will evolve as the demand for infrastructure changes location and volume and; 3) what vulnerabilities are introduced by these changing infrastructure topologies. This dissertation attempts to develop a methodology that will a) downscale the climate direct effect on the infrastructure; b) allow population to redistribute in response to increasing extreme events that will increase under climate impacts; and c) project new distributions of electricity demand in the mid-21st century.

The research was structured in three parts. The first used downscaling techniques to scale regional gridded atmospheric processes to measurements of local extreme events. These techniques illustrate the ability to move reasonably from regional to local effects. The second chapter explored how people migrated in response to the extreme events for which climate change will increase the frequency and intensity. The third chapter translated downscaled climate impacts and granular population movements into a national map of electricity demand.

The results of this research illustrates the feasibility of the three part approach to address possible future infrastructure vulnerabilities under varying policy options and technology assumptions. This methodology can be an important tool for increasing the robustness of the nation's infrastructure.

Table of Contents

List of Tables

List of Figures

Chapter 1

Introduction

With the onset of climate change, communities have begun to experience the realization of predicted increases in storm intensity, flooding, inundation, heat waves and wildfires; the risk they pose to infrastructure and neighborhoods; and the disruption they cause to the energy supply and its dependent infrastructure. Direct effects have included damage to power plants, roads, bridges, and communication towers; and resultant interruption of electrical energy, transportation, and communications sectors in cities.

As climate conditions continue to change, local communities and the infrastructure on which they depend will necessarily respond, adapt and evolve. Population will shift in response to sea level rise and increased frequency of extreme weather events, for example, and services that generate new economic activity in more environmentally stable locations will attract new workers and associated households. This shift will force demand locations for power to change. As a result, networked infrastructures will be required to accommodate new load centers and to minimize vulnerability to natural disaster. Power for these networks will depend upon access to economically viable and transportable fuel sources. To provide information about the complex interactions among climatic conditions, population shifts, and energy supply and use, new tools are needed to assess the impacts of climate drivers on urban areas. This dissertation develops and demonstrates a small suite of these tools for assessment of information for anticipating the evolution of infrastructure in the immediate and extended future.

Little research has been conducted to quantify potential climate-related impacts on the power grid when the system is at its operating limit. Two reasons for this gap are first, that until

recently, climate projections at high enough resolution to be compatible with infrastructure modeling have been unavailable; and second, that population migration data and analysis techniques capable of providing estimates of future energy demand have been missing and/or difficult to characterize. This dissertation will address the first of these issues by examining a new statistical method for downscaling heavy precipitation events and also by examining dynamically downscaled temperature data (Gao et al., 2012) within a neighborhood-scale infrastructure model framework. It will address the second by fitting curves to population data obtained both from the US Census and the from the US Internal Revenue Service to develop baseline population trends and then to recreate these trends and the anomalies imposed upon them by well-characterized population response to extreme events.

The first of the tools developed is a method of analysis of return periods of heavy rainfall events at point-gauge locations and the correlation of these events to ambient atmospheric conditions. Findings from this study will provide a way for downscaling climate model predictions of average grid cell precipitation to probabilities of heavy events for specific locations. The data examined for this study include tipping-bucket measurements from five cities in southern Sweden. This region was chosen because of its abundance of data and for ease of comparison of the results to previous studies of a similar nature (Olsson and Willen, 2010).

The second of the tools is one of population movement response to extreme hurricane events. This tool examines county-by-county patterns of population change in the state of Louisiana over the years 1970-2010 noting large disturbances in the patterns due to large events. Social theory,

statistical methods and agent based modeling methods are applied to develop a representation of exogenously driven population change in response to environmental stress and this mode's effect on otherwise typical population movements.

The model developed is then used to predict population redistribution for the future under the Representative Concentration Pathway scenario 8.5 (RCP 8.5). The final tool combines information learned from resultant population movement response to extreme climate events, predictions for increased demand due to temperature increase, and change in demand due to shifts in household size to predict geospatial locations of increase and decrease in demand for electricity. From these calculations, National Demand Maps for 2010, 2030 and 2050 are generated and differences calculated. Findings from the application of these tools can be used to inform the evolution of the electrical grid for future decades, and the tools themselves will become an ensemble framework linking climate, energy and infrastructure within a system that can generate scenarios useful to the production of a portfolio of options for electrical grid planning at local scale.

Climate Impacts on Infrastructure Evolution: Methodology Box Diagram

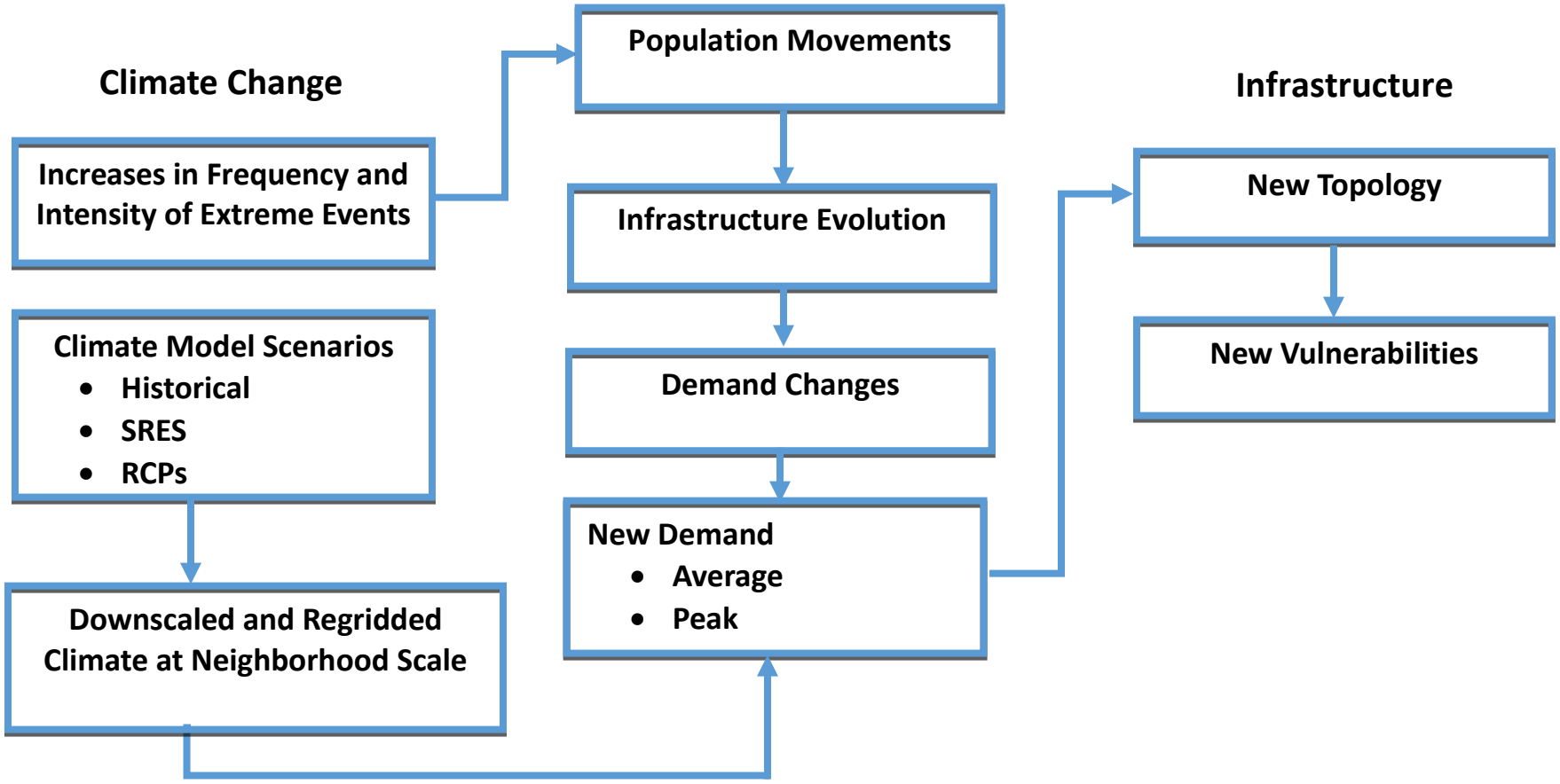

References

Gao, Y., J.S. Fu, J.B. Drake, Y. Liu, J-F Lamarque, 2012**.** Projected changes of extreme weather events in the eastern United States based on a high resolution climate modeling system**.** *Environ. Res. Lett.*, 7 (4), 044025.

Olsson, J., U. Willén, 2010. Downscaling extreme RCA3-precipitation for urban hydrological applications. *Mistra-SWECIA Working Paper No 3*.

Chapter 2

Problem Statement

2.1 Infrastructure Vulnerability to Environmental Stress

A functioning power infrastructure is critical to the environment, economy and human life, yet several incidents in recent past suggest that current US infrastructure is vulnerable to extreme weather and climate events such as heat waves, hurricanes and flooding. Because of these vulnerabilities, the US is further underprepared to cope with predicted increases in frequency and intensity of these events due to climate change. These vulnerabilities are particularly prevalent in regions such as coastal areas that

are more easily exposed to extreme weather, and they can lead to cascading consequences for the populations serviced by these and communicating sectors of the infrastructure.

The electrical grid is the most representative example of vulnerable infrastructure sectors since these systems are often the first affected by extreme weather phenomena, and since so much of the remaining infrastructure depends upon their proper functioning. Power failures can create a variety of threats to health including contamination of beaches, waterways and drinking water due to loss of electrically supported water pressure and/or flooding causing the release of sewage from water treatment plants. This sewage stream, then, can either flow into rivers, streams or lakes or back up into homes and businesses (Lee, 2011).

2.2 Vulnerability due to System Complexity

An illustration of the complications that can occur as a result of power failure is seen in the example of the San Diego Outage of September, 2011. On September 8, 2011, at 3:38pm, San Diego County suffered a massive power outage, which affected a large area stretching from

Orange County to Baja California and east into parts of Arizona. The two major power sources for the region became inoperable when a 500-kilovolt high-voltage transmission line from Arizona to California failed triggering a cascade of events that then knocked the San Onofre nuclear power plant offline (Gustafson, 2011). The outage was initiated by lack of vigilance during a routine repair at a station in Yuma, Arizona, which caused one of three turbines generating electricity at a plant east of Mexicali to create an imbalance in the line running south from the San Onofre Nuclear Generating Station. The problem was compounded by an inability to monitor activities in neighboring balancing authorities, which prevented staff from limiting the blackout (McDonald, 2011). The outage, thus, stopped power from coming into the county, halted the San Onofre nuclear power plant and shut down the entire system. The uncontained surge from the outage cut all power from a high-voltage transmission line connecting Arizona and California, and initiated a chain of events that also cut off the San Onofre plant (Keegan, 2011).

The failure cascaded in two ways. First, the grid instantly lost about a third of its power supply. Second, the customers normally served by the Arizona power line were transferred to nearby power grids, including that of San Diego, all of which are interconnected. The addition of more customers to these grids immediately increased the amount of power being demanded from San Onofre and overwhelmed the power plant's capabilities (Keegan, 2011).

Impacts to the affected communities were manifold. Electricity for millions of homes and businesses was unavailable for 12 hours. During the outage, non-operational generators in the

area caused water pressure in the distribution system to reduce significantly, resulting in backflow and contamination to the clean supply to and from homes and businesses. San Diego residents were ordered to boil water prior to consumption (Chillymanjaro, 2011). Once power was restored, two incidents of sewage spills occurred. One pump station caused approximately 2.6 million gallons of sewage to be spilled from three manholes onto Sorrento Valley Road and Sorrento Valley Boulevard into the storm drain system and ultimately into the Los Penasquitos Creek. The other spilled approximately 870,000 gallons of sewage into Sweetwater River and ultimately into San Diego Bay (NRCC Executive Summary, 2011).

2.3 Vulnerability due to Heat Waves

An additional complication in the San Diego blackout was that the outage occurred on the last day of a heat wave during which temperatures had consistently reached 12 degrees (Fahrenheit) above average (Gustafson, 2011). Combined with heating of the power lines due to the increased load of more customers using more power for indoor cooling, outdoor conditions also contributed to line fatigue and collapse. Similarly, in August 2003, when a high-voltage power line in northern Ohio made contact with overgrown trees and disconnected from the system as a result of line slackening due to excess heat from the high current flowing through the line along with elevated ambient temperatures, a power failure was instantiated. Although the incident should have activated an alarm in the control room of FirstEnergy Corporation, an Ohio-based utility company, it didn't, because the alarm system failed. As efforts were made to understand the events taking place, three other lines likewise sank into trees and switched off, forcing the remaining lines in service to operate at higher capacity. Because of the added load, these lines,

too, shut down, generating a cascade of failures throughout southeastern Canada and eight northeastern states (Minkel, 2008).

Millions of people in the Northeast lost electric power during the incident, but some of the most damaging effects were the result of water treatment plants and pumping stations shutting down. The blackout compromised the water supply in Detroit and Cleveland in at least two ways: first, by decreasing the pressure in water pumps, allowing bacteria to build up in municipal water systems; and second, by effectively shutting down sewage treatment facilities. As a result, millions of gallons of raw or partially treated sewage were discharged into the lake and streams from Ann Arbor, Michigan to communities east of Cleveland, Ohio. These discharges prompted officials in the Cleveland area to be on guard for signs of cryptosporidium, a parasite pathogen causing intestinal illness and even death in humans (Johnson and Lefebvre, 2003). Air quality in the region was also compromised, as FirstEnergy's coal-fired power plant in Eastlake, Ohio, spewed a huge cloud of ash over a more than half-mile radius from the plant two hours before the blackouts began (Johnson, 2003).

2.4 Vulnerability due to Hurricanes, Storm Activity and Flooding

A National Oceanic and Atmospheric Administration (NOAA) technical manual list of the deadliest and costliest hurricanes shows that large death totals were primarily a result of the 10 feet or greater rise of the ocean associated with most of the top thirty major hurricanes, and that a large portion of the damage in some of costliest tropical cyclones resulted from inland floods caused by torrential rain (Blake et al., 2011). Hurricane Katrina of 2005, for example, was

responsible for at least $108 billion of property damage and is by far the costliest hurricane ever to strike the United States. Irene (2005) sustained winds strong enough to damage power lines and cause widespread outages. It likewise brought enough rain to cause major flooding in a variety of regions (Weiss, Boyd, Wheeler, CBS, 2011). Flooding in many areas during these storms was compounded by aging infrastructure (Huffington Post, 2011; ASCE, 2009). Irene is blamed for 45 deaths in 13 states (Boyd and Leger, 2011). Causes of death included personal blows due to storm-related traffic accidents and falling trees, drowning as a result of flooding and broken pipes, carbon monoxide poisoning produced by generators, and fires ignited by fallen power lines (Associated Press, August 30, 2011). Additional impacts from Irene occurred in fifteen states, Connecticut, Delaware, Florida, Maine, Maryland, Massachusetts, New Hampshire, New Jersey, New York, North Carolina, Pennsylvania, Rhode Island, Vermont, Virginia and Washington, D.C. All of these states experienced power losses and flooding. Among the most severe additional consequences was a ruptured sewer main in the Baltimore Highlands area southwest of the city, which poured approximately 100 million gallons of raw sewage into the lower Patapsco River. Power outages also led to more than a dozen other sewage spills across the region (Wheeler, 2011).

As climate conditions change, populations shift, and requirements for power increase; infrastructure must evolve to accommodate demand, and simultaneously to prevent risk to human welfare. Symptoms of climate change are beginning to show: overall temperatures have risen in the past century resulting in longer heat waves and higher sea surface temperatures which have led to Arctic ice melt and sea level rise along with more frequent and more intense

hurricanes. If warnings are heeded, policy and preparedness plans developed, and new building codes and zoning laws enacted with regard to power generation and dependent infrastructure, future deaths can be minimized and large property losses avoided.

References

Blake, E.S., C.W. Landsea, E.J. Gibney (August, 2011). NOAA Technical Memorandum NWS NHC-6. "The Deadliest, Costliest, and Most Intense United States Tropical Cyclones from 1851 to 2010 (And Other Frequently Requested Hurricane Facts)".

Chillymanjaro, September 9, 2011, San Diego power outage caused 2 million gallons of raw sewage spilled into Los Penasquitos Lagoon and Sweetwater River. http://thewatchers.adorraeli.com/category/earth-changes/pollution-earth-changes

Gustafson, Craig, Sept. 8, 2011, Updated 6:01 a.m. , Sept. 9, 2011, Unprecedented outage left millions in the dark. http://signonsandiego.printthis.clickability.com/pt/cpt?expire=&title=Unprecedented+outage+left+millions+in+the+dark+-+SignOnSanDiego.com&urlID=460051427&action=cpt&partnerID=86541&fb=Y&url=http%3A%2F%2Fwww.signonsandiego.com%2Fnews%2F2011%2Fsep%2F08%2Fwidespread-power-outages-across-san-diego-county%2F

Johnson, Jeremy and Alex Lefebvre, August 20, 2003, US: Impact of Northeast Blackout Continues to Emerge, *World Socialist Web Site.* http://www.wsws.org/articles/2003/aug2003/blck-a20.shtml

Keegan, Kyle, Four Big Unanswered Blackout Questions, Posted: Friday, September 9, 2011 8:20 pm; Updated: 5:10 pm, Fri Oct 14, 2011. http://www.voiceofsandiego.org/data-drive/article_dc4aabe6-db5b-11e0-97ba-001cc4c03286.html

Lee, Morgan, Sept. 22, 2011, Grid operators didn't share info during blackout, SignOn San Diego. *http://www.signonsandiego.com/news/2011/sep/22/5-authorities-handle-electric-grid-didnt-share-inf*

Lee, Mike, September 27, 2011, Blackout's sewage spills 75 percent greater than reported. http://www.signonsandiego.com/news/2011/sep/27/blackouts-sewage-spills-far-greater-reported

McDonald, Jeff and Morgan Lee, September 16, 2011, Outage Had Roots in Mexico, too, *SignOn San Diego.* http://signonsandiego.printthis.clickability.com/pt/cpt?expire=&title=Outage+had+roots+in+Mexico%2C+too+%7C+SignOnSanDiego.com&urlID=460595072&action=cpt&partnerID=86541&fb=Y&url=http%3A%2F%2Fwww.signonsandiego.com%2Fnews%2F2011%2Fsep%2F16%2Foutage-had-roots-in-mexico-too%2F

Minkel, J.R. (2008). The 2003 Northeast Blackout—Five Years Later, *Scientific American*, http://www.scientificamerican.com/article.cfm?id=2003-blackout-five-years-later

Natural Resources and Culture Committee Executive Summary Sheet, September 22, 2011. "Impacts of the September 8, 2011 Countywide Blackout of the Public Utilities Department." City of San Diego.

Sinigalliano, C.D. et al. (2007) Impacts of Hurricanes Katrina and Rita on the microbial landscape of the New Orleans area, *PNAS*, May 22, 2007 vol. 104 no. 21 9029-9034 , doi: 10.1073/PNAS.0610552104. http://www.pnas.org/content/104/21/9029.full

U.S.-Canada Power System Outage Task Force, April 2004, Final Report on the August 14, 2003 Blackout in the United States and Canada: Causes and Recommendations. https://reports.energy.gov/

Chapter 3

Scientific Background

America's energy infrastructure was given the grade of D+ recently in the American Society for Civil Engineers' 2013 Report Card for America's Infrastructure (ASCE, 2013). Surprisingly, this grade indicates an improvement in power generation, distribution and maintenance over that of the previous grading period. While our energy infrastructure has now achieved a passing grade, however, it has not graduated from an overall grim assessment, granted fortified, fluid energy production and delivery proves a tough course to master. Complexity inherent in the power system complicates planning and preparedness for system failures. As previously illustrated, disruptions of the system, along with additional problems associated with cascading effects, were the impacts of the 2003 Northeastern blackout, the San Diego power outage, and the failures due to Hurricanes Irene and Katrina. This section focuses upon the causes of those failures; and upon the potential for much larger catastrophes due to climate change, should hardening measures not be taken.

3.1 Structure of "The Grid"

The North American power system is commonly referred to as "the grid," but the system actually comprises three distinct power grids. The Eastern Interconnection is located in and services the eastern two-thirds of the continental United States and Canada from Saskatchewan east to the Maritime Provinces, while the Western Interconnection covers the remaining western third of the continental United States (excluding Alaska), the Canadian provinces of Alberta and British Columbia, and a portion of Baja California Norte, Mexico. The third interconnection inhabits and services only Texas. The three interconnections are electrically independent of each other except for a few small direct current (DC) linkages (US Canada Task Force, 2004). Within each separate interconnection, electricity flows over virtually all transmission lines from generators to

loads; thus, a failure at a critical point in the network can quickly translate to failures within other sections of the same interconnection. These multiple failures can then cause cascading effects to additional infrastructure sectors such as water and wastewater treatment, transportation and public parks and recreation areas.

The US Canada Task Force, established to mitigate the effects of the 2003 Northeastern blackout, defines a cascading failure as "a dynamic phenomenon that cannot be stopped by human intervention once started. It occurs when there is a sequential tripping of numerous transmission lines and generators in a widening geographic area." (US Canada Task Force, 2004) Such cascades, a feature of each of the major outages previously described, are the development of a variety of factors: conductor contact with trees; overestimation of dynamic reactive output of system generators; inability of system operators or coordinators to visualize events on the entire system; failure to ensure that system operation was within safe limits; lack of coordination on system protection; ineffective communication; lack of "safety nets;" and inadequate training of operating personnel." (US Canada Task Force, 2004)

The 2009 Report Card focuses on two major weaknesses in the national electric grid: resilience and reliability. It states that utilities are generally prepared for local and regional responses, but that they lack the type of resilience needed should a much broader response be required. Regarding reliability, certain facilities are, for example, insufficiently girded against moderate wind loading. Pole failures in Florida due to Hurricane Wilma, whose winds were well below load design requirements, demonstrate

this weakness. “If these structures had been designed from the 90 mph winds required by NESE on transmission structures, distribution outages would have been reduced.”(ASCE, 2009). The complications and cascading consequences of the San Diego SDG&E blackout described previously are also illustrative of the weaknesses in the power infrastructure.

3.2 Vulnerability is Compounded by Climate Variability and Climate Change

As demonstrated in the previous section, many power failures are initiated by extreme weather events such as heat waves, hurricanes and flooding. According to studies cited in the Fourth Assessment Report of the Intergovernmental Panel on Climate Change Working Group I (IPCC AR4 WG I, 2007), the potential for such events to increase in intensity, duration and frequency with climate change is very high. While a wide range of extreme weather events is expected in most regions even with an unchanging climate, and observational data for model validation is limited to merely one and a half centuries, and several factors are usually in combination to produce one extreme event; it is nevertheless statistically reasonable to infer that substantial changes in the frequency of extreme events can result from a relatively small shift of the distribution of a weather or climate variable such as global temperature. Extremes are the infrequent events at the high and low end of the range of values of a particular variable,

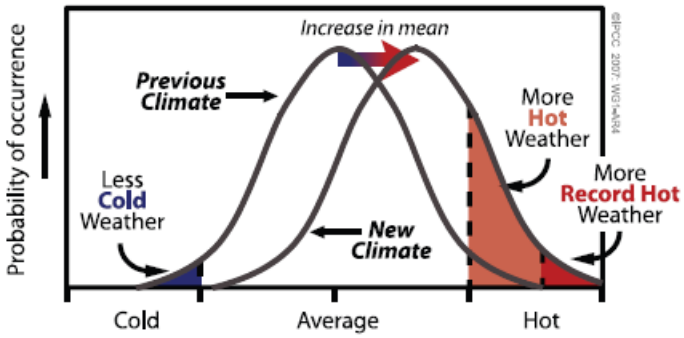

Figure 3.1 Climate Equilibrium Shift (IPCC WG I Technical Summary, 2007)

or, statistically speaking, at the tails of the frequency distribution. Figure 3.1 (above) illustrates this shift showing that as the mean of a normal distribution is shifted right, those events previously occupying only the highest percentiles now become a much higher probability.

The following extreme events, which are related to elevated temperatures, are those most likely to affect power generation and to expose its vulnerabilities and their potential for additional cascading effects.

3.3 Heat Waves

As illustrated by the figure above, a very real consequence of global temperature rise for many regions is an increase in the annual number of heat waves (defined as the mean annual consecutive 3-day warmest nighttime minima event, Meehl et al., 2004; Ganguly et al., 2009). The record-breaking heat wave over western and central Europe in the summer of 2003 is an example of such an exceptional extreme. Additionally, records show that eleven of the last 12 years rank among the 12 warmest years on record since 1850. Rates of surface warming

increased markedly in the mid-1970s and the global land surface has been warming at about double the rate of ocean surface warming since then (Brohan, 2006; Smith and Reynolds, 2005; Lugina et al., 2005; Hansen et al., 2001). In a modeling study performed more recently (Ganguly et al., 2009), it was found that observed heat wave intensities for the first decade of the 21st century were even higher than the previously-modeled worst-case model projections of the same decade, implying an even steeper temperature growth curve for further projections for the current century.

3.4 Hurricanes

Just as land surface and adjacent lower atmospheric temperatures continue to increase with climate change, sea surface temperatures also continue to rise. These temperature increases, along with increased atmospheric water vapor levels that higher sea surface temperatures induce, can foster the conditions leading to atmospheric convection and thunderstorms that generate hurricanes (although this climate change phenomenon is not fully understood--variability in additional global forces also have significant influence). Currently, hurricanes tend to form when sea surface temperatures exceed about 26 degrees Celsius. As sea surface temperatures increase, then, the area over which storms can potentially form expands.

The intensity of hurricanes, defined as the maximum wind speed achievable in a given thermodynamic environment (Emanuel, 2003), similarly depends critically on sea surface temperatures and atmospheric structure. According to the National Oceanic and Atmospheric Administration's (NOAA) Accumulated Cyclone Energy (ACE) index (Levinson and Waple,

2004), the collective intensity and duration of tropical storms and hurricanes during a given season is proportional to the maximum surface sustained winds squared. The power dissipation of a storm is proportional to the wind speed cubed. Thus, the effects of such storms are such that one large storm can have a much greater impact on the environment and the climate system than several smaller storms (IPCC AR4 WG I, 2007; Emanuel, 2005; 2013; Keim, 2007).

3.5 Sea Level Rise

Global sea level had risen by about 120 m during the several millennia that followed the end of the last ice age (approximately 21,000 years ago), and stabilized between 3,000 and 2,000 years ago. Various sea level indicators suggest that global sea level did not change significantly from then until the late 19th century. Modern observations of sea level change show evidence that sea level began again to rise during the 19th century. Estimates for the 20th century show that the global average sea level rose at a rate of about 1.7 mm yr–1 (IPCC AR4, WG I).

The rate of this sea level change over recent decades, however, has not been geographically uniform. Sea levels are forecast to rise more quickly over time from now on, especially in eastern North America and western Alaska (Zhang et al., 2000; Church et al., 2004; Meehl et al., 2007; Cooper et at., 2008; Wu, et al., 2009). Many previous studies have documented the correlations between rising sea levels, coastal and inland erosion, and more frequent and intense storms in the US (Meehl et al., 2007; Travis, 2010). Additionally, flooding resulting from sea level rise can present threats similar to those of the aftermath of hurricanes.

With regard to safeguarding power and other infrastructure, then, the key sources of climate vulnerability are increases in the frequency, intensity and duration of heat waves, hurricanes and tropical storms (although the probability of the storms making landfall may not necessarily increase), and associated precipitation. For storms making landfall, the damage from winds and flooding, as well as storm surge, are especially of concern. Likewise, chronic flooding caused by sea level rise may manifest similar consequences. The likelihood of infrastructure remaining vulnerable to these threats depends upon resilience and reliability maintained by structural and operational codes.

References

American Society of Civil Engineers, *2013 Report Card for America's Infrastructure*. http://www.infrastructurereportcard.org/a/documents/Energy.pdf

Brohan, P., et al., 2006: Uncertainty estimates in regional and global observed temperature changes: A new dataset from 1850. *J. Geophys. Res.*, **111**, D12106, doi:10.1029/2005JD006548.

Climate Change 2007 - The Physical Science Basis. Contribution of Working Group I to the Fourth Assessment Report of the IPCC. Solomon, S., D. Qin, M. Manning, Z. Chen, M. Marquis, K.B. Averyt, M. Tignor and H.L. Miller (eds.) Cambridge University Press, Cambridge, United Kingdom and New York, NY, USA.

Emanuel, K., 2003: Tropical cyclones. *Annu. Rev. Earth. Planet. Sci*., **31**, 75–104.

Emanuel, K. (2005). Increasing destructiveness of tropical cyclones over the past 30 years. *Nature*, **436**, 686–688.

Emanuel, K.A. (2013). Downscaling CMIP5 climate models shows increased tropical cyclone activity over the 21st century. *Proc. Nat. Acad. Sci*., **110**, doi/10.1073/pnas.1301293110.

Ganguly, A.R., K. Steinhauser, D.J. Erickson, III, M. Branstetter, E.S. Parish, N. Singh, J.B. Drake, L. Buja (2009). Higher trends but larger uncertainty and geographic variability in 21st century temperature and heat waves, *Proceedings of the National Academy of Sciences*, 106, 37, 15555 - 15559, doi:10.1073/pnas.0904495106.

Hansen, J., et al., 2001: A closer look at United States and global surface temperature change. *J. Geophys. Res.*, **106**, 23947–23963.

Keim, B.D., R.A. Muller and G.W. Stone (2007). Spatiotemporal Patterns and Return Periods of Tropical Storm and Hurricane Strikes from Texas to Maine, *Journal of Climate*, **20**, 3498-3509.

Levinson, D.H., and A.M. Waple (eds.), 2004: State of the climate in 2003. *Bull. Am. Meteorol. Soc*., **85**(6), S1–S72.

Lugina, K.M., et al., 2005: Monthly surface air temperature time series area-averaged over the 30-degree latitudinal belts of the globe, 1881-2004. In: *Trends: A Compendium of Data on Global Change.* Carbon Dioxide Information Analysis Center, Oak Ridge National Laboratory, US Department of Energy, Oak Ridge, TN, http://cdiac.esd.ornl.gov/trends/temp/lugina/lugina.html.

Meehl, G. A. & Tebaldi, C. More intense, more frequent, and longer lasting heat waves in the 21st century. *Science* **305**, 994-997 (2004).

Smith, T.M., and R.W. Reynolds, 2005: A global merged land and sea surface temperature reconstruction based on historical observations (1880–1997). *J. Clim.*, **18**, 2021–2036.

U.S.-Canada Power System Outage Task Force, April 2004, Final Report on the August 14, 2003 Blackout in the United States and Canada: Causes and Recommendations. https://reports.energy.gov/

Wu, S. Y., Najjar, R., & Siewert, J. (2009). Potential impacts of sea-level rise on the Midand Upper-Atlantic Region of the United States. *Climatic Change, 95*, 121–138.

Zhang, K.Q., Douglas, B.C., & Leatherman, S.P. (2000). Twentieth-century storm activity along the U.S. east coast. *Journal of Climate, 13*, 1748-1761.

Chapter 4

Compatibility of Scale among Climate and Critical Infrastructure Models

As climate models achieve higher resolution capability and more accurate regional predictions, the use of the information provided by the models is shifting towards policy-relevant impacts on human societies. Yet cities are complex systems that tend to grow from the bottom up, their size and shape following scaling laws pertaining to competition for space* based on demographic and economic decision-making activities over days, weeks and years and at spatial scales of 1km and less. Climate processes, on the other hand, are physical and chemical in nature, have only been reasonably resolved spatially to 4km and are studied commonly in terms of decadal trends. These climatic physical and chemical processes are computed in time steps of 30 minutes, while infrastructure operations such as power flow are computed in seconds, and population movement at yearly time steps. Because climate models work at different spatial and temporal scales from infrastructure and social models, to interface agent models to climate models with coupling and feedback mechanisms presents many new issues requiring new science and constructs for a global approach.

Over the last decade of research, climate models have become more granular, critical infrastructure models wider, data supporting detailed scenarios and interdependencies better understood, and questions of energy deployment and availability more tractable (Tables 4.1 and 4.2). Methods for communication among the various models has included statistical and dynamical downscaling and regridding of climate model data for input at compatible scales for critical infrastructure modeling, and aggregation and interpolation of results from the infrastructure models for input to climate models. Additionally, changes in file types must be made for interpretation of the data output by each model for input to the next. This process often

requires attention to grid types, projections, metadata and formatting in order to maintain as closely as possible the integrity of the data across computer architectures, computing platforms, and model frameworks.

Table 4.1 Temporal and Spatial Scales for Climate and Infrastructure Modeling, 2004

5 degr					Climate	Climate	Climate	Climate	Climate
2.5 deg					Climate	Climate	Climate	Climate	Climate
1 degr					Climate	Climate	Climate	Climate	Climate
36km									
12km									
4km									
1 km	Infrast	Infrast							
0	Minutes	Hourly	3-hrly	6-hrly	daily	monthly	yearly	decadal	century

Table 4.2 Temporal and Spatial Scales for Climate and Infrastructure Modleing, 2014

5 degr	Infrast	Infrast	Climate	Climate	Climate	Climate	Climate	Climate	Climate
2.5 deg	Infrast	Infrast	Climate	Climate	Climate	Climate	Climate	Climate	Climate
1 degr	Infrast	Infrast	Climate	Climate	Climate	Climate	Climate	Climate	Climate
36km	Infrast	Infrast	both	both	both	both	both	both	Climate
12km	Infrast	Infrast	both	both	both	both	both	both	Climate
4km	Infrast	Infrast	both	both	both	both	both	both	Climate
1 km	Infrast	Infrast	both	both	both	both	both	both	Climate
0	Minutes	Hourly	3-hrly	6-hrly	daily	monthly	yearly	decadal	century

*Batty, M. (2008). The Size, Scale, and Shape of Cities. *Science* **319**, 769-771.

Chapter 5

Can Regional Atmospheric Conditions Inform Bias Corrections for Model Downscaling of Extreme Precipitation?

Melissa R. Allen[1,2], Joshua S. Fu[1,2], Hamparsum Bozdogan[1]

[1]University of Tennessee, Knoxville

[2]Oak Ridge National Laboratory

Abstract

The determination of location-specific rainfall values from gridded data poses many challenges since precipitation is not a single variable, but instead a composite response to a variety of atmospheric conditions; and because spatial heterogeneity of rainfall within a model grid cell considerably affects the atmospheric state within it. Thus, the downscaling of modelled precipitation to specific locations requires more than simple bias correction, and statistical models incorporating ambient atmospheric conditions into the downscaling process can provide more accurate predictions of return periods of heavy events than those that do not include them. Multiple regression models for 99th percentile rainfall events in five locations in southern Sweden and two locations in the United States Gulf Coast region are evaluated using scores from four Information Complexity criteria for models including ten independent atmospheric variables. Results show that rainfall in these regions is exponentially distributed and that the moisture content of the atmosphere contributes the best information to downscaling calculations for heavy rainfall events from large grid cell averages to point-specific locations.

5.1. Introduction

As climate models achieve higher resolution capability and more accurate regional predictions, the use of the information provided by the models is shifting towards policy-relevant impacts on human societies. Many decision makers are concerned about extreme precipitation potential at specific locations (e.g., Wilbanks and Fernandez, 2012; Aerts et al., 2012; Pielke et al., 2000). Hydrological cycle predictions, for instance, play an important role in determining national and international resource allocation, viability of traditional and renewable energy technology, civil infrastructure design and operation procedures, and disaster risk aversion. Hydrologic variables such as rainfall, streamflow and runoff and their prediction are important to these calculations; yet rainfall, upon which these calculations are dependent (and especially extreme rainfall) remain difficult to predict. Additionally, the cost of the computing power required for dynamic climate modelling at neighbourhood scale is prohibitive even for the fastest supercomputers, let alone for urban planning budgets.

Climate models include parameterizations for a variety of factors affecting precipitation, but output of precipitation intensity is constrained by spatial and temporal resolution. Precipitation is output as averages over grid cells of at least a third of a degree latitude and longitude, and intensity is represented as a flux rather than as a discrete value for a given time period. Furthermore, the spatial heterogeneity of rainfall within a model grid cell considerably affects the atmospheric state and the mass balances within it, and without subgrid resolution in the model, even accurate values for the grid cell average can be difficult to attain. Thus, both location-specific extreme rainfall and the factors contributing to it are masked by the limits of

model resolution. Even models based on real-time measurements, such as reanalyses, must interpolate values between observation stations in order to provide a gridded product.

Thus, resolution of subgrid extreme precipitation has been treated statistically in both past (Eagleson, 1978; McKee et al., 1993; Wilks, 1995) and recent studies (Garavaglia et al., 2011; Benestad et al., 2012; Papalexiou, 2013). These studies investigate the applicability of a variety of extreme value distributions to extreme rainfall events such as Generalized Extreme Value, Exponential, Generalized Pareto, Lognormal, Log Pearson, Weibull, Kappa and Gamma, and give careful analysis of each for long data records at a large number of locations.

In addition, a variety of improvements on these methods have been proposed. For example, Perica and Foufoula-Georgiou (1996) suggested that rainfall fluctuations could be described with a Haar wavelet transformation informed by two components based upon the amount of convective available potential energy (CAPE, containing specific humidity, potential temperature and pressure relationships) available in the atmosphere, and that this information could be used to scale model output to successively finer resolution. Mannshardt-Shamseldin et al. (2010), in search of a simpler alternative, addressed differences between station measurements and reanalysis data sets by developing regression relationships between them. They found, however, that the residuals from their models showed spatial patterns for which they were unable to account. Olsson and Willen (2010), in a model that is simpler still, found that the averaged convective precipitation for Stockholm, Sweden could be scaled to the maximum within its grid cell using the high cloud cover fraction within the cell multiplied by a scaling

factor. From values obtained in this manner, the researchers found annual maxima that were used to compute return periods that matched those of the Stockholm station observations. The particular scaling factor derived for the Stockholm example in the Olsson and Willen study did not reliably forecast the annual maxima at other southern Sweden sites, however, but did predict consistently the pattern of extreme precipitation events for Stockholm.

Among the difficulties in characterizing extremes in location-based precipitation is that precipitation in general cannot be considered a single variable, but rather a composite response to a variety of atmospheric conditions. That is, predictions of the intensity of a given precipitation event must incorporate several atmospheric processes including evaporation, changes in atmospheric pressure, and uneven solar heating leading to convective activity. For instance, in European studies conducted by Hellstrom (2005), Gustafsson et al. (2010) and Zveryaev and Allan (2010), significant links were found between precipitation and evaporation from the European land surface, and from the Baltic Sea. Hellstrom also found that extreme precipitation in Sweden occurs predominantly under cyclonic atmospheric conditions. Since mean sea level pressure is co-located with vertical velocity in the mid troposphere (Lamb, 1950; Lavers et al. 2013), and is indicative of cyclonic development and precipitation, investigations into the effects of varying scales of mean sea level pressure values on regional precipitation have been conducted. Lavers et al. provide one such example for which European precipitation shows spatiotemporal variability when using large scale monthly mean sea level pressure fields (correlated with the North Atlantic Oscillation) throughout the year, while Thompson and Green (2004) note a clear relationship between local sea level pressure and precipitation in the

Mediterranean. May et al. (2012) and Richardson (1981) associate changes in precipitation patterns with changes in surface radiation. Shindell et al. (2012) further show that changes in thermal forcing and the resultant impact on poleward energy fluxes affect tropical precipitation patterns, but that changes in circulation affecting extra-tropical precipitation are more closely tied to anomalous flow around localized sea level pressure changes. Thus, regional precipitation is affected by both local and remote forces; and precipitation patterns differ from region to region.

In order to develop a simple method that examines the appropriateness of including atmospheric state variables in the construction of a model for downscaling grid cell averages to single-point heavy rainfall events, we use multiple regression analysis along with four information-complexity based model selection criteria in order to select a best model from ten atmospheric variables for a given location. We then check the result with a computation of intensity vs return period for the location using a determined best cumulative distribution function. Because the Olsson Willen model described above provides another simple model to which we can compare results, we use data from the same locations that they included in their study: Helsingborg, Malmo, Stockholm, Uppsala and Vaxjo. To further validate our method, we examine its performance using measurements from two locations in the United States Gulf Coast region as well, a region governed by very different atmospheric processes than those of southern Sweden, Baton Rouge, Louisiana and Canton, Mississippi. The time period of the study is years 1961-1982, which was chosen based upon the available data common to all locations investigated and to the reanalysis product. The success of this method can offer field hydrologists and urban

engineers a tool for evaluating global climate model output for the purpose of planning projects focused at a more local scale.

5.2. Methodology

This study begins by determining the probability density function that best fits the measurements at each location examined and then proceeds to develop a simple model from relevant multiple regression defined by the meteorological variables of most significance in the calculation of 99th percentile 24-hour rainfall intensities. Results are then transformed (per Chow, 1988 as described in section 2.3) to return period calculations.

5.2.1 Datasets and Initial Calculations

Tipping bucket measurements (resolution 0.1mm) obtained from five stations in southern Sweden for the years 1961-1982 (the years of quality data in common to all data sources) by the Swedish Meteorological and Hydrological Institute (SMHI) for 24-hour accumulation (from 06 UTC of the indicated day to 06 UTC of the following day) were used as the observational data for this study. Data were downloaded from http://www.smhi.se/klimdata/meteorologi/dataserier-2.1102 for the point gauge locations shown in Figure 5.1 and listed in Table 5.1. Gauge data used for validation of the method for the US Gulf Coast area are from the National Climatic Data Center (NCDC) hourly measurements aggregated to daily accumulation. Only two sites in this area contained complete measurement data sets for the years common to the Swedish data sets. These locations are also included in Table 6.1.

Gridded data comes from the European Centre for Medium-Range Weather Forecasts (ECMWF) ERA-40 global daily reanalysis fields output at 6-hourly intervals at 2.5 x 2.5 degree resolution. Meteorological values used as independent variables in the exponential regression include convective and large scale precipitation, total and high cloud cover fraction, evaporation, total column water and water vapour, surface and top of atmosphere thermal radiation, and mean sea level pressure. Precipitation values were summed for each day, while all other values were averaged daily. A table of these independent variables and the units used for each can be found in Appendix 6A.

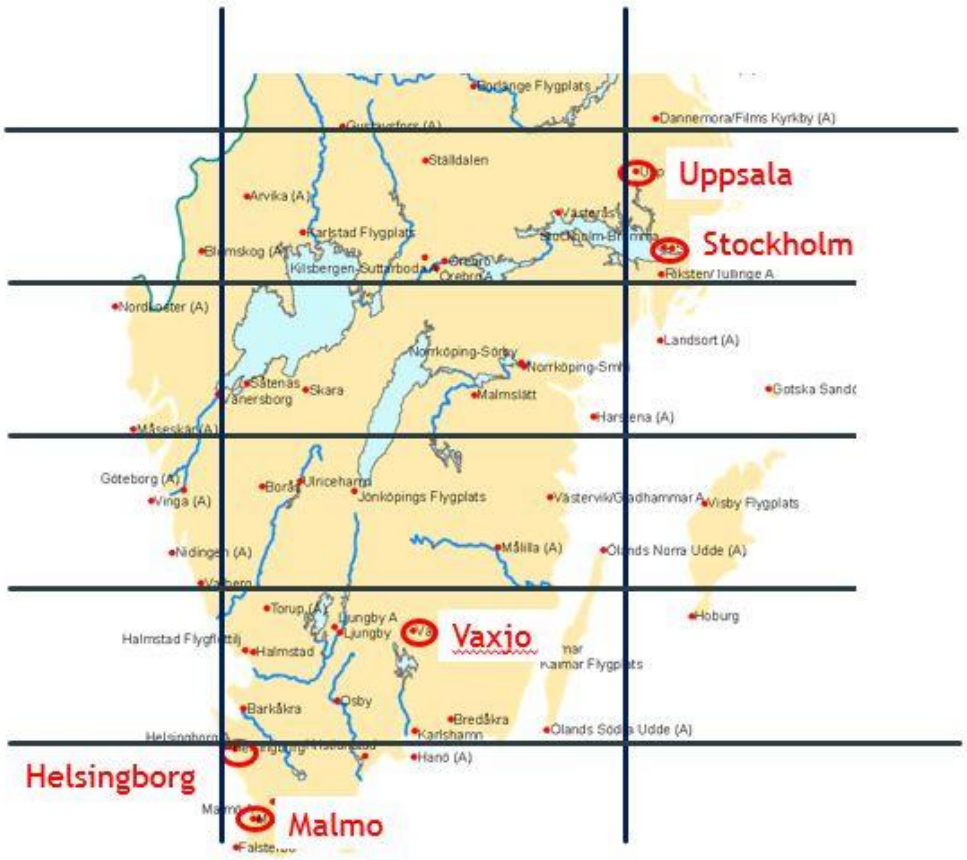

Figure 5.1. Southern Sweden Sites Examined

Although rainfall intensity in Sweden is lower than in many parts of the world, an accumulation of over 40mm in a 24-hour period is defined as an extreme event by SMHI, because above this limit the risk of flooding of rivers and landslides increases. Annual average 1-day maximum precipitation ranges between 25mm and 40mm (Gustafsson et al., 2010). Values included in the 99^{th} percentile intensities of 24-hour precipitation events in this study (which occur during the summer months as rain) vary between 16.6mm to 64.8mm, containing this range. For the US Gulf Coast state station measurements these values are much larger at 57.4mm to 304.5mm and occur during various months throughout the year.

Table 5.1. Precipitation Measurement Station Locations

Location	Station Number	Longitude	Latitude
Helsingborg	6203	12.69	56.04
Malmo	5336	13.03	55.58
Stockholm	9821	18.06	59.34
Uppsala	9752	17.63	59.86
Vaxjo	6452	14.82	56.84
Baton Rouge	160549	-91.15	30.53
Canton	221389	-90.03	32.6

5.2.2 Determination of Probability Density Function of the Measured Data

We begin by analysing the point gauge data from SMHI for the five locations in southern Sweden (and the two locations in the southern US) to determine the probability density function that provides the best fit for 99^{th} percentile precipitation events. To accomplish this task we apply two different methods: 1) Information Complexity Criteria and (results shown in Appendix 6B) 2) quantile-quantile comparison for visualization (Appendix 6C).

The Information Complexity Criteria methodology used to determine the suitability of various probability density functions to the measured data, described in more detail in section 2.6, employs four different scoring methods, the minima of which identify the best distribution fit. This method was used to compare the fit of Normal, Lognormal, Exponential, Gamma, Weibull, Uniform, Generalized Pareto (Peaks-Over-Threshold), Generalized Extreme Value and Log Pearson, Type III distributions to the data. Results of this procedure showed that of these distributions, the best fit for the data for each location and evaluation, the single parameter Exponential distribution matched the data best. (We do not consider here changes in temporal trend, i.e., nonstationarity, because the data span only 22 years. Moving averages (15- and 30-year windows) for precipitation have been investigated in in other studies (e.g., Livezey et al., 2007 and Kao and Ganguly, 2011 respectively)).

5.2.3 Frequency Analysis

The fundamental statistical method used to evaluate increasing frequency of extreme precipitation events is that of frequency analysis. The objective of frequency analysis is to relate the magnitude of events to the frequency of their occurrence using probabilistic methods. It is assumed that the events (data) are independently and identically distributed. Chow et al. (1988) suggest the following relationship between probability and frequency of events.

For a random variable X, and threshold level x_T, an extreme event occurs if $X \geq x_T$. The recurrence interval of the event is described as:

$$\tau = Time\ between\ occurrences\ of\ X \geq x_T \qquad (1)$$

The return period is then a function of τ, $E(\tau)$, which is the average recurrence interval between events equalling or exceeding a threshold. Therefore, if p is the probability of occurrence of an extreme event, then

$$E(\tau) = T = \frac{1}{p} \quad (2)$$

or

$$P(X \geq x_T) = \frac{1}{T} \quad (3)$$

The following sections describe the methods used to determine the frequency analyses used to describe the distribution of the most extreme (99^{th} percentile) rainfall events in each of the locations identified above.

5.2.4 Exponential Distribution

The single-parameter exponential cumulative distribution function (a special case of both the Gamma and the Generalized Pareto distributions) is:

$$F(x) = 1 - e^{-\lambda x}$$

With lambda equal to the reciprocal of the mean value of the distribution, $\lambda = 1/\mu$.

To obtain intensity vs return period, we apply a transformation in the manner of Chow (1988):

1) Define a reduced variate, y:

$$y = \lambda x \tag{4}$$

2) Substitute the reduced variate into the CDF:

$$F(x) = 1 - \mathrm{e}^{-y} \tag{5}$$

3) Solve for y:

$$y = -\ln[1 - \mathrm{F(x)}] \tag{6}$$

4) Recall from (3) and continue,

$$P(X \geq x_T) = \frac{1}{T} \tag{3}$$

5) Substitute into (6),

$$y_T = -\ln\left(\frac{1}{T}\right) \tag{7}$$

6) Relate x_T to y_T:

$$x_T = \mu y_T \tag{8}$$

5.2.5 Additional Physical Parameters Contributing to Extreme Precipitation

Using a multiple exponential regression scheme along with information-based model selection criteria (Bozdogan et al., 1986), we derive a subset of output variables from the ECMWF coarse grid dataset that best contribute to the calculation of extreme precipitation at each point location. (This data set does not include atmospheric chemical constituents, however, so the effect of aerosols or additional atmospheric chemistry on amount of precipitation is not taken into consideration.)

The objective of the model selection criteria used here is to evaluate the appropriateness of each of various models comprising a subset of independent variables drawn from the lower resolution ECMWF ERA-40 product output to represent the most extreme (99^{th} percentile) measured local precipitation events. A model is considered more appropriate the lower its score calculated by the criteria. This score represents an evaluation of the model's 'entropy,' or unpredictability, of the expected local precipitation measurement as characterized by the independent variables. This model selection method is chosen over that of hypothesis testing since these methods test only 'significance' of each independent variable and not the complexity of the model system (e.g., Akaike, 1973; Bozdogan, 1987; Anderson et al., 2000).

Four criteria are used to evaluate model subset selection. Each of these criteria evaluates both goodness of fit of the model parameters using Maximum Likelihood Estimates (MLE) and minimization of Kullback-Leibler Information (1951). The first criterion applied is the Akaike Information Criterion (AIC), which rewards the goodness of fit of a given model but penalizes

model complexity using a relative estimate of the information lost (Akaike, 1974). A second and related criterion, Consistent Akaike's Information Criterion (CAIC), is evaluated as a check on potential error due to small sample size (Bozdogan, 1987). The third criterion used is the Schwarz Bayesian Criterion (SBC), which is based on AIC but incorporates a higher penalty for complexity (in this case, additional parameters) in a model. Finally, we score the models using the Information Complexity (ICOMP) Criterion developed by Bozdogan (2000; Yang and Bozdogan, 2011). This criterion is derived from AIC, but takes into account the interdependencies of the parameter estimates as well as the dependencies of the model residuals by quantifying the concept of overall model complexity in terms of the estimated inverse-Fisher information matrix (Amari, 1985).

Briefly, a multiple linear regression model under normality is defined by

$$\boldsymbol{Y} = \boldsymbol{X\beta} + \boldsymbol{\varepsilon} \tag{9}$$

where $\boldsymbol{Y}$ is an (nx1) vector of observed values of the response variable, $\boldsymbol{X}$ is an (nxq) full rank matrix representing n observations with each one measured on k variables and $q = k + 1$, $\boldsymbol{\beta}$ is a (qx1) matrix of unknown regression coefficients, and $\boldsymbol{\varepsilon}$ is an (nx1) vector of independently and identically distributed random errors. Further, it is assumed that $\boldsymbol{Y} \sim N_n(\boldsymbol{X\beta}, \sigma^2\boldsymbol{I})$ and $\boldsymbol{\varepsilon} \sim N_n(\boldsymbol{0}, \sigma^2\boldsymbol{I})$ with σ^2 being the unknown variance of random errors.

Given the multiple regression model in Equation (9) the Maximum Likelihood Estimates (MLEs) of $\boldsymbol{\beta}$ and σ^2 are given by:

$$\hat{\beta} = (\mathbf{X}'\mathbf{X})^{-1}\mathbf{X}'\mathbf{Y} \quad (10)$$

$$\hat{\sigma}^2 = \frac{1}{n}(\mathbf{Y} - \mathbf{X}\,\widehat{\boldsymbol{\beta}})'(\mathbf{Y} - \mathbf{X}\,\widehat{\boldsymbol{\beta}}) \quad (11)$$

The maximized log likelihood function is:

$$logL(\widehat{\boldsymbol{\beta}}, \hat{\sigma}^2) = -\frac{1}{2}n\,log(2\pi) - \frac{n}{2}\log(\hat{\sigma}^2) - \frac{1}{2}n \quad (12)$$

The badness/lack of fit for the model is, then:

$$-2\log L(\widehat{\boldsymbol{\beta}}, \hat{\sigma}^2) = n\,log(2\pi) + n\log(\hat{\sigma}^2) + n \quad (13)$$

For each evaluation of model fitness, AIC, CAIC, SBC and ICOMP, both a badness of fit term (13) and a model complexity term add together to make up the fitness assessment. The model complexity terms for each are:

AIC: 2(k+1) k= degrees of freedom of the model

CAIC: [log(n)+1]k n=sample size

SBC: [log(n)]k

ICOMP: $C_1(\mathbf{F}^{-1})$

For ICOMP, the complexity term is a term defined by the complexity of the Inverse Fisher Information Matrix (IFIM), denoted: $C_1(\mathbf{F}^{-1})$. $\mathbf{F}^{-1}$ is defined as:

$$\mathbf{F^{-1}} = Est.Cov(\widehat{\boldsymbol{\beta}}, \hat{\sigma}^2) = \begin{bmatrix} \hat{\sigma}^2(\boldsymbol{X'X})^{-1} & \mathbf{0} \\ \mathbf{0'} & \frac{2\hat{\sigma}^4}{n} \end{bmatrix} \quad (14)$$

and the complexity measure that C_1 of $\mathbf{F}^{-1}$ is the scalar value given by:

$$C_1(\boldsymbol{F^{-1}}) = \frac{3}{2} log\left[\frac{tr(\boldsymbol{F^{-1}})}{s}\right] - \frac{1}{2} log|\boldsymbol{F^{-1}}| \quad (15)$$

where $s = \dim(\boldsymbol{F^{-1}}) = rank(\boldsymbol{F^{-1}})$

As the number of parameters increases (i.e., as the size of X increases), the error variance ($\hat{\sigma}^2$) decreases although the complexity increases. In addition, as $\hat{\sigma}^2$ increases, $(X'X)^{-1}$ decreases. Therefore $C_1(\widehat{\boldsymbol{F}}^{-1})$ negotiates between these two extremes to eliminate mullticollinearity in the selected model.

We pay special attention to this last scoring criterion as each formulation of ICOMP adjusts for the number of parameters and the sample size, which serve to control the risks of both insufficient and over parameterized models (Bozdogan, 2000).

For this study, we analyze the data under the assumption that the *y*-values are exponentially distributed, thus transforming the linear regression model to:

$$ln(\boldsymbol{Y}) = \boldsymbol{X\beta} + \boldsymbol{\varepsilon} \quad (16)$$

5.3. Results and Discussion

Both Information Complexity Criteria and quantile comparison for the 99th percentile of daily precipitation intensity measurements for the years 1961-1962 for each of the five locations in

southern Sweden suggest that the single-parameter exponential distribution best fits this data. This result corroborates the general finding of Benestad et al. (2012).

A comparison of the sum of convective and large scale precipitation at the same locations as given in the reanalysis data from the ECMWF for 99th percentile of precipitation intensity (Figure 5.2) demonstrates the well-known problem that grid cell averages of precipitation greatly underestimate the total precipitation amounts for events of extreme intensity.

Olsson and Willen (2010) address this problem by relating the convective component of the precipitation in a grid cell to the extreme value received at a single point using the fraction of high cloud cover (since it is associated with convective activity), assuming that the probability of precipitation is the same everywhere inside the grid cell and that precipitation occurring at an arbitrary point inside the grid cell equals the fractional precipitation area.

$$P_{point} = \frac{cp}{\alpha \times hcc} + lsp$$

with cp = convective precipitation component, hcc = high cloud cover fraction, lsp = large scale precipitation and α = scaling factor. Our findings, using their method with 24-hour precipitation values, showed a close match for Stockholm just as their results for 30 minute precipitation events were accurate to within 10% for Stockholm, but (as they discovered in their study) results using this method were not accurate for the other four locations examined (Figure 5.2.)

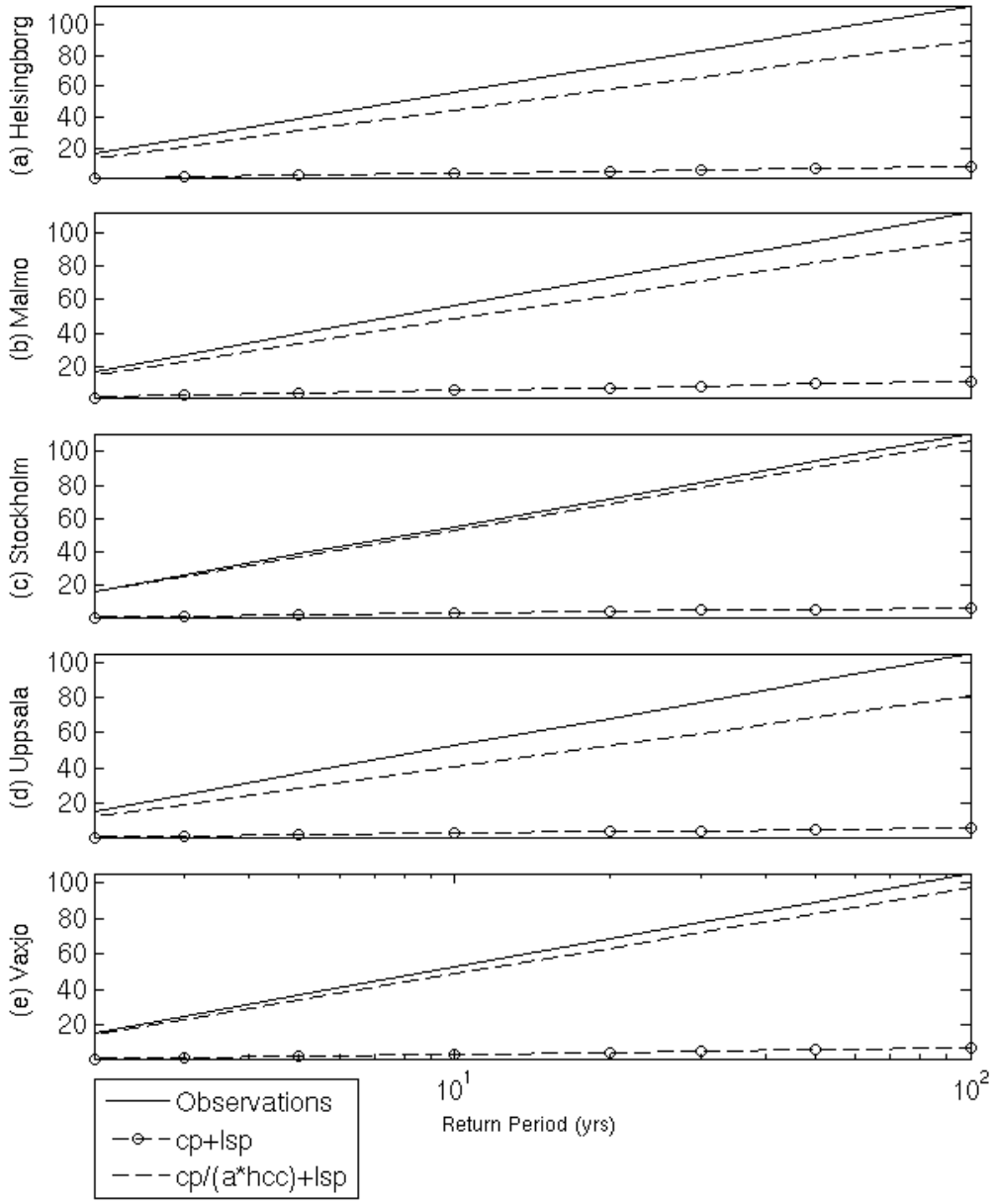

Figure 5.2. Results using the Olsson and Willen scaling method for calculating return periods for 99th percentile precipitation events at a given location using grid cell averaged values (dashed line) show good agreement for Stockholm measurements but much less agreement in the other southern Sweden locations. Simple addition of convective and large scale precipitation in the grid box is shown with the line marked '-o-'.

5.3.1 Results of Exponential Regression

To improve upon this result, we apply a multiple exponential regression using the SMHI point-gauge measurements as the dependent variable, and ten different meteorological variables (Appendix A) from the ECMWF data as the independent variables in order to look more deeply into the relationship between heavy daily rainfall at a specific location and regional atmospheric conditions. Using the Information Criteria based model selection procedure (Bozdogan et al., 1986), we determine which of the additional parameters may yield better predictability of extreme rainfall.

Results followed a form similar to that of the Hernebring (2006) IDF (Intensity, Duration, Frequency) equation, which sets precipitation intensity for each of 5 locations in Sweden equal to a multiplication of base e and Return period and Duration each raised to exponents found specifically and empirically for each location. Our models, however, incorporated the values associated with specific 1-day average meteorological variables in each grid cell into the formula, which simplifies the equation, is adaptable to all locations, and which applies to the 99th percentile of precipitation events. The models are as follows:

Helsingborg:

$$I = e^{(2.6824 + (0.5591 * total\ cloud\ fraction))}$$

Malmo:

$$I = e^{(2.8748 + (0.018 * total\ column\ water\ vapor))}$$

Stockholm:

$$I = e^{(3.1235 + (-0.0836 * convective\ precip) + (0.4039 * high\ cloud\ cover))}$$

Uppsala:

$$I = e^{(3.1011 + (-0.0685 * convective\ precipitation))}$$

Vaxjo:

$$I = e^{(2.9885 + (-0.027 * large\ scale\ precip) + (0.011 * column\ water\ vapor))}$$

Scores for each model by each criterion can be found in Appendix D. Comparison of probability density function and intensity vs return period for the 99th percentile events are shown in Figures 5.3-5.7.

The variation in regional precipitation patterns becomes evident as each best model comprises different atmospheric variables for best prediction of intensity vs return period of the measured data. For Helsingborg and Malmo, both on the western coast of southern Sweden and both contained in the same 2.5 x 2.5 ECMWF grid cell, a single atmospheric moisture variable is chosen as significant to prediction of heavy precipitation events. For Helsingborg (Figure 5.3), the variable is total cloud cover fraction, while for Malmo (Figure 5.4) it is total column water

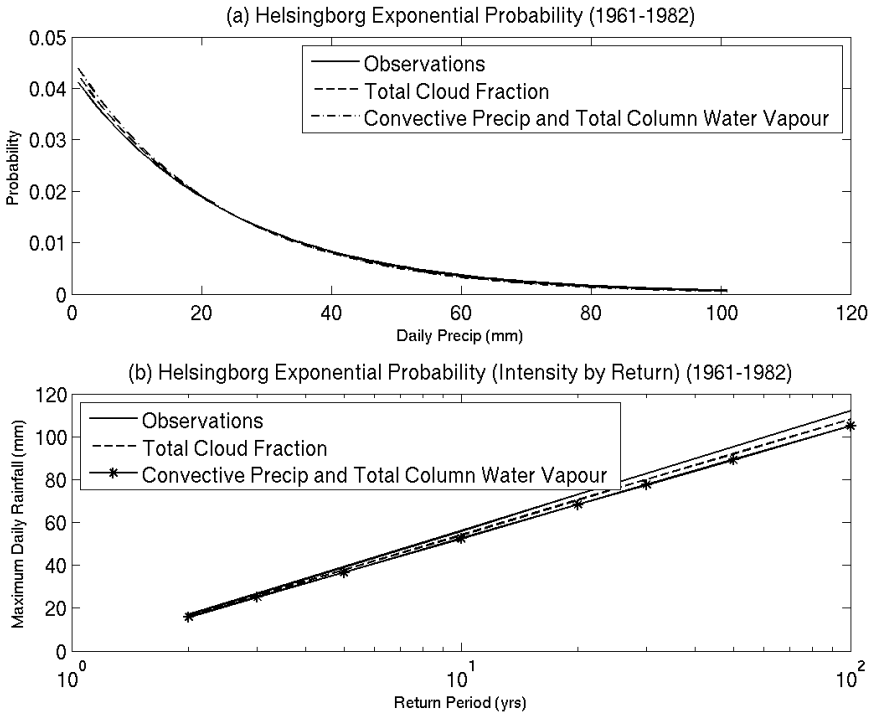

Figure 5.3. The probability of 99th percentile of rainfall events in Helsingborg, Sweden follows an exponential distribution (a). Results from the best models obtained from the exponential regression of corresponding local meteorological variables from the European Centre for Medium-Range Weather Forecasting (ECMWF) ERA-40 reanalysis data (at 2x2.5 degree resolution) are compared to point gauge measurements. The best model for this location was the one in which total cloud cover fraction was the only significant predictor. (b) A transformation to intensity vs return period of (a) shows that the regression model only slightly underestimates the intensity for return periods of the highest daily rainfall amounts found in the observations. The all-southern-Sweden model using convective precipitation and total column water vapour as predictors does slightly less well for this location.

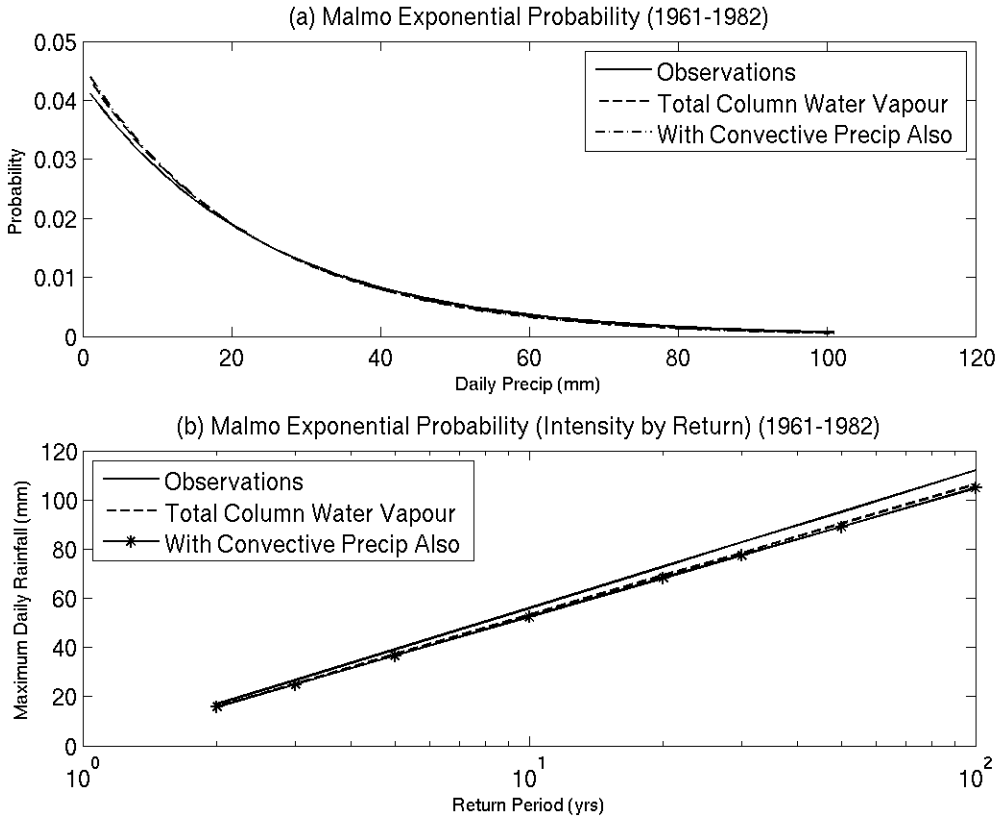

Figure 5.4. The probability of 99th percentile of rainfall events in Malmo, Sweden also follows an exponential distribution (a). For this location, the best model for is the one in which total column water vapour was the only significant predictor. (b) A transformation to intensity vs return period of (a) shows that the regression model only slightly underestimates the intensity for the return periods of the highest daily rainfall amounts found in the observations. The all-southern-Sweden model using convective precipitation and total column water vapour as predictors does nearly as well for this location.

vapour. Forsythe et al. (2012) show a relationship between the vertical structure of clouds and total precipitable water anomaly in the North Pacific (the Scandinavian region was not investigated)—that high clouds and deep clouds throughout the troposphere there are more likely at higher anomaly values; thus, these variables may not be truly independent, especially as predictors of larger rainfall events.

For the Stockholm and Uppsala locations (Figures 5.5 and 5.6), the amount of convective precipitation reported in the grid cell was the most significant predictor of heavy precipitation. In Stockholm, high cloud cover also played a large role in the calculation of precipitation intensity. This finding agrees to some extent with that of Olsson and Willen (2010) for Stockholm. It is also consistent with studies showing that cyclonic atmospheric conditions are predominantly responsible for extreme precipitation events in southern Sweden (Hellstrom, 2005; Gustafsson et al., 2010).

Vaxjo (Figure 5.7) is the only location at which the best model indicated that high precipitation intensity is dependent primarily on large scale precipitation, although total column water vapor is also significant in the model. This result may support the findings of previous work which show that moisture needed for precipitation in this inland region of southern Sweden is due to transport of moisture from the European continent and the Baltic Sea (Hellstrom, 2005; Gustafsson et al., 2010; and Zveryaev and Allan, 2010) and/or the climatological analysis of Hellstrom and Malmgren (2004) demonstrating that frontal activity is a dominant influence on extreme precipitation under non-cyclonic conditions.

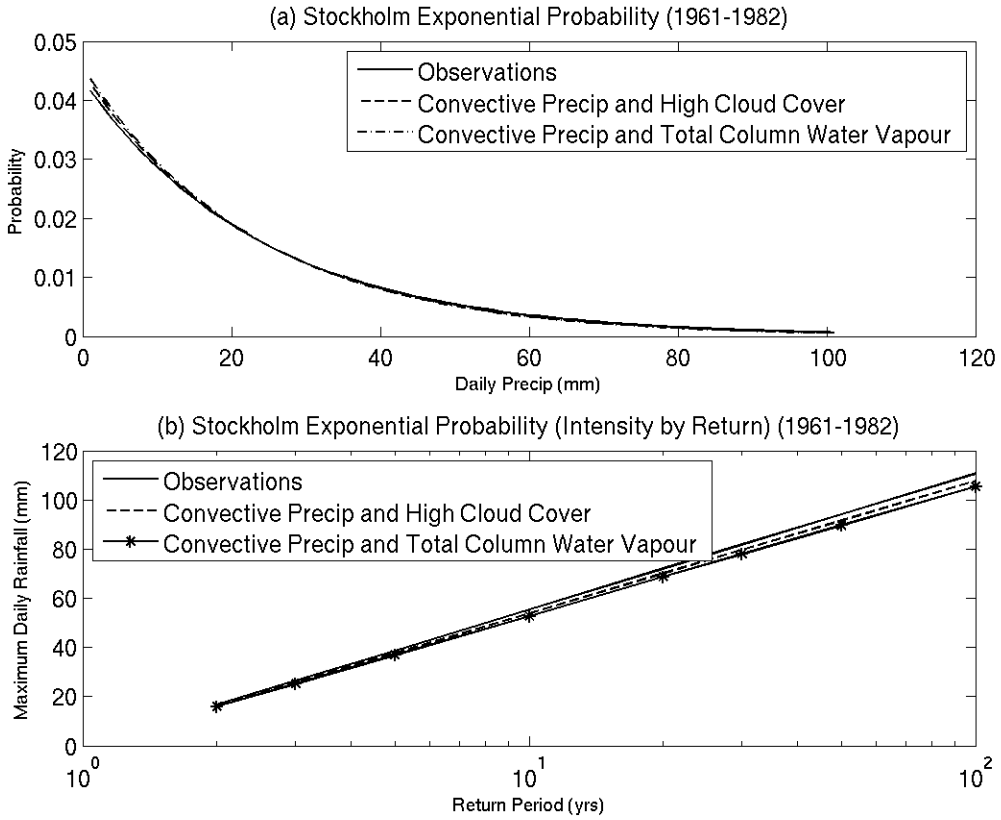

Figure 5.5. 99th percentile rainfall events in Stockholm, Sweden are exponentially distributed (a). The best model for Stockholm includes both convective precipitation and high cloud cover as significant predictors. (b) A transformation to intensity vs return period shows close agreement with that found for the highest daily rainfall amounts in the observations. The all-southern-Sweden model using convective precipitation and total column water vapour as predictors does slightly less well for this location.

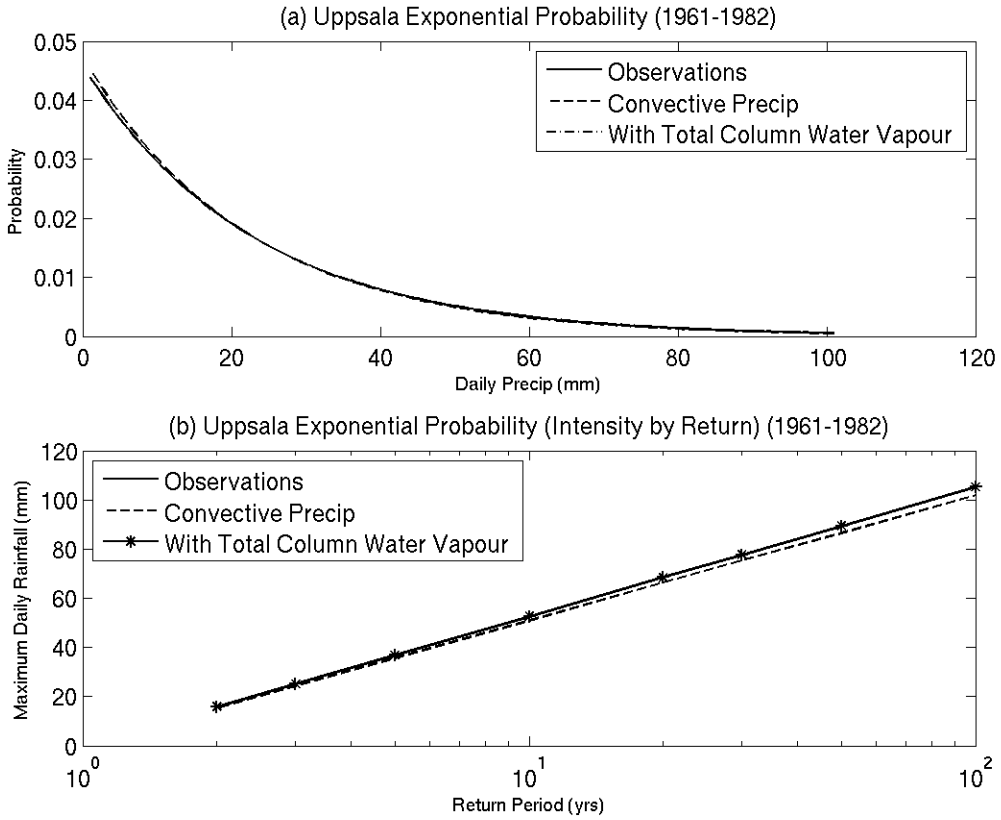

Figure 5.6. 99th percentile rainfall events in Uppsala, Sweden are exponentially distributed (a). The best model for Uppsala includes only convective precipitation as a significant predictor. (b) A transformation to intensity vs return period shows close agreement with that found for the highest daily rainfall amounts in the observations. The all-southern-Sweden model using convective precipitation and total column water vapour as predictors does better than convective precipitation alone for this location.

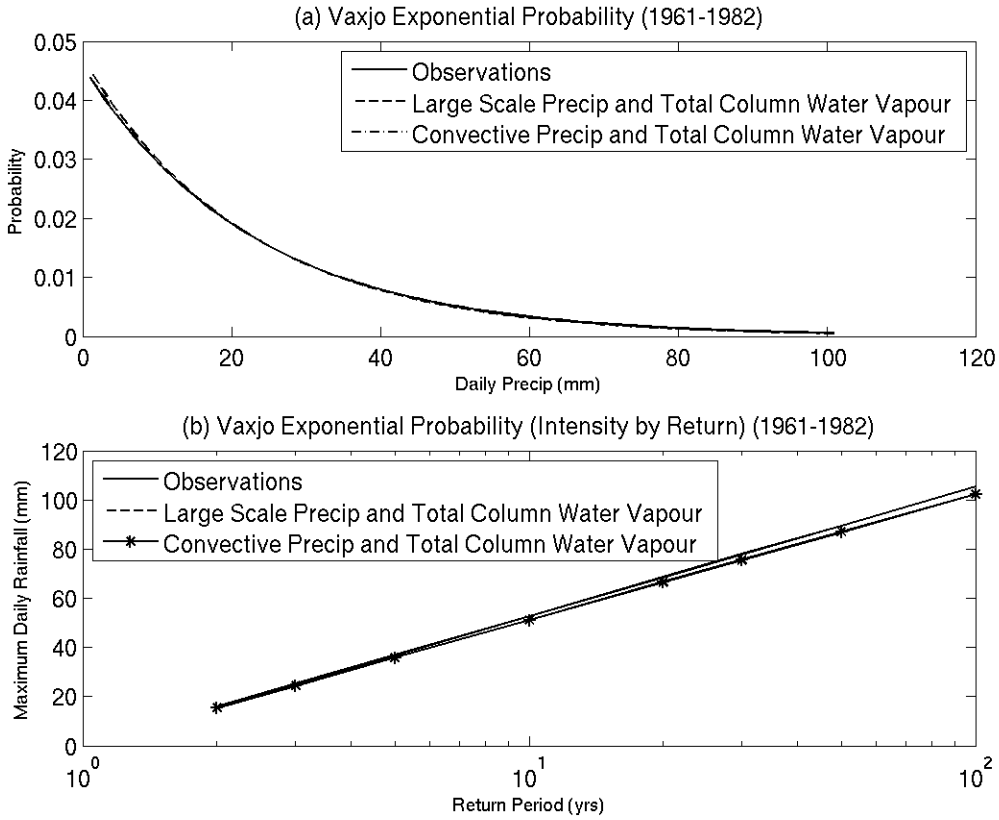

Figure 5.7. 99th percentile rainfall events in Vaxjo, Sweden are exponentially distributed (a). The best model for Vaxjo includes both large scale precipitation and total column water vapour as significant predictors. (b) A transformation to intensity vs return period shows close agreement with that found for the highest daily rainfall amounts in the observations. The all-southern-Sweden model using convective precipitation and total column water vapour as predictors does slightly better than the model chosen based on atmospheric variables for this location alone.

To investigate the possibility that a single model could characterize the heavy rainfall of all of southern Sweden, a final regression was performed in which the measurements from all of the gauges were concatenated to form a single dependent variable, and data for each independent variable were also concatenated accordingly. The resulting model gave convective precipitation and total column water vapour as the best predictors:

$$I = e^{(3.0087 - (0.071 * convective\ precip) + (0.0092 * total\ column\ water\ vapor))}$$

As shown in the figures as 'All 18,' this model slightly underestimates the extreme rainfall in two of the locations (Helsingborg and Stockholm), does as well as the model for the single station for two of the locations (Vaxjo and Malmo) and predicts Uppsala better than the model for the single station. This result may indicate that there is no real difference in heavy rainfall among the stations and that the larger sample size of the combined model compensated for any multicollinearity unsolved for by the scoring criteria.

Validation of the approach was performed using measurement data from Baton Rouge, Louisiana (Figure 5.8) and Canton, Mississippi (Figure 5.9). 99^{th} percentile rainfall in these locations was found also to be exponentially distributed, and models for both locations included total column water vapour and total column liquid water. Closely scoring alternative models to this included variables such as top thermal radiation and mean sea level pressure indicating conditions favourable to cyclonic activity (e.g., Emanuel et al., 2013).

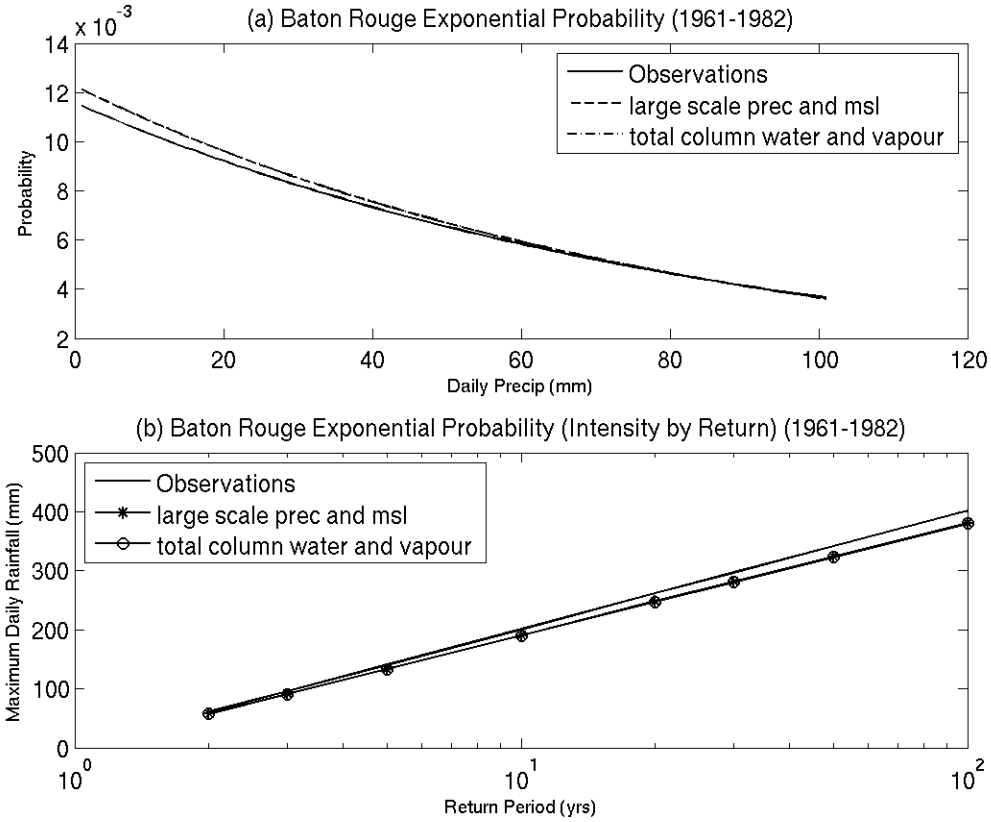

Figure 5.8. 99th percentile rainfall events in Baton Rouge, Louisiana are exponentially distributed (a). The best model for Baton Rouge includes total column water vapour and total column liquid water as significant predictors, although the model using large scale precipitation and mean sea level pressure does essentially as well. (b) A transformation to intensity vs return period shows close agreement with that found for the highest daily rainfall amounts in the observations.

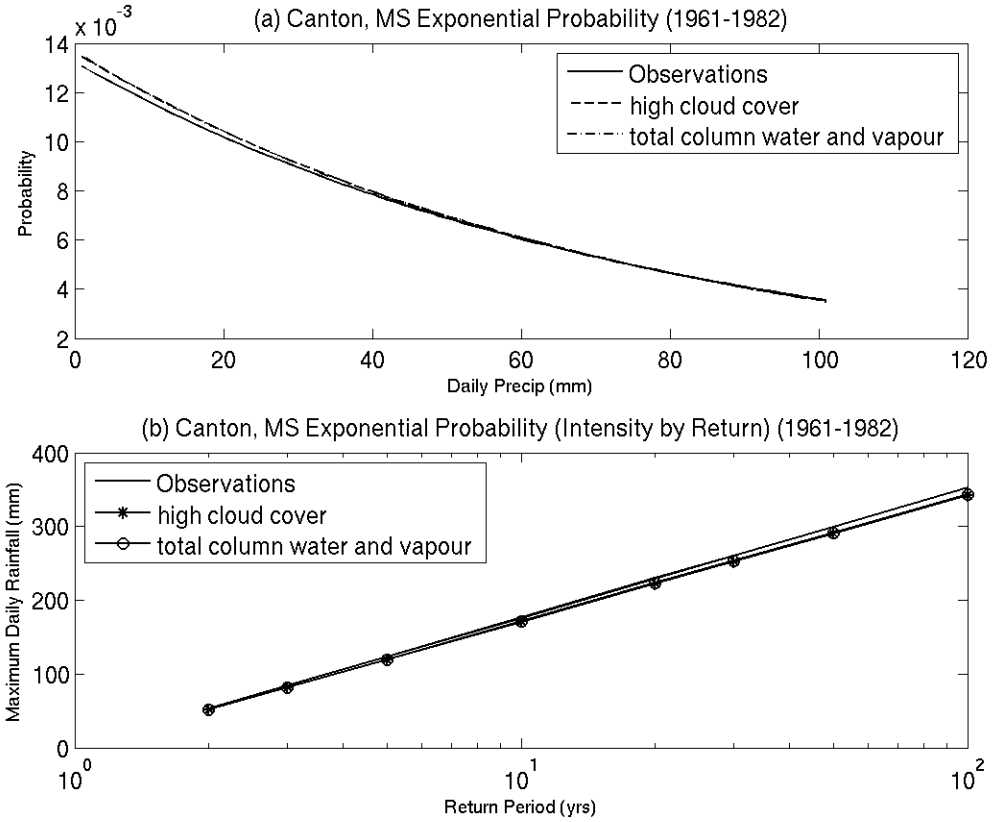

Figure 5.9. 99th percentile rainfall events in Canton, Mississippi are exponentially distributed (a). The best model for Canton includes total column water vapour and total column liquid water as significant predictors, although the model using high cloud cover, mean sea level pressure and top thermal radiation fits nearly as closely. (b) A transformation to intensity vs return period shows close agreement with that found for the highest daily rainfall amounts in the observations.

5.4. Conclusions and Future Work

Information Complexity Criteria (Bozdogan, 2000) provided a quantitative validation of apparent quantile-quantile analyses of the probability distributions of measured extreme rainfall events. Confirmation that the distributions were exponentially distributed allowed for meaningful multivariate regression using an exponential formulation. This analysis was an important first step in the process to inform the choice of regression used. Comparison of the results obtained by this method with results obtained from a linear regression (not discussed) of

the same atmospheric variables differed significantly in the models and variables selected. Matching the distribution of the model results with that of the dependent variable yielded much more robust predictions of return periods of significant rainfall events. The results showed that regional precipitation is affected by both local and remote forces; and precipitation patterns differ from region to region, yet in all of the cases examined, the heaviest rainfall at a given point was associated with the moisture content of the atmosphere either in the form of cloud cover or liquid or water vapour. (This finding is particularly important with regard to climate change, since with increases in atmospheric temperature more water is retained in the atmosphere.) Convective precipitation contributed significantly to heavy rainfall in Sweden whereas it was not highly correlated to heavy rainfall in the Gulf of Mexico. This is likely due in part to the fact that the heaviest rains in southern Sweden occur almost always in the months of July and August, whereas in the Gulf Coast area, the heaviest rains (generally at least twice the magnitude of those in southern Sweden) can occur in almost any season and, as such, can be associated either with large scale systems or with hurricanes, each of which involve very different atmospheric processes.

Additional steps in the development of a statistical downscaling scheme for the representation of precipitation at the local level from that at coarser scale could also include temporal and spatial relationships among grid cell values of convective and large scale precipitation and the significant variables identified. That is, examination of the correlation between atmospheric conditions before an extreme event occurs (possibly suggesting movement of systems from one location to another) may prove at least as significant to the point-specific downscaling as

concurrent ones. Results of these schemes should be compared to observational values, and predictive results to dynamical downscaling schemes such as those of high resolution models (e.g., Gao et al., 2012) and to spatial regression relationships (e.g., Hellstrom and Malmgren, 2004). The schemes may ultimately apply to predictions of local extremes using output of climate model simulations under various social (SRES) and radiative forcing (RCP) scenarios (Nakićenović and Swart, 2000; Moss et al., 2008, respectively).

We have shown a simple method for downscaling gridded average precipitation values to values for heavy precipitation events at specific locations by incorporating meteorological state variables into the calculations. The method represents a readily accessible way for field hydrologists and infrastructure developers to evaluate both historical data and climate model predictions, without the requirement of extensive computing power, as they plan for flood mitigation and minimization of urban consequences due to extreme precipitation events.

5.5 Acknowledgments

This manuscript has been authored by employees of UT-Battelle, LLC, under contract DE-AC05-00OR22725 with the U.S. Department of Energy. Accordingly, the United States Government retains and the publisher, by accepting the article for publication, acknowledges that the United States Government retains a non-exclusive, paid-up, irrevocable, world-wide license to publish or reproduce the published form of this manuscript, or allow others to do so, for United States Government purposes. The authors would like to acknowledge the financial support for this research from the US Government for the development real time simulation of

power grid disruptions, an Oak Ridge National Laboratory Directed Research and Development (LDRD) project and from the Bredesen Center at the University of Tennessee.

References

Aerts, J., W. Botzen, M.J. Bowman, P.J. Ward and P. Dircke, 2012. *Climate Adaptation and Flood Risk in Coastal Cities*, Earthscan: London, New York.

Akaike, H., 1973. Information theory and an extension of the maximum likelihood principle, in B. N. Petrov and F. Csaki (Eds.), *Second international symposium on information theory*. Budapest: Academiai Kiado.

Akaike, Hirotugu, 1974. A new look at the statistical model identification. *IEEE Transactions on Automatic Control,* 19 (6), 716–723.

Amari, S., 1985. Differential-geometrical methods in statistics, *Lecture Notes in Statistics* 28. New York, Springer-Verlag.

Anderson, D.R., Burnham, K.P. and Thompson, W.L., 2000. Null hypothesis testing: problems, prevalence, and an alternative. *Journal of Wildlife Management*, 64, 912-923.

Benestad, R., D. Nychka, and L. Mearns, 2012. Specification of wet-day daily rainfall quantiles from the mean value. *Tellus A*, 64 (14981), 1-14.

Bozdogan, H., 1986. Multi-Sample Cluster Analysis as an Alternative to Multiple Comparison Procedures. *Bulletin of Informatics and Cybernetics*, 22, 1-2.

Bozdogan, H., 1987. Model selection and Akaike's Information Criterion (AIC): The general theory and its analytical extensions. *Psychometrika*, 52 (3), 345-370.

Bozdogan, H., 2000. Akaike's Information Criterion and Recent Developments in Information Complexity. *Journal of Mathematical Psychology,* 44, 62-91.

Chow, V.T., Maidment, D.R., Mays, L.W., 1988. *Applied Hydrology*. New York: McGraw-Hill.

Eagleson, P. S., 1978. Climate, soil, and vegetation: 2. The distribution of annual precipitation derived from observed storm sequences. *Water Resour. Res*., **14**(5), 713–721.

Emanuel, Kerry, Susan Solomon, Doris Folini, Sean Davis, Chiara Cagnazzo (2013). Influence of Tropical Tropopause Layer Cooling on Atlantic Hurricane Activity. *J. Climate*, **26**, 2288–2301.

Emori, S., and S.J. Brown, 2005. Dynamic and thermodynamic changes in mean and extreme precipitation under changed climate. *Geophys. Res. Lett*., **32**, L17706.

Forsythe, J. M., J.B. Dodson, P.T. Partain, S.Q. Kidder, T.H. Vonder Haar, 2012. How Total Precipitable Water Vapor Anomalies Relate to Cloud Vertical Structure. *J. Hydrometeor*, 13, 709–721.

Gao, Y., J.S. Fu, J.B. Drake, Y. Liu, J-F Lamarque, 2012**.** Projected changes of extreme weather events in the eastern United States based on a high resolution climate modeling system**.** *Environ. Res. Lett.*, 7 (4), 044025.

Garavaglia, F., M. Lang, E. Paquet, J. Gailhard, R. Garçon, and B. Renard, 2011. Reliability and robustness of rainfall compound distribution model based on weather pattern sub-sampling. *Hydrol. Earth Syst. Sci.*, 15 (2), 519–532.

Gustafsson, M., D. Rayner, and D. Chen, 2010. Extreme rainfall events in southern Sweden: Where does the moisture come from? *Tellus A*, 62, 605–616.

Hellström, C. and Malmgren, B., 2004. Spatial analysis of extreme precipitation in Sweden 1961–2000. *Ambio.* 33, 187–192.

Hellström, C., 2005. Atmospheric conditions during extreme and non-extreme precipitation events in Sweden. *Int. J. Climatol.* 25, 631–648.

Hernebring, C., 2006. 10-års regnets återkomst förr och nu (Design storms in Sweden then and now). *VAforsk publ. Nr. 2006-04*, Svenskt Vatten, Stockholm (in Swedish).

Kao, S.-C. and A.R. Ganguly, 2011. Intensity, duration, and frequency of precipitation extremes under 21st-century warming scenarios. *Journal of Geophysical Research - Atmospheres*, 116, D16119.

Kullback, S., and Leibler, R., 1951. On information and sufficiency, *Annals of Mathematical Statistics*. 22, 79-86.

Lamb, H.H., 1950. Types and spells of weather around the year in the British Isles. *Q. J. R. Meteorol. Soc*. 76, 393–438.

Lavers , D., C. Prudhomme and D.M. Hannah, 2013. European precipitation connections with large-scale mean sea-level pressure (MSLP) fields. *Hydrol. Sci. J.*, 58 (2), 310-327.

Livezey, Robert E., Konstantin Y. Vinnikov, Marina M. Timofeyeva, Richard Tinker, Huug M. van den Dool, 2007: Estimation and Extrapolation of Climate Normals and Climatic Trends. *Journal of Applied Meteorology and Climatology* 46, 1759–1776.

McKee, T. B., N. J. Doesken, and J. Kleist, 1993. The relationship of drought frequency and duration to time scales. *In: Preprints, Eighth Conf. on Applied Climatology, Anaheim, CA, American Meteorological Society*, 179–184.

Mannshardt-Shamseldin, Elizabeth C., Smith, Richard L., Sain, Stephan R., Mearns, Linda O., Cooley, Daniel, 2010. Downscaling extremes: A comparison of extreme value distributions in point-source and gridded precipitation data. *The Annals of Applied Statistics,* 4 (1), 484--502.

May, P.T., C.N. Long, A. Protat, 2012. The Diurnal Cycle of the Boundary Layer, Convection, Clouds, and Surface Radiation in a Coastal Monsoon Environment (Darwin, Australia). *J. Climate*, 25, 5309–5326.

Min, S.-K., X. Zhang, F. W. Zwiers, and G. C. Hegerl, 2011. Human contribution to more-intense precipitation extremes. *Nature*, 470, 378–381.

Moss, R., *et al.*, 2008. *Towards New Scenarios for Analysis of Emissions, Climate Change, Impacts, and Response Strategies*. Intergovernmental Panel on Climate Change, Geneva.

Olsson, J., U. Willén, 2010. Downscaling extreme RCA3-precipitation for urban hydrological applications. *Mistra-SWECIA Working Paper No 3*.

Papalexiou, S. M., Koutsoyiannis, D., and Makropoulos, C., 2013. How extreme is extreme? An assessment of daily rainfall distribution tails. *Hydrol. Earth Syst. Sci*., 17, 851-862.

Perica, S., E. Foufoula-Georgiou, 1996. Model for multiscale disaggregation of spatial rainfall based on coupling meteorological and scaling descriptions. *J. Geophys. Res.*, 101D21, 26, 347–26, 361.

Pielke, R.A., M.W. Downton, 2000. Precipitation and Damaging Floods: Trends in the United States, 1932–97. *J. Climate*, 13, 3625–3637.

Richardson, C. W., 1981. Stochastic simulation of daily precipitation, temperature, and solar radiation, *Water Resour. Res.*, 17 (1), 182–190.

Schwarz, G.,1978. Estimating the dimension of a model, *Annals of Statistics*, **6**, 461-464.

Shindell, D.T., A. Voulgarakis, G. Faluvegi, and G. Milly, 2012. Precipitation response to regional radiative forcing. *Atmos. Chem. Phys.*, 12, 6969-6982.

Swedish Meteorological and Hydrological Institute Point Gauge Precipitation observations, 1961-1982.

Thompson, R., and Green, D., 2004. Mediterranean precipitation and its relationship with sea level pressure patterns. *Annals Of Geophysics*, 47 (5), 1617-1633.

Uppala, S.M., *et al.*, 2005. The ERA-40 re-analysis. *Quart. J. R. Meteorol. Soc.*, 131, 2961-3012.

Wilbanks, T.J. and Fernandez S.J., 2012. Climate Change and Infrastructure, Urban Systems, and Vulnerabilities. *Technical Report for the U.S. Department of Energy in Support of the National Climate Assessment*, February 29.

Yang, H. and Bozdogan, H., 2011. Model Selection with Information Complexity in Multiple Linear Regression Modeling. *Multiple Linear Regression Viewpoints, 2011*, 37 (2), 1-13.

Zveryaev, I. I., and R. P. Allan, 2010. Summertime precipitation variability over Europe and its links to atmospheric dynamics and evaporation. *Journal of Geophysical Research*, 115, D12102.

Appendix 5A. Tables of Independent Variables and Precipitation Amounts

Table 5A.1 Independent Atmospheric Variables and Units

Vector	Variable Name	Abbreviation	Units
X1	Convective Precipitation	cp	mm
X2	Evaporation	evp	mm
X3	High Cloud Cover	hcc	fraction
X4	Large Scale Precipitation	lsp	mm
X5	Mean Sea Level Pressure	mslp	Pa/10000
X6	Surface Thermal Radiation	str	W mm^{-2} s^{-1}
X7	Total Cloud Cover	tcc	fraction
X8	Total Column Water Vapour	tcv	kg mm^{-2}
X9	Total Column Water	ttw	kg mm^{-2}
X10	Top Thermal Radiation	ttr	W mm^{-2} s^{-1}

Table 5A.2 Number of Total Wet Days 1961-1982 and Range of 99th Percentile Precipitation Amounts

Location	Number of Wet Days	Range of 99th Percentile Amounts	Number of Events over 40mm
Helsingborg	3517	17.2 – 58.5 mm	5
Malmo	3728	16.6 – 64.8 mm	7
Stockholm	3793	17.4 – 59.8 mm	3
Uppsala	3709	16.8 – 44.1 mm	2
Vaxjo	4135	16.7 – 54.9 mm	2
Baton Rouge	1863	57.4 – 304.5mm	All in 99th percentile
Canton	1244	55.9 – 185.4mm	All in 99th percentile

Appendix 5B. Information Complexity Criteria for Determination of Probability Density of 99th Percentile Precipitation Events

Table 5B.1 Helsingborg (asterisks denote lowest criterion score)

PDF	AIC	CAIC	SBC	ICOMP_misspec
Normal	445.9199	452.684	450.684	446.4426
Lognormal	387.5288	394.2929	392.2929	387.0671
Exponential	237.8061*	241.1881*	240.1881*	238.1743*
Gamma	408.2506	415.0147	413.0147	408.1538
Weibull	438.0713	444.8353	442.8353	438.5043
Uniform	467.6009	474.3649	472.3649	468.8605
GEV	377.307	387.4536	384.4536	375.0406
GP	426.4604	433.2244	431.2244	427.1782
LogPears3	435.9961	442.7601	440.7601	436.3534

Table 5B.2 Malmo

PDF	AIC	CAIC	SBC	ICOMP_misspec
Normal	489.2355	495.9996	493.9996	489.5125
Lognormal	419.5797	426.3438	424.3438	418.0946
Exponential	292.1813*	295.5633*	294.5633*	290.7802*
Gamma	469.3002	450.6196	448.6196	443.0245
Weibull	469.3002	476.0642	474.0642	469.141
Uniform	506.6451	513.4091	511.4091	507.743
GEV	509.1115	519.2575	516.2575	507.274
GP	451.5604	458.3245	456.3245	451.6793
LogPears3	477.6274	484.3915	482.3915	477.6312

Table 5B.3 Stockholm

PDF	AIC	CAIC	SBC	ICOMP_misspec
Normal	430.8147	437.5787	435.5787	431.8145
Lognormal	384.1018	390.8659	388.8659	384.4779
Exponential	252.3234*	255.7054*	254.7054*	253.3339*
Gamma	400.4427	407.2068	405.2068	401.0626
Weibull	427.9892	434.7533	432.7533	429.0052
Uniform	452.7543	459.5183	457.5183	454.4044
GEV	275.7936	285.9397	282.9397	271.5917
GP	410.9467	417.7108	415.7108	412.2057
LogPears3	422.6599	429.4239	427.4239	423.5559

Table 5B.4 Uppsala

PDF	AIC	CAIC	SBC	ICOMP_misspec
Normal	386.1272	392.8912	390.8912	384.9349
Lognormal	324.4522	331.2163	329.2163	322.2391
Exponential	179.0663*	182.4484*	181.4484*	178.6825*
Gamma	345.7314	352.4954	350.4954	343.8216
Weibull	388.0524	394.8165	392.8165	386.8424
Uniform	402.8738	409.6379	407.6379	402.4455
GEV	417.8574	428.0035	425.0035	415.4318
GP	385.0455	391.8096	389.8096	384.3477
LogPears3	374.9635	381.7276	379.7276	373.5674

Table 5B.5 Vaxjo

PDF	AIC	CAIC	SBC	ICOMP_misspec
Normal	422.7214	429.4854	427.4854	423.0772
Lognormal	370.9961	377.7601	375.7601	370.4929
Exponential	215.2236*	218.6057*	217.6057*	214.6833*
Gamma	389.1184	395.8825	393.8825	388.954
Weibull	419.4484	426.2124	424.2124	419.8068
Uniform	443.3231	450.0871	448.0871	444.4282
GEV	356.2384	366.3845	363.3845	353.0281
GP	401.1203	407.8844	405.8844	401.7928
LogPears3	413.6096	420.3736	418.3736	413.8234

Table 5B.6 Baton Rouge, LA

PDF	AIC	CAIC	SBC	ICOMP misspec
Normal	699.1469	705.8858	703.8858	704.4221
Lognormal	647.5532	654.2921	652.2921	652.2983
Exponential	585.0011*	588.3705*	587.3705*	591.0315*
Gamma	665.7681	672.507	670.507	670.7417
Weibull	681.6376	688.3765	686.3765	686.8257
Uniform	717.5719	724.3108	722.3108	723.3249
GEV	596.623	606.7313	603.7313	594.6193
GP	659.0842	665.8231	663.8231	664.2943
LogPears3	692.8222	699.5611	697.5611	698.0398

Table 5B.7 Canton, MS

PDF	AIC	CAIC	SBC	ICOMP misspec
Normal	592.1043	598.8432	596.8432	595.2659
Lognormal	537.8143	544.5532	542.5532	540.3587
Exponential	390.4411*	393.8105*	392.8105*	393.562*
Gamma	557.2317	563.9706	561.9706	560.0235
Weibull	589.8812	596.6201	594.6201	593.0739
Uniform	614.8341	621.573	619.573	618.668
GEV	470.4601	480.5685	477.5685	468.2059
GP	571.3512	578.0901	576.0901	574.8612
LogPears3	585.2338	591.9727	589.9727	588.32

Appendix 5C. Q-Q Plots for Distribution of Heavy Rainfall Events

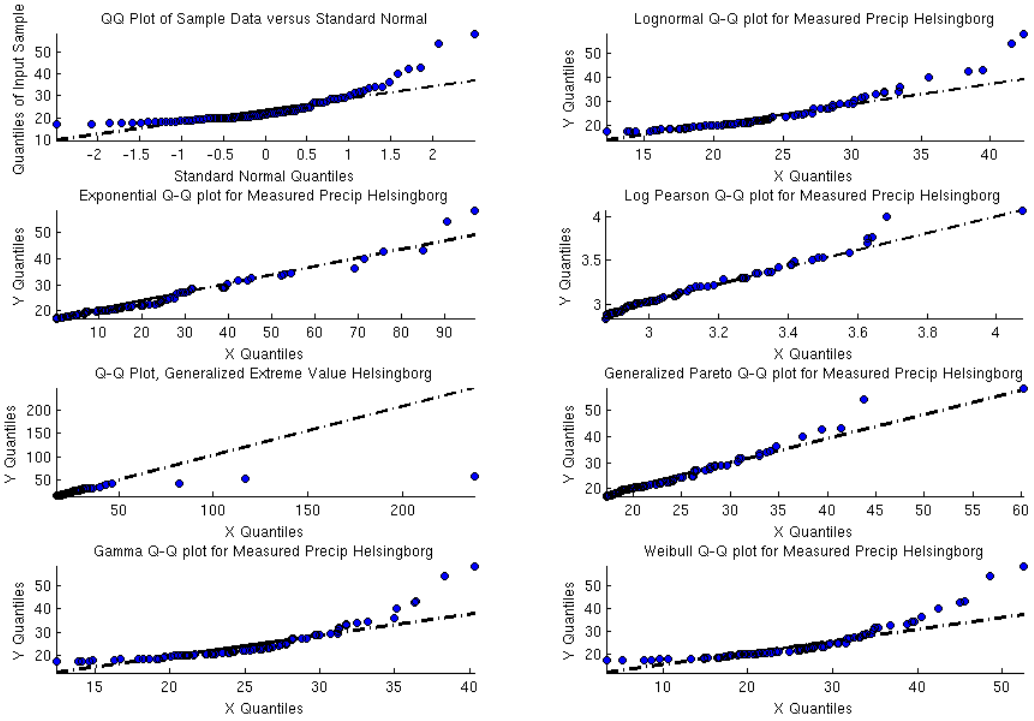

Figure C-1. Q-Q plots for Helsingborg, Sweden. The data most closely follow an exponential distribution.

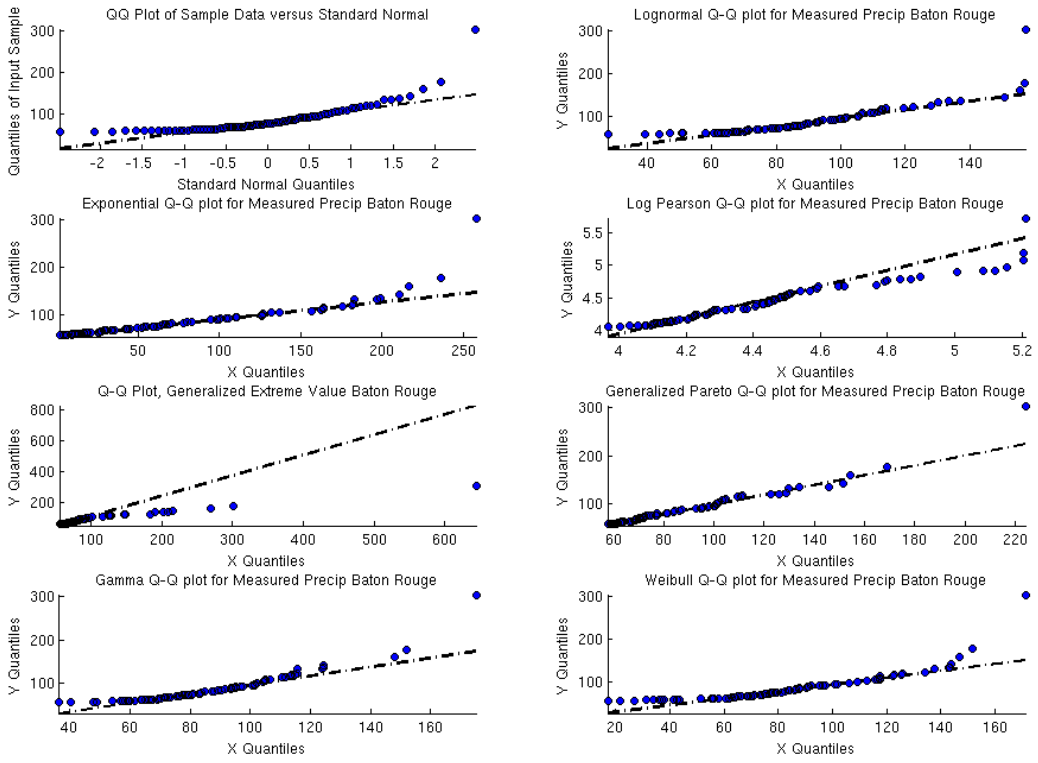

Figure C-2. Q-Q plots for Baton Rouge, Louisiana. The data most closely follow an exponential distribution.

Appendix 5D. Scores for Each Exponential Regression Model

Vars Selected	AIC	ICOMP	CAIC	SBC	R^2
Helsingborg					
0 7	**7.7634**	**3.1133**	**35.7035**	**34.0686**	**0.1109****
(0 = constant; 7 = Total Cloud Cover Fraction)					
Malmo					
0 8	**36.2182**	**35.6072**	**69.7810**	**68.4047**	**0.1486*****
(0 = constant; 8 = Total Column Water Vapour)					
Stockholm					
0 1 3	**-9.6560**	**-16.2580**	**27.3300**	**25.5686**	**0.1130****
(0 = constant; 1 = Convective Precipitation; 3 = High Cloud Cover Fraction)					
Uppsala					
0 1	**-1.1686**	**-5.9239**	**28.6059**	**27.4048**	**0.0195****
(0 = constant; 1 = Convective Precipitation)					
Vaxjo					
0 4 8	**-5.30879**	**-5.29883**	**42.6832**	**40.7667**	**0.124***
(0 = constant; 4 = Large Scale Precipitation, 8 = Total Column Water Vapour)					
Southern Sweden					
0 1 8	**40.9206**	**40.9995**	**95.4418**	**93.7174**	**0.06922*****
(0 = constant; 1 = Convective Precipitation; 8 = Total Column Water Vapour)					
Baton Rouge					
0 8 9	**45.9344**	**79.698**	**37.0877**	**34.9223**	**0.00078***
(0 = constant; 8 = Total Column Water Vapour; 9 = Total Column Liquid Water)					
Canton					
0 8 9	**1.08938**	**36.1851**	**-5.44225**	**-7.43747**	**0.0169***
(0 = constant; 8 = Total Column Water Vapour; 9 = Total Column Liquid Water)					

*Asterisks indicate the number of model scores minus one that were minimized for the given model; e.g., three asterisks indicate that all four scoring systems were minimized for the model. In the case of Vaxjo, Baton Rouge and Canton, there were several models that were minimized by only two scoring systems. In these cases, the lowest scores for the other two criteria determined the best model.

Chapter 6

Electricity Demand Evolution Driven by Storm Motivated Population Movement

Melissa R. Allen[1,2], Steven J. Fernandez[2,1], Joshua S. Fu[1,2]

[1]University of Tennessee, Knoxville

[2]Oak Ridge National Laboratory

Abstract

Managing the risks to reliable delivery of energy to vulnerable populations posed by local effects of climate change on energy production and delivery is a challenge for communities worldwide. Climate effects such as sea level rise and increased frequency and intensity of natural disasters can force populations to move locations. These moves result in changing geographic patterns of demand for infrastructure services. Thus, infrastructures will evolve to accommodate new load centers while some parts of the network are underused, and these changes will create emerging vulnerabilities. Forecasting the location of these vulnerabilities by combining climate predictions and agent based population movement models shows promise for defining these future population distributions and changes in coastal infrastructure configurations. In this work, we created a prototype agent based population distribution model and developed a methodology to establish utility functions that provide insight about new infrastructure vulnerabilities that might result from these new electric power topologies. Combining climate and weather data, engineering algorithms and social theory, we use the new Department of Energy (DOE) Connected Infrastructure Dynamics Models (CIDM) to examine electricity demand response to increased temperatures, population migration in response to extreme cyclonic events, consequent net population changes and new regional patterns in electricity demand. This work suggests that

the importance of established evacuation routes that move large populations repeatedly through convergence points as an indicator may be under recognized.

6.1 Introduction

New demands for increased energy and power in new and different locations will challenge the power grid as it evolves over the next decades. Climate change and resulting extreme weather events will affect these challenges as electricity demand will rise with temperature rise (Hadley et al., 2006) and population will move in response to extreme weather events to locations less vulnerable to environmental hazards (Perch-Nielsen et al., 2008; McLeman, 2013; Shumway et al., 2014)

Migration has been defined as "the residential relocation of an individual, family or group from one place to another" (Nel, 2010). Migration in response to extreme weather events occurs in part as a result of individual decisions to relocate to less vulnerable regions (Maslow, 1954; Graves, 1976) and in part as a result of businesses closing and rebuilding elsewhere after natural disaster (Lam et al, 2009). Although these decisions can significantly affect regional electricity demand, the implications of these shifts are little studied because the character of the influence of natural disaster on migration flow remains uncertain. Modeling of migration flow and the changes these flows create in the power grid topology require integration of disparate fields and theories and only recently have data from these fields at the required scale become available. Permann (2007) and Amal (2011) surveyed past attempts to connect people movement, power topology changes and their combined effect on the robustness and resilience of the resulting

power grid. To provide a testbed for the interaction and interdependencies of these forces, Oak Ridge National Laboratory (ORNL) developed a suite of tools including Visualizing Energy Resources Dynamically on Earth (VERDE) (http://web.ornl.gov/sci/electricdelivery/research_verde.shtml), Energy Awareness and Resiliency Standardized Services (EARSS) (http://cda.ornl.gov/publications_2013/Publication%2040621.pdf), Homeland security Extreme weather Awareness Tool (HEAT) (Fernandez et al., 2013) and Connected Infrastructure Dynamics Models (CIDM) (Allen et al., 2013).

This suite provides a common spatial scale for climate-infrastructure-population migration modeling by coupling high-resolution climate models with the neighborhood-scale infrastructure modules. Integration of the models provides a framework for placing existing high-resolution climate modeling output (Allen et al., 2013), ORNL infrastructure model data and population movements in a common reference grid so these domains can operate on the same spatial and temporal scales.

6.2. Methodology

6.2.1 Projections of Changing Electricity Demand

The US Energy Information Administration (EIA) makes historical electricity demand tables available by state for each year (http://www.eia.gov/electricity/data.cfm). Comparison of the demand over several decades shows the effects of various economic and demographic characteristics of a population such as changes in household size, increases in personal electronic

devices, changes in efficiency of heating, cooling and appliance technology, and the effect of energy prices on demand. There are large demand differences evident between years, however, which could represent outmigration from environmental or economic disaster areas and significant increases in population in other locations. Characterizing these changes over time is important for accurate prediction of changes in production and transmission necessary for the adaptation of the electrical grid to the changing climate.

Electric power demand is projected by the EIA by state for future years. For the projections, changes in power demand are calculated using broadly-defined determinants of energy consumption for the commercial and residential sectors. While economic and demographic effects of consumption are considered in each of these sectors, changes in these effects due to migration, and especially large migration due to cataclysmic events, is not included. We examine the additional effects of migration on electricity demand using LandScan population data at 1km resolution aggregated to the county level, along with by-county annual changes in migration as reported by the US Census.

6.2.2 Calculation of Electrical Customer Demand

As population relocates and businesses rebuild in new locations, electricity demand shifts. To calculate the electrical customer demand it is necessary first to convert the population count into electricity customer count using a conversion factor that varies geographically. This Bailey Young (Young et al., 2009) correction factor is derived for a given county as the population for a

given decennial year (in this case, 2000) divided by the sum of the households and the firms in the county.

6.2.3 Datasets and Approach

We use population migration and growth projections to estimate energy demand resident within CIDM developed as part of the LandScan population suite. Natural population fluxes such as births and deaths and new businesses moving into an area change the customer electricity demand in a somewhat predictable way, but the most startling and less predictable changes occur after a disaster of some kind for which the effects can last for at least a decade (Blanchard and Katz, 1992; Wilbanks and Fernandez, 2012). These migration models are agent based models allowing agents to move from cell to cell based on balance between attractors and repelling forces upon which the climate drivers act. The modeling framework allows stochastic examination of different migration theories and assumptions about adaptation options. We derived relationships between historical population data and energy demand data at the same spatial resolution as climate data and extrapolate to relative change in energy demand as future populations migrate. This relationship consequently estimates future energy demand levels and their spatial distribution.

To develop the utility functions upon which the agents in the models act we examine existing data from a variety of sources and derive a relationship based upon multiple linear regression scored by information complexity criteria. Selection of the data is based upon the decision-making metrics given in recognized social theory. Decisions by households as to whether to

remain in the same location or to relocate tend to be economically and culturally motivated (Maslow, 1954). It is reasonable, then, to assume that individuals' economic, social and cultural characteristics influence their mobility. To some extent, both early and later gravity models captured this idea as communities' "attractiveness" based on factors such as low unemployment and per capita wages (Lowry, 1964; Rogers, 1967) earning potential and social interaction opportunities among individuals of the same race (McHugh, 1988; Raphael and Riker, 1999). Our approach uses an expanded set of these same variables, but is evaluated in such a way as to to take into account the decision making of composite individuals.

Raphael and Riker (1999) show, however, that there are demographic types who perceive themselves to be mobile in the face of unexpected displacement from work whom we might expect to seek a livelihood elsewhere. These individuals include more men than women, more Caucasian than other races, more military households (Li et al., 2005) than civilian, and households with fewer than average occupants.

We took as our model a linear equation to examine the tendencies of individuals to stay or move to a chosen destination based upon their own demographic characteristics.

The basic equation is of the form:

$$\boldsymbol{Y = X\beta + \varepsilon}$$

and is generated via least squares regression analysis and evaluated by four Information Complexity Criteria (Bozdogan, 2000). The difference between the evaluation of this equation and those used for traditional single-equation regression migration models is the preprocessing stage. We do not use **Y** as a vector of values associated with a subset of all possible destinations but as a vector that represents agents associated with a single destination—namely a vector of ones and zeroes that represent the percentage of the population that moved from the origin to the specific destination (Fernandez et al., 2010). The length of the vector is determined by the amount of computing available for the regression process. We have arbitrarily chosen that number to be 1000.

Likewise, the **X** vectors are each random distributions of ones and zeroes representing the demographic attributes of the parish of origin. These demographic attributes are listed in Table 7.1. As agents were developed from these attributes, care was taken to represent mutually exclusive data as such during the stochastic process—that is, because citizens reporting race identified as either black or white alone, then the stochastically assigned ones for blacks did not overlap those for whites. Citizens reporting mixed race are counted implicitly as "other" by their absence. The decision to include only two racial choices was made to limit the number of independent variables and because blacks and whites make up at least 95% of the population in 2005 in most parishes. Studies (Groen and Polivka, 2010) have indicated an increase, however, in Hispanic residents from 3.2% in 2005 to 6.6% in 2007 driven by migration into the affected areas.) Likewise, as reported by the Bureau of Labor employed civilian population counts, individuals work in only one sector of the economy, so there is no overlap of career. Thus the

employment categories were partitioned among the thousand agents and stochastically assigned each within its own partition. Data were compiled from several sources: US Census (population, gender, married households, education, race, and veterans), Internal Revenue Service (IRS) (to and from migration), Louisiana State Government (employed civilian population), and Louisiana Department of Revenue (poverty rates). Since migration rates were taken from IRS tax records, we chose to focus on the working population and therefore did not consider age (such as retirees) among our explanatory variables.

Table 6.1. Demographics of Origin Populations

Model Ref	Type	%Jeff	%Orlea	%Plaqu	%St B	%St C	% St T
1	Gender female	52%	53%	49.9%	51.5%	51%	51.1%
2	Married	34%	34%	58%	54%	65%	65%
3	College Education	18%	18%	18%	18%	18%	18%
4	Below Poverty Level	13.7%	27.9%	18%	13.1%	11.4%	9.7%
5	White	70%	28.9%	71%	88.1%	72.2%	86.8%
6	Black	25%	67.6%	22.8%	9.0%	25.9%	10.6%
7	Ag/forest/fish Career	1.9%	1%	12.2%	1.9%	1.6%	2.6%
8	Construction Career	7.7%	4.9%	7.2%	9.2%	9.9%	9.1%
9	Manufacturing Career	8.3%	5.2%	9.0%	10.8%	17.9%	7.8%
10	Retail/Trade Career	4.7%	9.8%	3.7%	12.4%	10.5%	13.0%
11	Transportation/Utilities	5.9%	5.9%	10.6%	7%	8.1%	4.9%
12	Finance Career	6.9%	2.4%	4.1%	6.8%	4.9%	6.9%
13	Professional/Scientific	10.2%	9.9%	8.1%	8.1%	7.3%	10.1%
14	Education Career	19.4%	25.7%	15.1%	17%	18.1%	20.2%
15	Artistic Career	10.2%	15.3%	8.2%	9.7%	6.5%	8.5%
16	Military Veteran	9.0%	8.0%	7.9%	9.5%	8.3%	10.6%

6.3. Results

6.3.1 Regional Demand Map After Hurricane-Induced Redistribution

In order to demonstrate how this methodology might work, we examined county-by-county changes in electricity demand for the years surrounding the hurricane season of 2005. We

downscaled the state by state electricity sales data for the years 2004-2006 provided by the Energy Information Administration (EIA) using LandScan population counts for 2004 aggregated to the county level and converted to customer counts using the Bailey Young conversion factors (Section 2.2). To obtain population counts for subsequent years, by-county proportional changes in population as recorded by the US Census were used to convert population counts from 2004 to those in subsequent years. Figures 6.1-6.4 show the results as energy use in million kilowatt-hours by county in nine southeastern states.

A comparison of Figures 6.1 and 6.2 indicated little change in electricity demand occurred between 2004 and 2005 because only marginal population shifts occurred (-7% to 20% per county). Much larger differences appear between 2005 and 2006 as Figure 6.4 illustrates changes in population ranged between -76% and 13%. Most notable in the plots is the reduction in demand in south Florida; Plaquemines, Jefferson, St. Bernard (-76%) and Orleans due to migration in response to Hurricane Wilma Parishes in Louisiana in response to Hurricane Katrina; and in Cameron Parish Louisiana and several southeastern Texas counties in response to Hurricane Rita. Significant increases in demand as a result of Hurricane Katrina are evidenced in the largely populated areas of in which even a small percent increase produces a significant increase in power usage, Harris, Bexar, Dallas, Tarrant, Collin and Denton, TX as well as Harrison County, MS and East Baton Rouge and Lafayette, LA. Increases in demand shown in Caddo, Louisiana are due to influx of Rita evacuees.

6.3.2 Power Demand Increases Correlate with Evacuation Routes

Hurricane Katrina (August 23, 2005 - August 30, 2005) made landfall along the U.S. Gulf Coast on August 29, 2005, sustaining 110-knot winds, which extended 205 miles outward from the center of the storm. Extensive flooding in the City of New Orleans, Louisiana, resulted due to storm surge from adjacent Lake Pontchartrain and several levee failures. Damage from the storm displaced more than 1,000,000 Gulf Coast residents from their homes.

Hurricane Rita (September 19, 2005 – September 25, 2005) made landfall along the Gulf Coasts of western Louisiana and eastern Texas one month later on September 24, 2005. Sustained winds were reported above 140 knots with extent 80 miles from the center of the storm. Storm surge flooding reached 15 feet in Cameron Parish. New Orleans experienced additional flooding and levee failures from Hurricane Rita, and 600,000 households in that city remained displaced (Wilbanks and Fernandez, 2012). According to the Cable News Network (CNN) and the American Red Cross in 2005, evacuees resided predominantly in 2 states during this time: 55,000 evacuees in LA and 56,000 evacuees in TX. Forced evacuations, destroyed homes, disruption of economic activity, and the ruin of community infrastructures ($145 billion in damages) in the wake of these storms led to population shifts in the Gulf Coast Region.

The population shifts resulting from the hurricanes' damage recorded in the IRS data shows that the most attractive destination for the refugees was Harris County, TX. Tables 7.2 and 7.3 show the counties that received the most migrants from parishes affected by the storms for the years

2005-2006 and 2006-2007. Table 7.4 indicates the difference between population in 2005 and population in 2007.

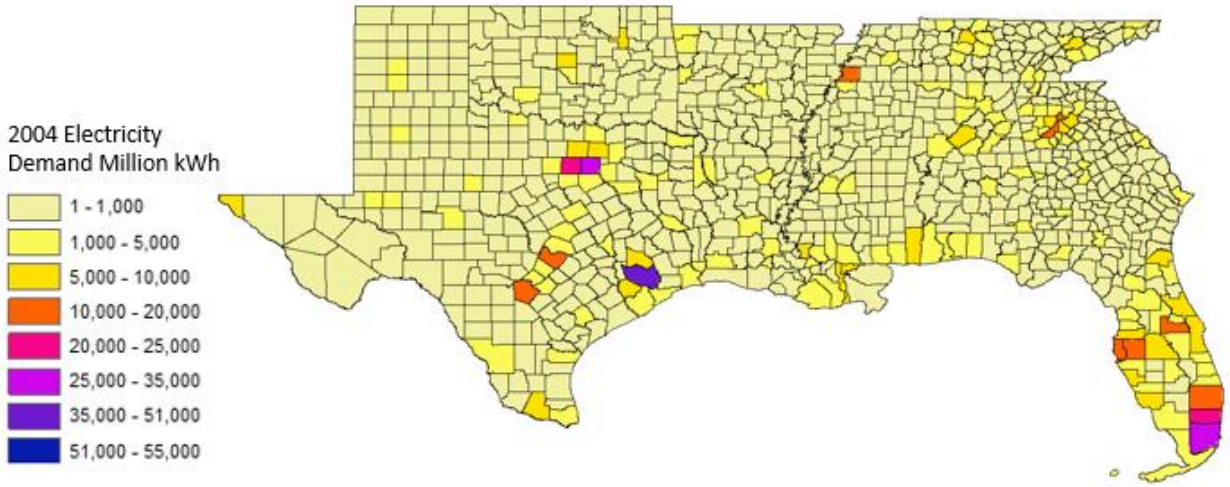

Figure 6.1 Electricity demand for southeastern states, 2004 in million kWh.

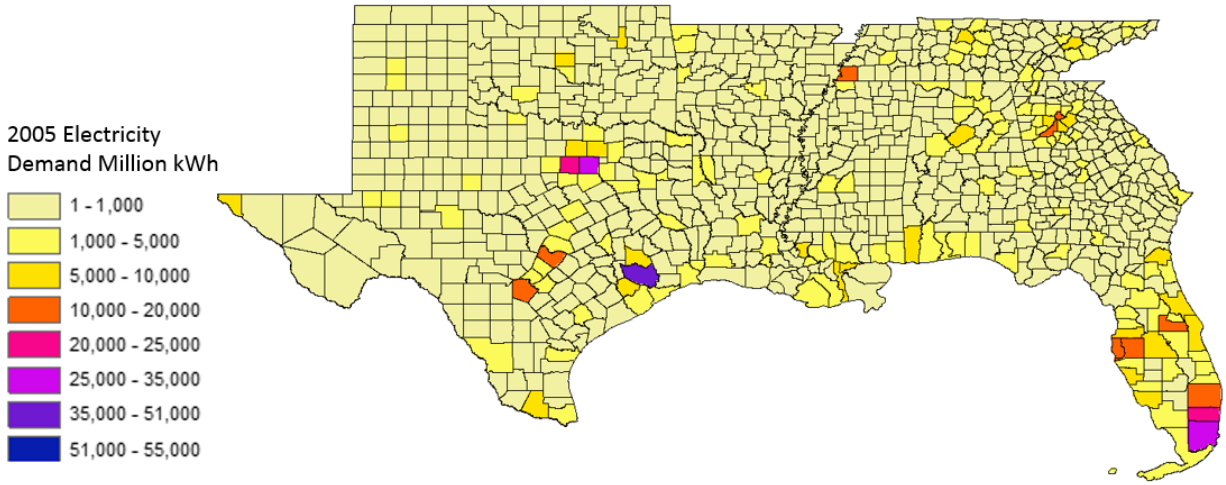

Figure 6.2. Electricity demand for southeastern states, 2005 in million kWh.

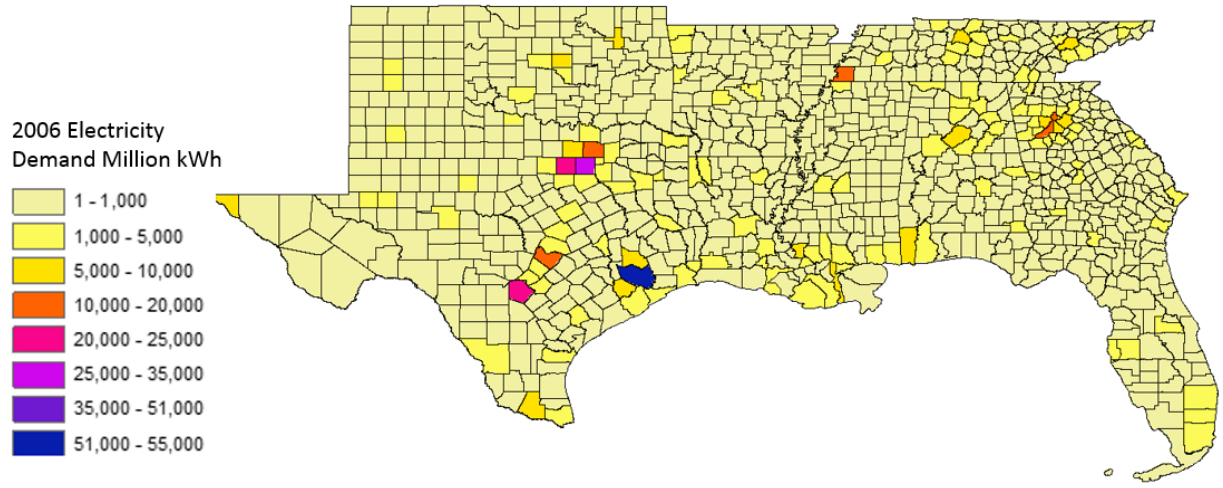

Figure 6.3. Electricity demand in southeastern states for the year 2006, shows large decreases in southeast Florida due to population losses from Hurricane Wilma. Large decreases in southeast Louisiana and southwest Mississippi are indicative of population losses due to Hurricane Katrina. Increases are shown in Harris, Bexar, Dallas and Tarrant counties in Texas, and to a lesser but significant extent in Shelby County, TN and Fulon County, GA. These were counties that provided the most refuge for Katrina evacuees.

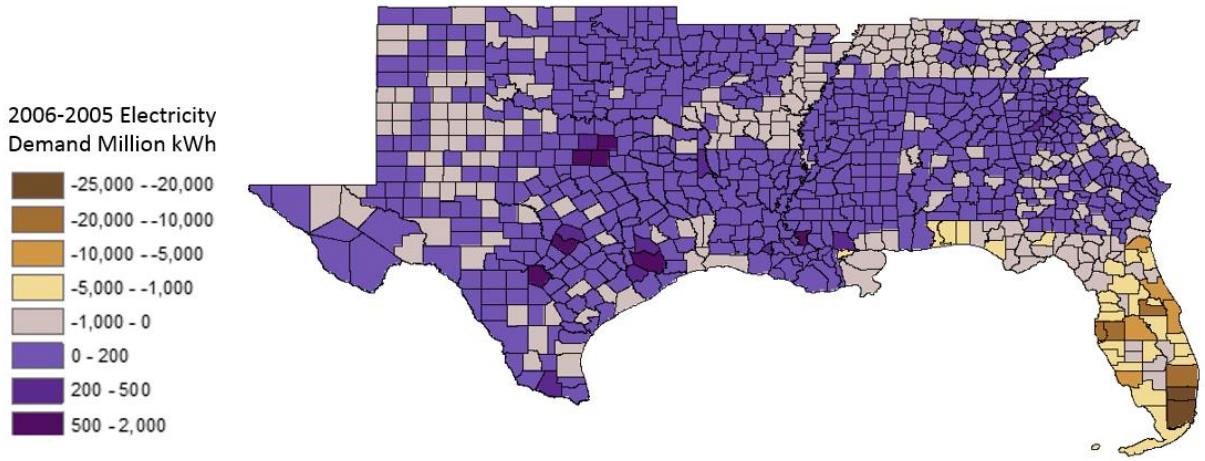

Figure 6.4. Differences in demand in the southeast from 2005 to 2006 reveal gains and losses in population due to hurricane events.

The tables illustrate that between the years of 2005 and 2006, population moved out of Katrina- and Rita-impacted areas and predominantly into three Texas counties. East Baton Rouge, Jefferson, St. Tammany and Tangipahoa Parishes, however, were the most popular in-state destinations. Between the years of 2006 and 2007, as counties recover, population begins to move back to pre-hurricane locations. By 2007, numbers of in-migrants are nearing pre-Katrina/Rita values. Orleans and St. Bernard parishes show increases in numbers of in-migrants from 2005 to 2007 indicating recovery of the parishes.

Table 6.2. Between the years of 2005 and 2006, population moved out of Katrina-devastated areas and predominantly into three Texas counties. East Baton Rouge, Jefferson, St. Tammany and Tangipahoa Parishes were the most popular in-state destinations.

Rank	To State (FIPS)	To County (FIPS)	County Name	Migrants
1	22	51	Jefferson,LA	11820
2	22	71	Orleans, LA	7707
3	22	103	St. Tammany, LA	5751
4	28	47	Harrison, MS	2780
5	28	59	Jackson, MS	2225
6	22	95	St. John Baptist, LA	1816
7	48	201	Harris, TX	1809
8	22	89	St. Charles, LA	1732
9	22	87	St. Bernard, LA	1611
10	22	33	E Baton Rouge, LA	1509
11	28	45	Hancock, MS	1351
12	22	105	Tangipahoa, LA	1280
13	28	109	Pearl River, MS	1240
14	22	75	Plaquemines, LA	983
15	1	97	Mobile, AL	824
16	6	73	San Diego, CA	586
17	48	113	Dallas, TX	555
18	22	117	Washington, LA	553
19	48	439	Tarrant, TX	464
20	22	55	Lafayette, LA	451

2004-2005

Rank	To State (FIPS)	To County (FIPS)	County Name	Migrants
1	48	201	Harris, TX	37933
2	22	51	Jefferson, LA	26113
3	22	33	E Baton Rouge, LA	14148
4	22	103	St. Tammany, LA	13484
5	48	113	Dallas, TX	10143
6	48	439	Tarrant, TX	5683
7	22	105	Tangipahoa, LA	4630
8	22	71	Orleans, LA	4549
9	48	29	Bexar, TX	3642
10	28	59	Jackson, MS	3413
11	28	109	Pearl River, MS	3387
12	22	95	St. John Baptist, LA	3328
13	22	55	Lafayette, LA	3255
14	47	157	Shelby, TN	3085
15	22	89	St. Charles, LA	2997
16	13	89	DeKalb, GA	2966
17	28	47	Harrison, MS	2922
18	13	121	Fulton, GA	2922
19	22	5	Ascension, LA	2693
20	13	67	Cobb, GA	2684

2005-2006

Table 6.3. Between the years of 2006 and 2007, as counties recover, population begins to move back to pre-Katrina parishes.

Rank	To State (FIPS)	To County (FIPS)	County Name	Migrants
1	48	201	Harris, TX	37933
2	22	51	Jefferson, LA	26113
3	22	33	E Baton Rouge, LA	14148
4	22	103	St. Tammany, LA	13484
5	48	113	Dallas, TX	10143
6	48	439	Tarrant, TX	5683
7	22	105	Tangipahoa, LA	4630
8	22	71	Orleans, LA	4549
9	48	29	Bexar, TX	3642
10	28	59	Jackson, MS	3413
11	28	109	Pearl River, MS	3387
12	22	95	St. John Baptist, LA	3328
13	22	55	Lafayette, LA	3255
14	47	157	Shelby, TN	3085
15	22	89	St. Charles, LA	2997
16	13	89	DeKalb, GA	2966
17	28	47	Harrison, MS	2922
18	13	121	Fulton, GA	2922
19	22	5	Ascension, LA	2693
20	13	67	Cobb, GA	2684

2005-2006

Rank	To State (FIPS)	To County (FIPS)	County Name	Migrants
1	22	51	Jefferson, LA	8653
2	22	71	Orleans, LA	7991
3	48	201	Harris, TX	4508
4	22	103	St. Tammany, LA	3787
5	22	33	E. Baton Rouge, LA	2796
6	22	87	St. Bernard, LA	2395
7	28	47	Harrison, MS	2097
8	28	59	Jackson, MS	1946
9	22	105	Tangipahoa, LA	1889
10	22	89	St. Charles, LA	1634
11	22	95	St. John the Bap, LA	1588
12	28	109	Pearl River, MS	1249
13	48	113	Dallas, TX	1224
14	22	5	Ascension, LA	1055
15	1	97	Mobile, AL	1041
16	48	439	Tarrant, TX	868
17	22	63	Livingston, LA	801
18	28	45	Hancock, MS	741
19	48	157	Fort Bend, TX	720
20	22	75	Plaquemines, LA	712

2006-2007

Table 6.4. By 2007, numbers of migrants are nearing pre-Katrina values. Orleans and St. Bernard parishes show increases in numbers of in-migrants from 2005 to 2007 indicating recovery of the parishes.

Rank	To State (FIPS)	To County (FIPS)	County Name	Migrants
1	22	51	Jefferson,LA	11820
2	22	71	Orleans, LA	7707
3	22	103	St. Tammany, LA	5751
4	28	47	Harrison, MS	2780
5	28	59	Jackson, MS	2225
6	22	95	St. John Baptist, LA	1816
7	48	201	Harris, TX	1809
8	22	89	St. Charles, LA	1732
9	22	87	St. Bernard, LA	1611
10	22	33	E Baton Rouge, LA	1509
11	28	45	Hancock, MS	1351
12	22	105	Tangipahoa, LA	1280
13	28	109	Pearl River, MS	1240
14	22	75	Plaquemines, LA	983
15	1	97	Mobile, AL	824
16	6	73	San Diego, CA	586
17	48	113	Dallas, TX	555
18	22	117	Washington, LA	553
19	48	439	Tarrant, TX	464
20	22	55	Lafayette, LA	451

2004-2005

Rank	To State (FIPS)	To County (FIPS)	County Name	Migrants
1	22	51	Jefferson, LA	8653
2	22	71	Orleans, LA	7991
3	48	201	Harris, TX	4508
4	22	103	St. Tammany, LA	3787
5	22	33	E. Baton Rouge, LA	2796
6	22	87	St. Bernard, LA	2395
7	28	47	Harrison, MS	2097
8	28	59	Jackson, MS	1946
9	22	105	Tangipahoa, LA	1889
10	22	89	St. Charles, LA	1634
11	22	95	St. John the Bap, LA	1588
12	28	109	Pearl River, MS	1249
13	48	113	Dallas, TX	1224
14	22	5	Ascension, LA	1055
15	1	97	Mobile, AL	1041
16	48	439	Tarrant, TX	868
17	22	63	Livingston, LA	801
18	28	45	Hancock, MS	741
19	48	157	Fort Bend, TX	720
20	22	75	Plaquemines, LA	712

2006-2007

Influence of Evacuation Routes on Migration

The state of Louisiana has published directions for phased evacuation in the event of a hurricane, and in which contraflow routes are established to allow traffic to use all lanes available to exit the impacted area. Planning models and logistics include the determination of the fuel required for all vehicles, the designation of public transit to evacuate disabled population, and mobilization strategies for emergency response personnel and emergency medical equipment. Evacuation routes direct traffic away from potential areas of congestion and toward maximum flow. They are also routed toward emergency shelters that have been preselected based on estimates of flooding potential for at-risk geographic areas in storm scenarios (Liu and Tuttle, 2008). For the most intense evacuation procedures, busses carry those without transportation to designated shelters. Those with personal transportation drive to the nearest safe area and take cover until the storm has passed, waters recede and cleanup has completed. As the nearest hotels reach capacity, evacuees must continue along a given route to find the next nearest hotels with vacancies. Thus, nearest hotels fill up first and more distant hotels reach occupancy later.

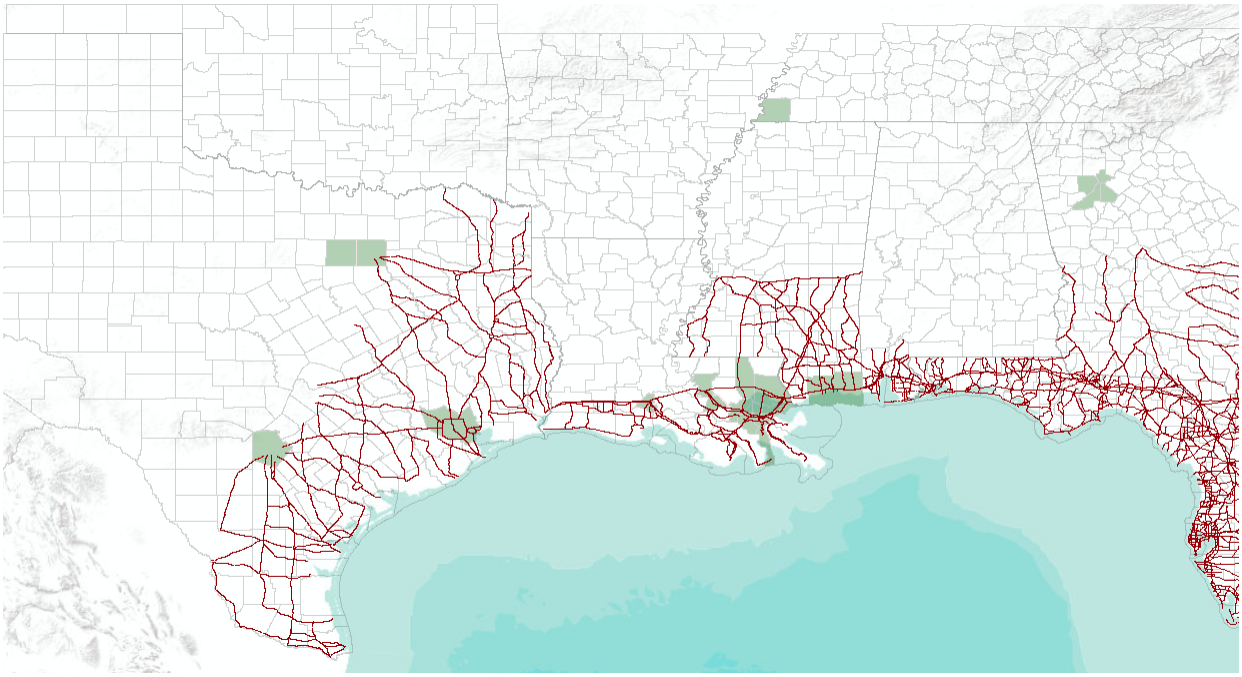

Figure 6.5. Contraflow Routes for Gulf Coast states take outflow to nearest habitable areas on the designated routes and their highway extensions. 15 of the top 20 receiving counties of Katrina refugees are located on the contraflow routes.

Implicit in Groen and Polevka (2010) about decisions of evacuees to return to affected counties after Katrina is that the alternative is to remain in the location of displacement. The IRS data show that of the top twenty locations to which Katrina refugees migrated in 2006, only five were not located on branches of the evacuation routes (see Figure 6.5). One of these counties, Tarrant County, TX is adjacent to Dallas County, TX, which is a terminus. The other four (Shelby, TN; DeKalb, Fulton and Cobb, GA) are located on the extensions of the major highways designated as contraflow routes for the initial exodus from Louisiana. Thus, perhaps the longer a population remains displaced, the more likely it is to settle in place, finding and retaining employment in the temporary location.

Influence of Demographics on Relocation Choice

Results of the multi-agent regression indicate several key findings. First, there was no one model that could be applied to every parish's population relocation choices. For each parish, county-specific demographics sets were selected to represent the characteristics of the individuals who chose to locate in the counties they did following the hurricane. Second, those who returned, those who relocated, and the counties to which they relocated were determined primarily by economics in some parishes, and in others by race, gender or educational attainment. As noted in (Lam et al., 2009) the economic sector to make the fastest recovery among the affected parishes was that of the Professional, Scientific and Technical. In many cases these companies were the largest and the most lucrative in the area, so they were the companies that could afford rapid recovery efforts. Our study supports this finding as this group had the highest tendency to return especially to the parishes of St. Tammany and St. Bernard. Those in agricultural, fishing and wildlife also tended to stay or to return quickly to their origins.

The model that best fit the Orleans Parish to Bexar County (San Antonio), TX flow included only construction and retail workers. Correspondingly, city data for Bexar County reports the number of new house construction building permits for the county in 2005 as 10, 298 buildings at an average cost of $146,700 and in 2006 as 9219 buildings at an average cost: $156,000. Numbers of similar permits in previous and subsequent years was approximately half those levels.

Individuals living below the poverty level moved mostly to the suburbs (Plyer and Ortiz, 2012). Models showed that parish citizens living below the poverty level moved from Orleans to Jefferson, Jefferson to Tangipahoa and St. Charles, and St. Charles to East Baton Rouge. For poverty-level households from Jefferson, models best describing the population flux included four demographics, the poverty demographic was associated with a slightly negative (on the order of 10^{-2}) coefficient, whereas if the poverty demographic was one of fewer than four explanatory variables, the coefficient was positive. Plyer and Ortiz (2012) show that one of the results of this migration is the change in poverty per parish from the year 1999 to the years 2008-2010 (average). In Tangipahoa, this number is statistically higher for the later period. This type of shift in parish income demographic profile has an additional effect on electricity demand (http://www.eia.gov/consumption/residential/data/2005/).

If we track population moves from a single parish outward, Plaquemines, for example, we note that black and white households moved to different places. White households moved from Plaquemines to Jefferson, St. Tammany, Tangipahoa, Lafayette and St. Mary parishes. Black households did not return to their original parishes (Groen and Polivka, 2010) but moved to Orleans (the parish with the highest black population before Hurriane Katrina) from other parishes.

Our results also suggest that women-led households moved farther from their original residences than other groups did. For example, these households moved from St. Tammany and Orleans to Dallas and to Tarrant Counties in Texas. Longer in-state moves for females were from St.

Bernard to Ascension Parish. Groen and Polevka (2010) report that in high-damage areas, evacuees with children were less likely to return than those without children.

Heads of Households with a college education (along with a Professional/Scientific/Technical career) stayed in St. Bernard Parish and moved to Parishes with large universities such as East Baton Rouge. These households also moved to Washington, St. Charles and Ascension Parishes.

Veterans favored parishes or counties with military facilities such as Jefferson (Coast Guard, US Air Force Department, Patrician military housing (Naval Base)), St. Tammany (Coast Guard, National Guard, Arm and Navy facilities), Ascension (National Guard and Louisiana National Guard), St. Mary (National Guard, Army Base, Civil Air Patrol), Terrebonne (Coast Guard and National Guard), and Fulton County in Georgia (Fort McPherson).

6.3.3 Framework for Long-term Evacuation Evaluation

In order to explore the balance of the influence of evacuation routes and of the demographics of a population on migration, we developed FLEE (Framework for Long-term Evacuation Evaluation), an agent based model that moves the evacuating population along the established routes. As each agent approaches a possible destination parish or county, it makes a "decision" as to whether to stay (relocate there) based upon its demographic components (as determined by the method described in section 2.4). The model ran for each of nine parishes of origin: five for response to Hurricane Katrina and four for response to Hurricane Rita. The four Rita parishes were those which experienced intense impacts from both Hurricane Rita in 2005 and Hurricane

Gustav in 2008. Model results obtained for the Hurricane Rita parishes were then compared to the same parishes' responses to Hurricane Gustav in 2008.

Previous research (Wilmot et al., 2006) suggests that the sequence in which evacuees approach locations with hotel or motel availability significantly affects an individual's choice of location of temporary refuge. That is, the sequence of opportunities to choose shelter site is sensitive to the direction of evacuation relative to the path of the storm. Apparent from the simulations was that the starting location determined initial evacuation destination decisions for the agents. This observation led to the simulation of agent evacuation based upon random movement along the flow routes in the direction of the contraflow mandated by state emergency procedures. Next, simulations with the full model, including weighted demographics were run. Results from these simulations are shown in Table 6.5.

Table 6.5 indicates that the FLEE model does well (0-20% error) at predicting destination parishes for long-term evacuees, but not as well for return population projections for storm-affected parishes of origin. In fact, the more intensely a parish suffered from each storm, the less accurate the model population projection was for long-term relocation to that parish. Figure 6.6 illustrates this idea showing wind swaths from both Katrina and Rita along with the percentages by which FLEE under- or over-estimated 2006 population counts (as indicated by the legend). The red shading in the hurricane swaths represents the areas which sustained 59-74 knot winds. The yellow shading indicates 40-58 knot winds, and the blue shading 39 knot winds.

Because the model employs geographically sequential decision-making for choice of destination, it tends mostly to underestimate the return of the population to the parish of origin. The model also tended to predict better the long-term destinations for Rita evacuees than it did for Katrina evacuees. Additionally, since migration patterns after Gustav for 2009 were similar to those after Rita for 2006, the model used for Rita showed good agreement with migration figures after Gustav.

Using values generated by FLEE, calculations using the Connected Infrastructure Dynamics Model (CIDM) of the values shown in Figure 6.5 matched reasonably well with the EIA actual figures, except for those in the most heavily affected areas. Differences between the FLEE model results and the EIA data are shown in Figure 6.6.

6.3.4 Robustness and Resilience

In determining a population's likelihood to stay or to leave an area affected by extreme weather events, it is useful to evaluate a community's robustness to these events and its resilience once subject to them. Infrastructure is robust to extreme climate activity if it is capable of withstanding stress. For example, a robust power plant may withstand a 100-year storm and continue to provide full service without interruption indicating a probability of reduced service equal to zero, even though the probability of the climate stressor is 1 percent (Wilbanks and Fernandez, 2012). Infrastructure is resilient if, once exposed to a stressor, it is capable of repair and renewal within a short time. Different regions have different amounts of robustness and resilience, and these differences among regions can be quantified using fragility curves.

Table 6.5. Differences between 2006 population migration results from FLEE model and US Census counts for parishes of origin and destination

Parish	Hurricane	LS+IRS Pop 2005	FracTo	ABM Pop 2006	LS+IRS Pop 2006	Difference	Pcnt Diff
Beauregard, LA	Rita	34645	0.214	9581.886381	35235	-25653.11	-72.81
Calcasieu, LA		185496	0.036	179802.5101	185311	-5508.49	-2.97
Vernon, LA		48737	0.227	56601.415	46966	9635.42	20.52
Allen, LA		25375	0.115	30503.463	25582	4921.46	19.24
Harris, TX		3711496	0.038	3715487.997	3833176	-117688.0	-3.07
Lafayette, LA		197439	0.003	197571.932	203930	-6358.07	-3.12
Jeff Davis, LA		31312	0	30623.136	31537	-913.86	-2.90
E. Baton Rouge		412029	0.004	426575.695	431397	-4821.30	-1.12
Rapides, LA		128404	0.03	129628.846	130727	-1098.15	-0.84
Orange, TX		85253	0.005	86180.48	84497	1683.48	1.99
Jefferson, TX		247585	0.001	247770.496	244309	3461.50	1.42
Cameron, LA		9635	0.002	9103.666603	7811	1292.67	16.55
Vermilion, LA		55485	0	55485	56242	-757.00	-1.35
Acadia, LA		59368	0	59461.936	60580	-1118.06	-1.85
Jefferson, LA	Katrina	452553	0.704	342406.359	432799	-90392.64	-20.89
Orleans, LA		455286	0.05	466113.455	224927	241186.46	107.23
St Tammany		220024	0.007	22130.15	230825	-208694.9	-90.41
Dallas, TX		2312519	0	2312739.024	2349871	-37131.98	-1.58
St Charles, LA		50744	0.02	59795.06	52959	6836.06	12.91
St John, LA		46340	0.013	52223.189	48737	3486.19	7.15
Tarrant, TX		1623670	0.001	1624180.547	1675427	-51246.45	-3.06
Tangipahoa, LA		106550	0.038	163151.238	113561	49590.24	43.67
Evangeline, LA		35726	0	35726	36178	-452.00	-1.25
St. Landry, LA		90129	0.005	90285.56	92027	-1741.44	-1.89
Bexar, TX		1519552	0	1519552	1558634	-39082.00	-2.51
Fulton, GA		840041	0	840041	863210	-23169.00	-2.68
DeKalb, GA		686803	0	686803	696352	-9549.00	-1.37
Shelby, TN		910530	0.003	911895.858	916294	-4398.14	-0.48
Plaquemines	Katrina	28997	0.223	6466.331	22585	-16118.67	-71.37
Terrebonne, LA		107729	0.027	108511.919	109996	-1484.08	-1.35
St Mary, LA		51515	0.001	51543.997	52173	-629.00	-1.21
St Bernard, LA	Katrina	65165	0.234	15248.61	15518	-269.39	-1.74
Pearl River, MS		52576	0.053	65490.777	57227	8263.78	14.44
Livingston, LA		108906	0.005	109231.825	114750	-5518.18	-4.81
Ascension, LA		90773	0.003	90968.495	97686	-6717.51	-6.88
Washingtn, LA		44487	0.028	50647.672	44962	5685.67	12.65
Montgmry, TX		378410	0	378410	397641	-19231.00	-4.84

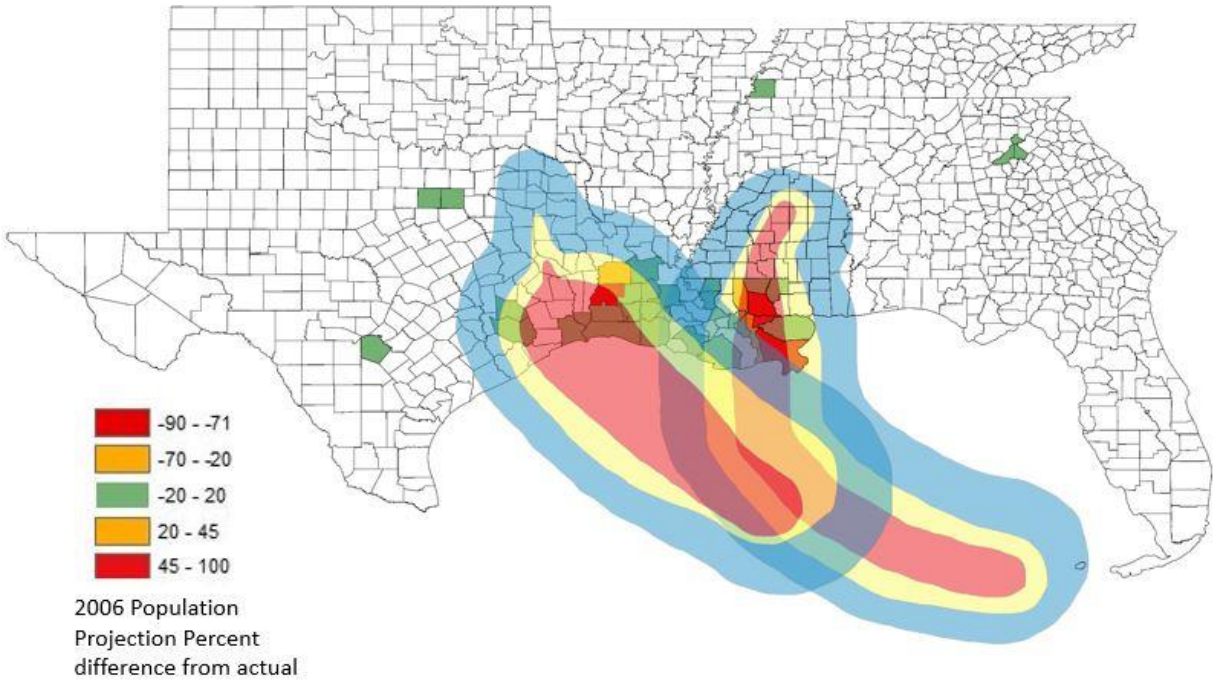

Figure 6.5. Uncertainty for population migration is greatest for locations experiencing the highest intensities of the storms. Wind swath shading: Red = 59-74 knot winds, Yellow = 40-58 knot winds, Blue = 39 knot winds.

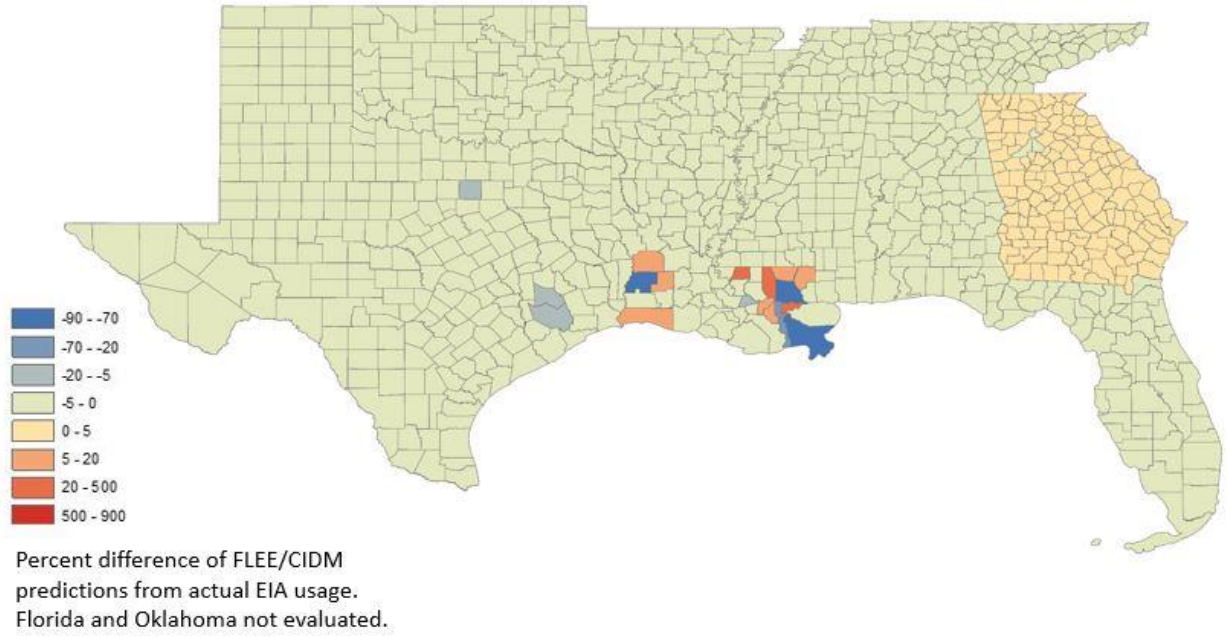

Figure 6.6. Percent difference between model calculations of by-county energy demand for 2006 and EIA values.

Fragility Curves

Fragility curves provide a powerful approach for understanding total environmental damage potential and the number of outages observed for a particular area during an extreme weather event. These curves depict the relationship between a weather variable (wind speed, gust speed, ice accumulation, precipitation rate) and the observed outages for a targeted infrastructure network (Fernandez et al, 2014). The ability to predict such outages based on the robustness of the local power grid against environmental damage potential given the outages observed for a particular area during an extreme weather event, and the capability of the operators of that local system to bring the power back online, can become a measure of both robustness and resilience of the community's infrastructure as a whole.

Issues affecting the fragility of the grid from location to location include physical and structural, informational, geospatial, procedural and societal components, but the prediction of fragility relies solely on customer outage and atmospheric data. Fragility, expressed as the bivariate relationship between wind speeds and number of observed power outages at time periods for a large (multi-county) region, follows an exponential curve, the extremity of which can vary empirically, but which is closely approximated by that developed by the Electric Power Research Institute (EPRI). Using this curve, counties with increased or decreased robustness can be characterized by terrain more or less susceptible to persistent flooding in areas where above ground poles have located their foundations. This information, then, can be applied to the calculation of the proportion of people expected to return to an area affected by severe flooding, and the timing of their return (Lam et al., 2009; Groen and Polivka, 2010).

Time to Restoration

Once an outage has occurred, the number of crew members per county available for repair may be estimated according to local resources, and the amount of time to restoration calculated as a result. This provides a measure of resiliency within a community to electrical outage, and represents a first step toward complete restoration of a community's infrastructure.

6.3.5 Influence of County Resilience on Population Return

A major influence on the rapidity with which the population returns to a county after a disastrous event is the resilience of the county (Li et al., 2005; Lam et al., 2009; Groen and Polivka, 2010). Comparison of the population between Hurricane Katrina in 2005 and Hurricane Isaac seven years later supports this observation (Lam et al., 2012; Fernandez et al., 2014). In the time intervening, the Army Corps of Engineers completed a Risk Reduction System (2012) and a mandatory evacuation for Hurricane Isaac was not issued. While the storm caused more damage than expected, and more than a million people were without power from three to six days, the costs to New Orleans citizens was far less than it was in the aftermath of Katrina and the city resumed its normal activity in much less time (Lam et al., 2009). Migration patterns for this year did not exceed typical outflow). Because of this response, we can posit that the vulnerability of its power transmission and distribution system, along with the length of time it takes for the utility to restore power to its residents is an indicator of the robustness and resilience of its infrastructure and the overall resilience of the community to extreme events (Lam et al., 2012). Because of the extreme ire that Katrina provoked, however, little outage information is available for hindcast predictions of its fragility or its resilience.

Resilience Indicators

Li et al. (2005) demonstrated that school reopenings played a major role in indicating the ability of a community to rebound and to signal its citizens that the community was operating again. Groen and Polivka (2010) confirm this finding. Other socioeconomic resilience indicators investigated by Li include employment rate increase, increase in sales tax earnings, and severance taxes (levied on production of natural resources taken from land or water) as indicators of a returning economy. Before any of these indicators can take effect and be recognized, however, basic infrastructure and places of employment must be repaired and in place. The demographic attributes that best described the population who returned within eight months is employment. As Li and Fernandez (2014) show, the most easily rebuilt businesses are those whose workers return first. In Plaquemines Parish, this business was manufacturing. St. Bernard also included agriculture, retail, professional/scientific, and artistic careers. Jefferson's returning employees were in transportation, finance, education, and artistic careers. The most likely to stay in St. Tammany were those living below the poverty level, while no variables had positive coefficients indicating that they stayed in Orleans or St. Charles Parishes.

6.4. Conclusions and Future Work

In this work, we created a prototype agent based population distribution model to be coupled to infrastructure models to anticipate emerging power grid vulnerabilities. If, as projected in climate models, the frequency of storms increases in the coming decades, populations will continue to shift in response to these extreme weather events. These shifts in turn will place new power consumption demands on the electrical infrastructure. This work suggests that while demographics and decision making are important to the final destinations of a population moving

in response to an extreme weather event, the importance of established evacuation routes that move large populations repeatedly through convergence points as an indicator may be under recognized. One of the limitations of the tool, however, is its capability for predicting the percentage of the population that chooses to return home to rebuild after having evacuated in advance of a storm. Variables related to infrastructure resiliency of parishes of origin should be incorporated into the next version of the model. Furthermore, additional studies of repeated evacuations is required before this type of anticipatory model can be used to assess the impact on the nation's critical infrastructure including an examination of the response of populations in counties that have experienced hurricanes in close succession. Ultimately, however, these models may allow key studies on future states of critical infrastructure resulting from increasing frequency of extreme events at vulnerable locations.

6.5. Acknowledgements

This manuscript has been authored by employees of UT-Battelle, LLC, under contract DE-AC05-00OR22725 with the U.S. Department of Energy. The authors would also like to acknowledge the financial support for this research by the Integrated Assessment Research Program of the U.S. Department of Energy¹s Office of Science.

References

Allen, MR, Sulewski LS, Fernandez SJ (2013). Effects of Climate Change on Coastal Population Migration and Changes in Regional Energy Demand. 2013 Carbon Management Technology Conference, Alexandria, VA.

Amala, A.J. and M. Ponnavaikko (2011), Optimal Substation Location and Network Routing using an Improved GA Based Solution Approach, Int. J. of Power System Optimization and Control:Articles, 3,1,47-60.

Blanchard, O.J. and L.F. Katz (1992). Regional Evolutions, *Brookings Papers on Economic Activitiy*, **1**, 1-75.

Bozdogan, H., (2000). Akaike's Information Criterion and Recent Developments in Information Complexity, *Journal of Mathematical Psychology*, **44**, 62-91.

http://cda.ornl.gov/publications_2013/Publication%2040621.pdf

http://www.eia.gov/electricity/data.cfm

http://www.eia.gov/consumption/residential/data/2005/

Fernandez, S.J., A.N. Rose, E.A. Bright, J.M. Beaver, C.T. Symons, and O.A. Omitaomu (2010). Construction of Synthetic Populations with Key Attributes: Simulation Set-up while Accommodating Multiple Approaches within a Flexible Simulation Platform. *IEEE Second International Conference on Social Computing* (SocialCom), 701-706.

Fernandez,SJ, Omitaomu OA, Allen,MR Sulewski, LS (2013). Methods for Exploring Evolution of the Power Grid Under Climate Drivers at Neighborhood Scale. 2013 Carbon Management Technology Conference, Alexandria, VA.

Fernandez, S.J., M.R. Allen, O.A. Omitaomu, K.A. Walker (2014). Application of Hybrid Geo-spatially Granular Fragility Curves to Improve Power Outage Predictions, *Journal of Homeland Security and Emergency Management*, In Review.

Graves, P.E. (1976). A reexamination of migration, economic opportunity and the quality of life. *Journal of Regional Science*, 16(1), 107-12.

Groen, J.A. and A.E. Polivka (2010). Going Home after Hurricane Katrina: Determinants of Return Migration and Changes in Affected Areas, *Demography*, 47(4), 821-844.

Hadley, S.W**.,** D.J. Erickson III, J.L. Hernandez, C.T. Broniak, T.J. Blasing (2006). Responses of energy use to climate change: A climate modeling study, *Geophysical Research Letters*, Vol. 33, L17703, doi:10.1029/2006GL026652.

Lam NSN, Pace K, Campanella R, LeSage J, Arenas H (2009). Business Return in New Orleans: Decision Making Amid Post-Katrina Uncertainty, *PLoS ONE* 4(8): e6765. doi:10.1371/journal.pone.0006765.

Lam NSN, Arenas H, Pace K, LeSage J, Campanella R (2012). Predictors of Business Return in New Orleans after Hurricane Katrina, *PLoS ONE* 7(10): e47935. doi:10.1371/journal.pone.0047935.

Li, H., S.J. Fernandez, and A. Ganguly (2005). Racial Geography, Economic Growth and Natural Disaster Resilience, *The Role of Social Science Research in Disaster Preparedness and Response*, Hearing before the Subcommittee on Research, Committee on Science, House of Representatives, One Hundred Ninth Congress, First Session, November 10, 2005. Serial Number 109-32. http://www.house.gov/science .

Li, H., and S.J. Fernandez (2014). Racial Geography, Economic Growth and Natural Disaster Resilience, *Geography and Natural Disasters,* Accepted.

Liu C., and M. Tuttle (2008). Emergency Evacuation Plan Maintenance. In: Shekhar, S, and Hui Xiong, (Eds). *Encyclopedia of GIS*, 2008. Springer-Verlag.

Lowry, I.S (1964). A Model of Metropolis RAND Memorandum 4025-RC.

McHugh, K.E. (1988). Determinants of Black Interstate Migration, 1965-70 and 1975-80. *Annals of Regional Science* **22**, 36-48.

McLeman, R. (2013). Developments in modelling of climate change-related migration, *Climatic Change*, **117**, 599–611.

Maslow, A.H. (1954). *Motivation and Personality*, Harper & Row Publishers, New York.

Nel, E. (2010), *The Dictionary of Human Geography*, 5th edition – Edited by Derek Gregory, Ron Johnston, Geraldine Pratt, Michael J. Watts and Sarah Whatmore. New Zealand Geographer, **66**, 234–236. doi: 10.1111/j.1745-7939.2010.01189_4.x.

Perch-Nielsen, S. L., Bättig, M. B. and Imboden, D. (2008). Exploring the link between climate change and migration. *Climatic Change*, **91**, 375-393.

Permann,M.R., (2007) Genetic Algorithms for Agent Based Infrastructure Interdependency Modeling and Analysis, INL/CON-07-12317.

Plyer, A. and E. Ortiz (2012). Poverty in Southeast Louisiana Post-Katrina. Greater New Orleans Community Data Center (GNOCDC).

Raphael, S. and Riker, D.A. (1999). Geographic Mobility, Race and Wage Differentials. *Journal of Urban Economics*, **45**, 17-46.

Rogers, A. (1967). A Regression Analysis of Interregional Migration in California. *The Review of Economics and Statistics*, **49/2**, 262-267.

Shumway, J.M., S. Otterstrom, and S. Glavac (2014). Environmental Hazards as Disamenities: Selective Migration and Income Change in the United States from 2000–2010. *Annals of the Association of American Geographers*, **104**(2), 280-291.

Technical Report: HSDRRS in New Orleans, Louisiana (2012). EQECAT, Inc.

http://web.ornl.gov/sci/electricdelivery/research_verde.shtml

http://web.ornl.gov/sci/landscan/

Wilbanks, T.J. and S.J. Fernandez (2012). Climate Change and Infrastructure, Urban Systems, and Vulnerabilities. *Technical Report for the U.S. Department of Energy in Support of the National Climate Assessment*. February 29.

Wilmot, C.G., N. Modali, and B. Chen (2006). Modeling Hurricane Evacuation Traffic: Testing the Gravity and Intervening Opportunity Models as Models of Destination Choice in

Hurricane Evacuation. Louisiana Transportation Research Center Project no. 03-1SS, State Project No. 736-99-1116.

Young, B.S., S.J. Fernandez and O.A. Omitaomu (2009). Dynamic Modeling of Components on the Electric Grid, Oak Ridge National Laboratory Report ORNL/TM-0000/00.

Appendix 6A. Best 2005-2006 County to County Migration Models as Determined by Information Complexity Criteria

Harris, TX

Jefferson	Bernard	Tammany	Orleans
0 11 14	0 -13	-2 5	0 -16
14	5	0 2	0 7

To Harris

2 Married	11 Transportation career
5 white	14 Education Career
7 Ag career	16 Veteran

Jefferson, LA

Stay	*Orleans	*Plaquemines	Bernard	*Charles	*Tammany
0 7 11 12 14 15	0 4	0 -12	0 1	2 9 13	0 16
	0 -7	5			

To Jefferson

1 Gender female	11 Transportation career**
2 Married	12 Finance career**
4 Below Poverty Level++	13 Professional/Sci career
5 white	14 Education career**
7 Ag career**	15 Artistic career**
9 Manufacturing career	16 Veteran

East Baton Rouge, LA

Jefferson	Plaquemines	Bernard	Charles	Tammany	Orleans
2 10	13 14	0 3 11 16	4	6	0 -9
		5		8	6

To E Baton Rouge

2 Married	10 Retail career
3 College Education	11 Transportation career
4 Below Poverty	13 Professional/Scientific
8 Construction career	14 Education Career
9 Manufacturing career	16 Veteran

St. Tammany, LA

Stay	*Jefferson	Plaquemines	Bernard	Charles	*Orleans
0 4	0 14	-3 5 12 14	0 12	8 10 15	0 2 7
			0 16		1

To St. Tammany

1 Gender female
2 Married
3 College education
4 below poverty level**
5 white
8 Construction career
10 Retail career
12 Finance Career
14 Education career
15 Artistic
16 Veteran

Dallas, TX

Jefferson	Tammany	Orleans
14	1 12	0 7

To Dallas

1 Gender female
7 Ag career
12 Finance career
14 Education career

Tarrant, TX

Jefferson	Tammany	Orleans	Plaquemines
4 7 9 15	13	0 6	5 12 14
4 7 9		1	
		5	

To Tarrant

1 Gender female
5 white
6 black
12 Finance career
13 Professional/ Sci career
14 Education career

Tangipahoa, LA

*Jefferson	Bernard	*Tammany	Plaquemines	*Charles
1 6 7 13	5	5	8 10 11 13 15	2
6 7				

To Tangipahoa

2 Married
4 Below poverty level++
5 white
7 Ag career
8 Construction career
9 Manufacturing career
10 Retail career
11 Transportation career
13 Professional/Sci career
14 Education career
15 Artistic career

Orleans, LA

Stay	*Jefferson	Plaquemines	Bernard	Charles	*Tammany
0 -7	4 11	6 9	2	10	4 6 8
0 -9			5		

To Orleans

2 Married
4 Below poverty level++
5 white
6 black
7 Ag career**
8 Construction career
9 Manufacturing career**
10 Retail career
11 Transportation career

Bexar, TX

Orleans
8 10

To Bexar

8 Construction career
10 Retail career

Pearl River, MS

St. Bernard	*St. Tammany
5	5

To Pearl River

5 white

St. John the Baptist, LA

*Jefferson
5

To St. John the Baptist

5 white

Lafayette, LA

Plaquemines
2

To Lafayette

2 Married

St. Charles, LA

Stay	*Jefferson
0 -7	2 3 11
0 -3	-1 2 3 11
	-1 2 3 6 11

To St. Charles

1 female
2 married
3 College education**
6 black
7 Ag career**
11 Transportation career

DeKalb, GA

Orleans
2
4

To DeKalb

2 Married
4 Below poverty level

Fulton, GA

Orleans
12
16

To Fulton
12 Finance career
16 Veteran

Ascension, LA

St. Bernard	St. Charles
1	0 3 -5 -6
5	

To Ascension
1 Gender female
3 College education
5 white
6 black

Plaquemines, LA

Stay
0 -12
0 9

Stayed in Plaquemines
9 Manufacturing career**

St. Bernard, LA

Stay
0 3 7 9 10 13 15

Stayed in St. Bernard
3 College education**
7 Ag career**
9 Manufacturing career**
10 Retail career**
13 Professional/Sci**
15 Artistic career**

St. Mary. LA

Plaquemines
5
5 16

To St. Mary
5 white
16 veteran

Terrebonne, LA

Plaquemines
2 4 16

To Terrebonne
2 Married
4 Below poverty line
16 Veteran

Livingston, LA

St. Bernard
5 8 14
5

To Livingston
5 white
8 Construction career
14 Education career

Lafourche, LA

***St. Charles**
10
4

To Lafourche
4 Below Poverty level++

Washington, LA

***St. Tammany**
3 12 15

To Washington
3 College education
12 Finance career
15 Artistic career

Appendix 6.B. Percent of Customers out of Power in the Days after Katrina

Utility	Parish	%/100 Out Kat 8-29	%/100 Out Kat 8-30	%/100 Out Kat 8-31	%/100 Out Kat 9-01
SLEMCO	Acadia	0.74	0.72	0.72	0.73
ENOI	Ascension	1	0.94	1	0.93
EGSL	Assumption	0.34	0.28	0.22	0.15
CLECO	Avoyelles	0.27	0.31	0.31	0.31
ELL	Bienville	0.63	0.64	0.64	0.6
EGSL	Calcasieu	0.34	0.28	0.22	0.15
ELL	Caldwell	0.63	0.64	0.64	0.6
EGSL	E Baton Rouge	0.34	0.28	0.22	0.15
ELL	E Carroll	0.63	0.64	0.64	0.6
DEMCO	E Feliciana	0.7	0.66	0.43	0.28
CLECO	Evangeline	0.27	0.31	0.31	0.31
CLECO	Grant	0.27	0.31	0.31	0.31
CLECO	Iberia	0.27	0.31	0.31	0.31
EGSL	Iberville	0.34	0.28	0.22	0.15
ELL	Jackson	0.63	0.64	0.64	0.6
ENOI	Jefferson	1	0.94	1	0.93
EGSL	Jefferson Davis	0.34	0.28	0.22	0.15
ENOI	Lafourche	1	0.94	1	0.93
DEMCO	Livingston	0.7	0.66	0.43	0.28
ELL	Madison	0.63	0.64	0.64	0.6
ELL	Morehouse	0.63	0.64	0.64	0.6
ENOI	Orleans	1	0.94	1	0.93
ELL	Ouachita	0.63	0.64	0.64	0.6
ENOI	Plaquemines	1	0.94	1	0.93
CLECO	Rapides	0.27	0.31	0.31	0.31
ENOI	St. Bernard	1	0.94	1	0.93
ENOI	St. Charles	1	0.94	1	0.93
DEMCO	St. Helena	0.7	0.66	0.43	0.28
ENOI	St. James	1	0.94	1	0.93
ENOI	St. John Baptist	1	0.94	1	0.93
SLEMCO	St. Landry	0.74	0.72	0.72	0.73
CLECO	St. Martin	0.27	0.31	0.31	0.31
CLECO	St. Mary	0.27	0.31	0.31	0.31
WST	St. Tammany	0.48	0.48	0.48	0.48
ELL	Tangipahoa	0.63	0.64	0.64	0.6
ELL	Tensas	0.63	0.64	0.64	0.6
SLEMCO	Vermilion	0.74	0.72	0.72	0.73
WST	Washington	0.48	0.48	0.48	0.48
EGSL	West Baton Rouge	0.34	0.28	0.22	0.15
DEMCO	West Feliciana	0.7	0.66	0.43	0.28
ELL	Winn	0.63	0.64	0.64	0.6

Chapter 7

The Impacts of Climate Change on Subregional Electricity Demand

Melissa R. Allen[1,2], Steven J. Fernandez[2,1], Joshua S. Fu[1,2]

[1]University of Tennessee, Knoxville
[2]Oak Ridge National Laboratory

Abstract

We employ new tools to develop an electricity demand map for the southeastern United States at neighborhood resolution to serve as a baseline from which to project increases in electricity demand due to a rise in global and local temperature and to population shifts, both typical and those motivated by extreme weather events due to climate change. Improved resolution in both population and climate projections provides more locally useful modeling results than have previously been available to utilities and to local urban planners.

7.1. Introduction

One of the most important sectors of the interconnected urban infrastructure is that of electricity. Because of the current limitations of the electrical grid due to physical aging and outdated technology (ASCE, 2013); and the need to incorporate new and cleaner generation; it is well understood that the grid must evolve. How and where the evolution will take place from generation to consumption are two of the prevailing questions among planners. Without accurate estimates of present and future demand, however, it is difficult to determine how much electricity must be generated, how and where it must be transmitted, and how the grid should adapt. Integrated Assessment Modeling of climate change impacts on infrastructure has provided general insight in the past, but has fallen short of providing grid-specific information for planning purposes. Various organizations such as the Eastern Interconnection Planning

Committee (EIPC, Phase 1, 2011) and the Electricity Information Administration (EIA, http://www.eia.gov/forecasts/aeo/data.cfm) have made projections regarding energy use, capacity and generation; but within their modeling efforts, they do not consider the climatic effects of either temperature rise or population movements, and neither considers to very high resolution the spatial distribution of the electricity demand or supply.

One of the symptoms of climate change will be increases in intensity and frequency of storms including hurricanes making landfall in coastal areas. For instance, hurricane wind speeds will increase over the century by a factor of up to 1.15 (Emanuel et al., 2005; 2013). This prediction upgrades tropical depressions, tropical storms and hurricanes. Additionally, return periods for Category 3+ hurricanes may decrease by a factor of as much as 2.3 (Keim,2010). That is, some locations will experience this intensity of hurricane 2.3 times as often by the end of the century as they do now. Because damage rises by about a factor of four for every category increase (Pielke et al., 2008), population stresses associated with hurricanes are likely to increase with the increase in hurricane intensity, and these stresses will cause some of the population to move to less vulnerable locations.

We address these issues by simulating, at neighborhood scale, how electricity demand might be altered due to a rise in global and local temperature and to population shifts, both typical and those motivated by extreme weather events due to climate change. This information can inform where and when we should plan for extra electricity generation and capacity, and where less electricity will be required due to climate and environmental changes in the future. This paper

extends the current state of the science in three significant ways. 1) We employ a spatial methodology for electric load forecasting for grid planning in which a cost distance algorithm based on regional population is used to determine the service area for a given substation. The advantage of using this methodology is that the algorithm can redistribute the service areas of the existing substations based upon projected growth and decline in population of various regions. 2) We apply satellite population observations (LandScan) and predictions based upon Census and Internal Revenue Service (IRS) data to project spatial shifts in demand in the southeastern US region. We also incorporate into the study several sudden redistributions of population in response to a 2005-like hurricane season at the predicted return period for such events in the region based on recent climate science. 3) To analyze further the effect of increases in global temperature and resulting regional electricity demand consequences, we calculate local percent change in electricity demand given temperature changes from dynamically downscaled (12km resolution) climate model projections for the region.

Because the growth of every small area is linked to causes and forces located elsewhere in the region and by demographic and economic interactions, the process of regional growth and resulting electricity demand changes is hard to characterize (Willis and Aguero, 2007). A variety of commercial models for forecasting electric load spatially based on land use projections have been used in the past to generate scenarios for long range planning. Among the first were linear urban models based on Ira Lowry's (1964) gravity model for population movement and generalized by Garin (1966) to a set of matrix computations. While these models take into consideration projected development of various types of electricity customers (residential,

commercial, industrial), they do less well at predicting the ways in which re-development of land use will occur. Therefore, the US Geological Survey (Clark and Leonard, 1998), Duke Energy (Integral Analytics, 2010) and the California Energy Commission (Auffhammer and Aroonruengsawat, 2012), among others, have added development to such models that incorporate economic and demographic weights for the determination various redevelopment types using agent based modeling.

For each of these models, the critical components are those of the spatial distribution of the population among their places of residence and their places of business, and the way changes in those distributions are projected for the future. With the high-resolution (1km) satellite population data (LandScan) for both day (work) and night (residential) population locations available for our use in this study, we are able to determine electricity customer service areas to a high degree of accuracy. Additionally, population projections using locally-adaptive, spatially-explicit dasymetric methods (McKee et al., 2014), with this satellite data as a base case, couple the appropriate land use predictions (Mays et al., 2012) with highly accurate initial conditions to provide more accurate inputs to the cost distance evaluation for the determination of the service areas yielding more reliable planning scenarios. Population projections included methods for modeling suitability, service area planning, consequence assessment, mitigation planning and implementation, and assessment of spatially-vulnerable populations. To these population projections we add, at the predicted return periods (Keim,2010), population response to a 2005-like hurricane season.

Strides have been made regarding predictions of increases in electricity demand in response to increases in global temperature expected with climate change. Using the Electricity Information Administration National Energy Modeling System (NEMS), Hadley et al. (2006) showed that for most US locations, the savings of electricity in the winter months due to fewer cooling degree days do not offset the added expenditures on electricity in the summer for the increase in heating degree days. The climate inputs used in the Hadley study, however, were global model output at 2.5 degree resolution, so while the study was able to capture electricity customer response to some general trends in future temperature, it was unable to resolve regional differences in temperature in both base and future cases. To improve upon such predictions, the California Energy Commission (Hidalgo et al., 2008) employs a Constructed Analogues method for statistically downscaling global climate model output at coarse resolution (2.5 degrees) to fine (~13km) resolution using analogues from present regional climate. With this method, along with electricity utility billing data, and demographic information, they have made projections regarding increases in residential electricity use according to geographic and economic boundaries of the population in the state.

While many statistical downscaling methods such as the Constructed Analogues method provide computationally frugal ways for deriving regional climate variable values from global ones, they lack the physical and chemical robustness possible with dynamical downscaling, a process by which global climate output is used as initial and boundary conditions for a more highly resolved regional weather model based on equations for physical and chemical processes. Our calculation uses temperature projections dynamically downscaled to 12km from a member of the

Intergovernmental Panel on Climate Change Coupled Model Intercomparison Project, Phase 5 (CMIP5) ensemble to inform the calculation of change in electricity demand due to temperature change. We present the full methodology and results of our study in the following sections.

7.2. Methodology

Increases in demand as a result of large population shifts can place extra stress on infrastructure as a whole, especially at locations of regional convergence; that is, convergence of critical infrastructure components through a specific geographical location. The determination substation vulnerability to demand increases due to storm-related population movements involves a variety of datasets and several processing steps. Both typical population changes and changes due to migration after a storm must be estimated as well as substation capacity for a given service area and peak and average customer demand for each service area. Each of these procedures is described in the following sections.

7.2.1 Initial Assessment

We can make an initial assessment of the locations experiencing the greatest changes in electricity demand due to both temperature and population change by examining simultaneously the predictions for these variables for the 2050s. Figure 7.1 shows the areas which have potential for extreme increase in demand as a result of intense temperature increase along with population influx. (The population projections for this map are based on typical population shifts rather than those induced by extreme climate. Additions of these considerations are discussed in the following sections.) High density of dots suggests high population density, while darker red

shading indicates temperature increase. Values are projections for the 2050s. The two areas most affected in the United States are the Denver, Colorado area and the Chicago, IL area. Incorporation of LandScan population data sets within CIDM allow GIS integration to link the climate impacts to the affected built infrastructure systems and population movements at the same 1×1 km resolution (Gao et al., 2012).

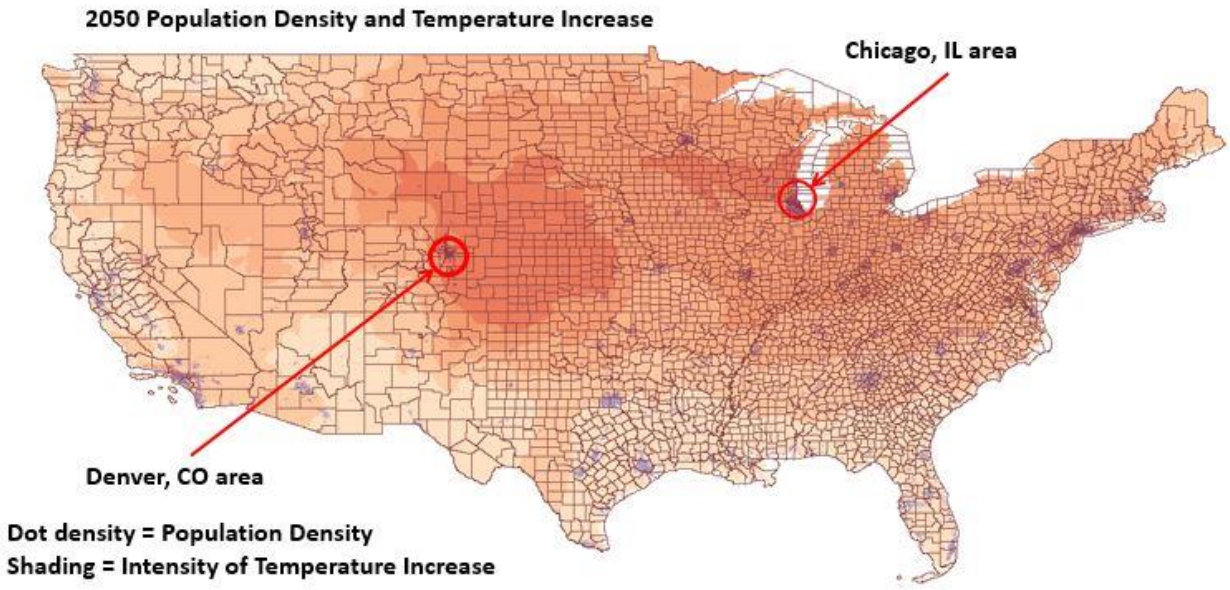

Figure 7.1. Locations at risk for Regional Convergence of Population Movement and Temperature Increase

7.2.2 Datasets

Datasets used include Oak Ridge National Laboratory (ORNL) Geographic Information Science and Technology (GIST) files including substation location and capacity, LandScan population data sets for 2011 and projections for 2030 and 2050, Energy Information Administration (EIA)

state by state total electricity consumption records for 2011 and predictions for 2040, and Internal Revenue (IRS) Data sets for by-county in- and out-migration for the years 2004-2007.

7.2.3 Determining the Service Areas for the Substations

The first step in determining the amount of stress placed on substation capacity in an area is to estimate the service area for each substation based on its location and its capacity. This is accomplished using a process developed by Omitaomu (2008) and described in the ORNL Power Distribution Model (PoDiuM) Technical Report (Omitaomu et al., 2012). PoDiuM is a cost distance based algorithm that compares cost units to geographical units to determine maximum distance to customers served. In this cost approach, the lower the demand, the higher the cost, and the greater the transmission distance, the larger the cost.

The service area cost is computed with the following equation, where P = population of a given 1km cell in the LandScan dataset and $\sum P$ = the sum of the population in a study region and S = the capacity sum of the substations in the region. Study regions were bounded by state borders here.

$$D_{inv} = \frac{1}{\frac{P}{\sum P} * S} \quad (1)$$

Geographical cells (again, 1km resolution) are allocated to a given substation based upon the lowest accumulated cost to reach the source from the cell. Accumulated cost is calculated as the sum of two values: c1 = the average of D_{inv} for the starting cell and the ending cell (each multiplied by length = 1, which is the spatial resolution in kilometers); and c2 = the average of

D_{inv} for the starting cell and the midpoint cell (again each multiplied by 1) as shown in Figure 7.1.

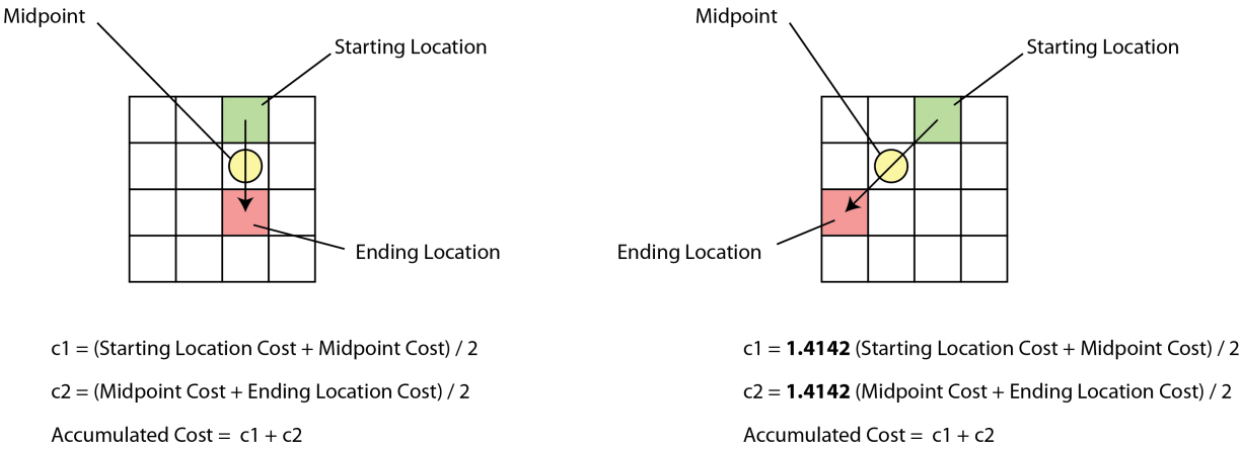

Figure 7.1. Accumulative Cost Calculation (ESRI, 2007)

For diagonal transmission distance traveled, length increases to $\sqrt{2}$ = 1.414, so each average value is multiplied by this amount. Cells which contain the substations, or source cells are given a D_{inv} value of 0. Since no D_{inv} calculation can be made from the "no data" cells, these cells act as barriers to the movement of the allocation process. Cost allocation is performed as an iterative process beginning with the cost evaluation of the source cell, then extending to the eight neighboring cells of the source cell. For each concentric square of cells, the cells that help form the least cost path outward from the source are added to the service area of the source. Changing of allocated cells is possible, for instance, if a new, cheaper route is found by adjusting choices on inner squares to access less expensive cells on outer squares (Figure 7.2). This process continues until all of the cells are allocated, or an optional maximum distance threshold is met.

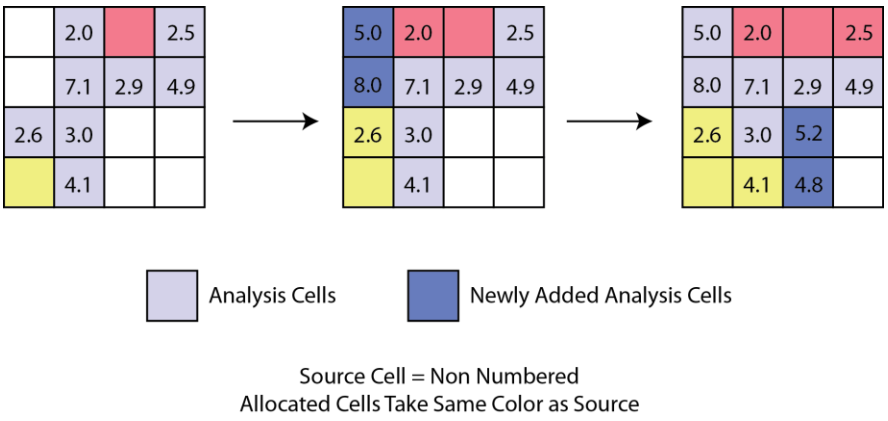

Figure 7.2. Cost Allocation (ESRI, 2007)

7.2.3 Population Shifts Due to Storm Motivated Migration

While the United States Census and others (e.g., McKee et al., 2014) have made viable projections of population distribution for future years, the projections do not include changes due to environmental stresses caused by climate change (sea level rise, drought) or extreme weather events (storms, wildfires). For this study, we investigate the impacts of further population redistribution on the overall spatial and electricity demand by including in those projections an adjustment for a 2005-type hurricane season applied at the 20-year return period for such a season indicated as probable by the climate community (Emanuel, 2005, 2013; Keim, 2007) as the 21st century continues (Appendix 7A).

To simulate this impact, we apply by-county migration rates from 2005-2006 and 2006-2007 to the study region as a hurricane migration component. If we assume that the migration rates as given by the IRS ((in-out)/(nonmigrants+out)) for 2004-2005 are typical of the various counties in the nine-state region, we can subtract these rates from each of the rates of the two following years, then use the results as factors to calculate the additional hurricane component. For the

population response by 2032, for instance, to a hurricane inserted at the year 2030, the calculation would be:

$$((pcntChange2005\_2006 - pcntChange2004\_2005)/100) * Pop\_2030 + Pop\_2030 \quad (2)$$

$$((pcntChange2006\_2007 - pcntChange2004\_2005)/100) * Pop\_2031 + Pop\_2031 \quad (3)$$

The initial 2030 population is taken from the projections made from LandScan by McKee et al. (2014). To calculate additional population response by 2052 from another 2005 hurricane season in 2050 (which takes into account population that relocated after the 2030 storm), we make the same calculation using 2050 population projections with the difference between the calculated 2032 values and the initial 2030 values added to the 2050 dataset.

7.2.4 Total Average Customer Demand Per Service Area

To project the total average customer demand per service area for the future, we take as a base average per-customer demand value the total consumption in GWh/year per state divided by the number of customers in the state and then further divided by the number of hours in a year (365.25*24) and multiplied by 1000 to convert gigawatts to megawatts.

$$GWh\_AverageCustomerConsumption = \frac{TotalStateConsumption}{StateTotalCustomers} \quad (4)$$

$$MW\_AverageCustomerDemand = 1000 * \frac{GWh\_AverageCustomerConsumption}{(365.35*24)} \quad (5)$$

Total number of customers in a location, however, is not the same as the total population. In order to convert from population to customers, we must apply a county-by-county varying conversion factor, which is equal to the population for a given decennial year (in this case, 2000) divided by the sum of the households and the firms in the county for that year (Young et al., 2010).

Once the average customer demand is calculated, we can calculate the total average customer demand per substation service area by multiplying this value by the number of customers within the service area.

7.2.5 Peak Customer Demand Per Service Area

For an electric utility company, peak demand is defined as the single half hour or hour-long period during which highest amount of customer consumption of electricity occurs. Since the amount of electricity over a certain threshold must often be purchased from additional providers during this time, the cost to provide that electricity is much more than that produced up to that threshold. Therefore, the utility companies calculate a peak-to-average demand ratio to be used in assessing their own costs to provide the electricity and the costs they pass on to the consumers. This amount is found by relating the peak of the electricity use curve to the area underneath the curve. Assuming Gaussian distribution and area A, the height of the peak is:

$$H = f(\mu) = \frac{A}{\sigma\sqrt{2\pi}} e^{\frac{-(\mu-\mu)^2}{2\sigma^2}} = \frac{0.3989A}{\sigma} \qquad (6)$$

and

$$\frac{H}{A} = \frac{0.3989}{\sigma} \quad (7)$$

With $\sigma = FWHM/2.35$ and FWHM (Full Width at Half Maximum) measured in the data from the utility readings.

The peak to average demand ratios calculated by the Electric Reliability Council of Texas (ERCOT) and by the Southeastern Reliability Council (SERC) for the years 1993–2012 are shown below in Figures 7.3 and 7.4. To these time series, we fit a linear trend in order to project peak to average demand ratios for future years, 2030 and 2050. With this information, we calculate peak demand for those years for each of the states (ERCOT values for Texas, SERC values for the other states) included in our southeastern study region.

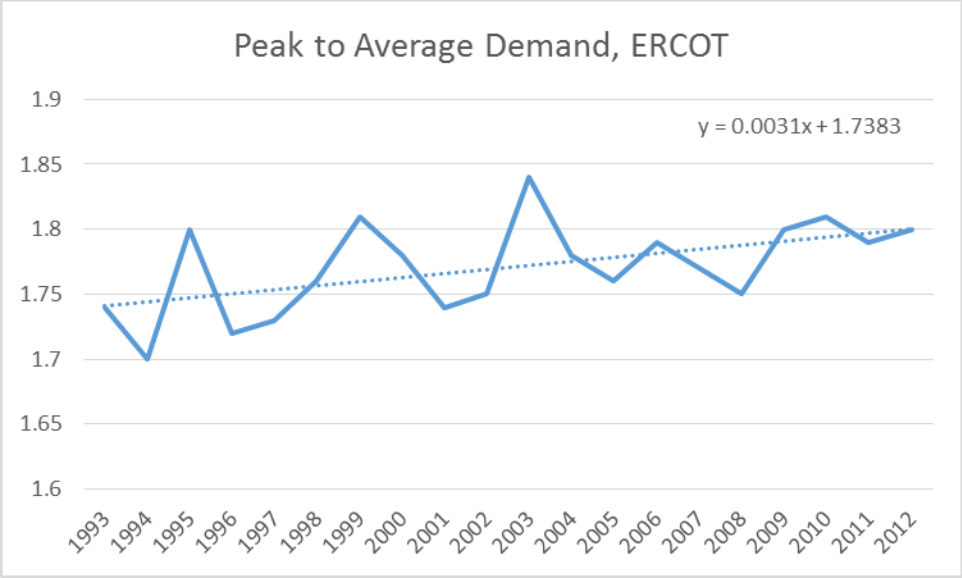

Figure 7.3. ERCOT Peak to Average Demand Ratios with linear fit.

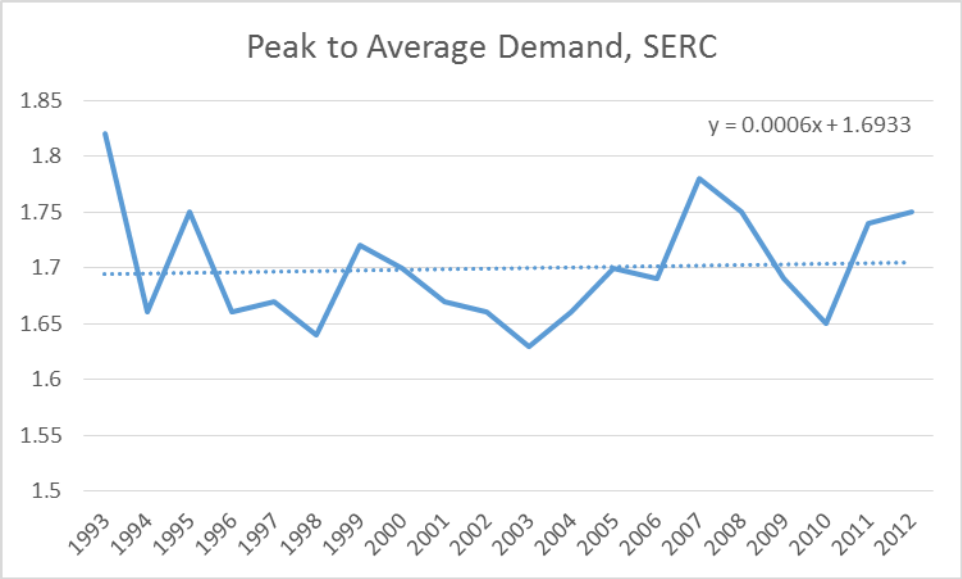

Figure 7.4. SERC Peak to Average Demand Ratios with linear fit.

7.2.6 Demand Change in Response to Temperature Rise

Increased power demand in response to rising temperatures has been well established by the utility industry, and has a latitudinal dependence. The percent increase in electricity demand for a county due to temperature rise is calculated (Toole et al., 2006):

$$I = (5.33 - 0.067L_{centroid}) * \Delta T$$

With I = percent increase in electricity demand, $L_{centroid}$ equal to the latitude in decimal degrees at the centroid of the county and ΔT equal to the change in maximum annual temperature in degrees Fahrenheit.

New demand as a result of this increase is calculated:

$$D = D_{av} * N * (1 + \frac{I}{100})$$

With D=total demand for the study area, D_{av} = average customer use and N=number of customers.

As temperature input to these formulae, we use historical and Representative Concentration Pathway scenarios (RCP 4.5 and RCP 8.5) generated by the Community Earth System Model (CESM) at three-hour intervals as initial and boundary conditions for a set of Weather Regional Forecasting (WRF) domain simulations (36×36km centered at 97°W, 40°N). This set contains boundary conditions for a further downscaled domain (12×12km in North America), which in turn serves as boundary conditions to 4×4km resolution domains. Both surface and three-dimensional variables extracted from the Community Atmosphere Model, Version 4 (CAM4) and the Community Land Model, Version 4 (CLM) history outputs comprise the initial and boundary conditions. Two-meter reference height temperature is horizontally interpolated from CESM (CAM4 and CLM4, 0.9° x 1.25° spatial resolution in latitude/longitude) to WRF simulation domains using the WRF Preprocessing System (WPS). The WRF 4km data sets are then incorporated as dBASE file tables into a Geographical Information System (GIS) platform and joined to additional energy and infrastructure layers for further analysis.

7.3. Results

Results show that population shifts in general, and specifically those that result from storm motivated migration have the largest effects on changes in electricity demand. Additionally, an overall rise in temperature, especially for the more northerly region of the study area, will add to the electricity demand, but with much smaller impact.

7.3.1 Development of a Demand Map for the Southeastern United States

Projections of future energy capacity and use are made by the Electricity Information Administration for each National Energy Reliability Council (NERC) region for each year from 2011 through 2040. Each NERC region is projected to sustain a demand of between approximately 40%-50% of the generating capacity available for each region (Figure 7.5). What these predictions are unable to do, however, is to predict stresses at specific locations where local demand may, either on average or during peak hours, exceed the peak load of substation capacity causing, in extreme cases, potential for blackouts, or in more mild cases, for utility companies to incur extra expense because of the necessity to buy power from other producers. Our results show these potential outcomes at the resolution of the electricity service area.

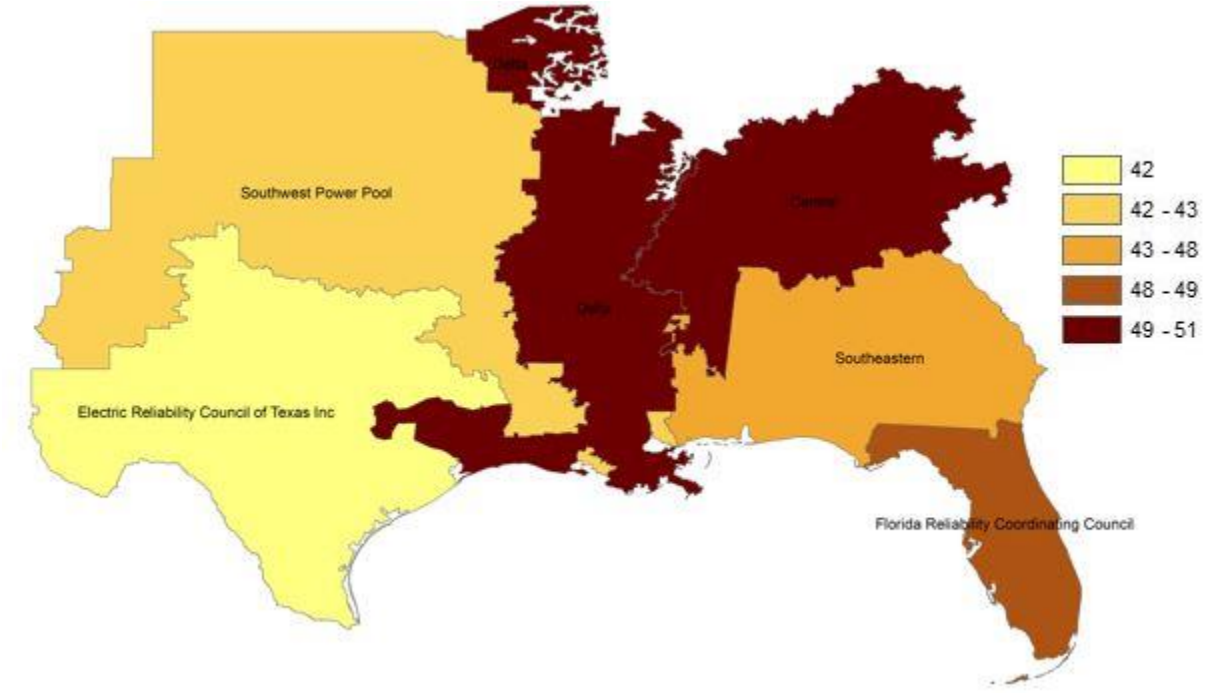

Figure 7.5. Calculation of Percent Demand of Capacity in each NERC Region based on EIA 2030 projections

To establish a baseline for these predictions, we first generated a demand map for the southeastern United States that outlines potential service areas based on the spatial pattern of the location of the population (discussed in Section 2.2). We then determined the percent of capacity of the substations that is used on average by customers in a service area, based on 2011 average statewide electricity consumption as reported by the EIA. Figure 7.6 shows the results for average customer demand. Additionally, because it is in the interest of electricity providers to retain enough capacity to serve its customers during peak demand hours, we also produced a baseline map that shows the percent of capacity used for peak demand (Figure 7.7). The maps show that there are several large service areas in both Alabama and Georgia that are operating at

80% or greater substation capacity for the service areas. A few smaller areas in Louisiana and Florida also show this situation. These areas grow with the added demand for peak hours.

Next, two types of differences in service area demand and capacity were investigated for future years 2030 and 2050. First, we retained the service area delineations as determined by the 2011 population and examined the effect of changes in electricity demand in those established service areas due to projected population shifts for the 2030s and 2050s. Second, the service areas were recalibrated based on the new distributions of population for the 2030s and 2050s before calculating the demand to capacity percentages. The difference between these two approaches is that in the plots with the recalibrated service areas, the extremes in the demand are distributed more evenly among the substations available so that fewer service areas showed demand in excess of 80% capacity.

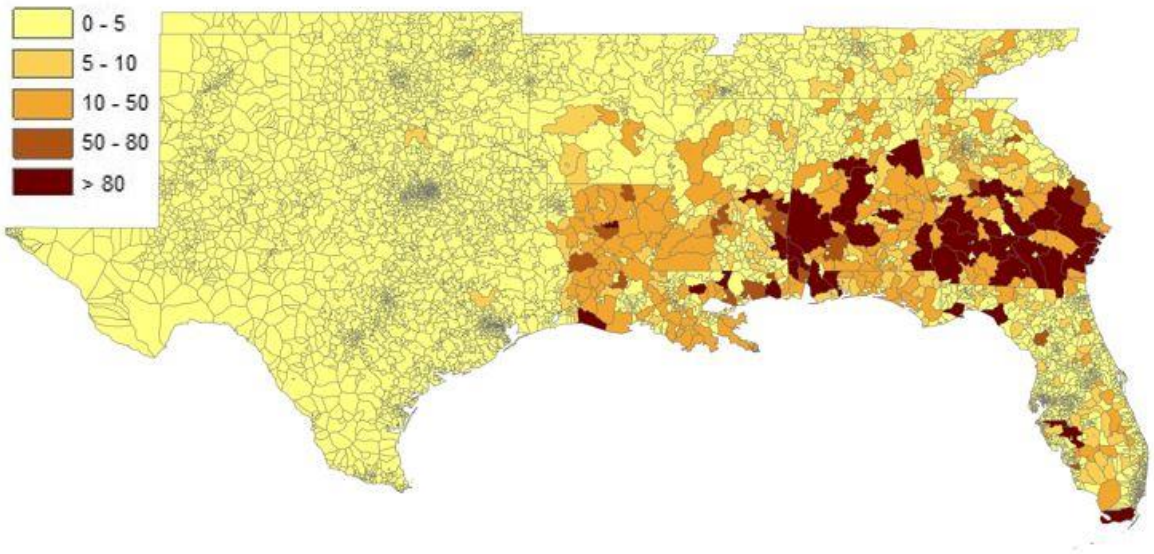

Figure 7.6. Percent Capacity Average Use per Substation Service Area, 2011

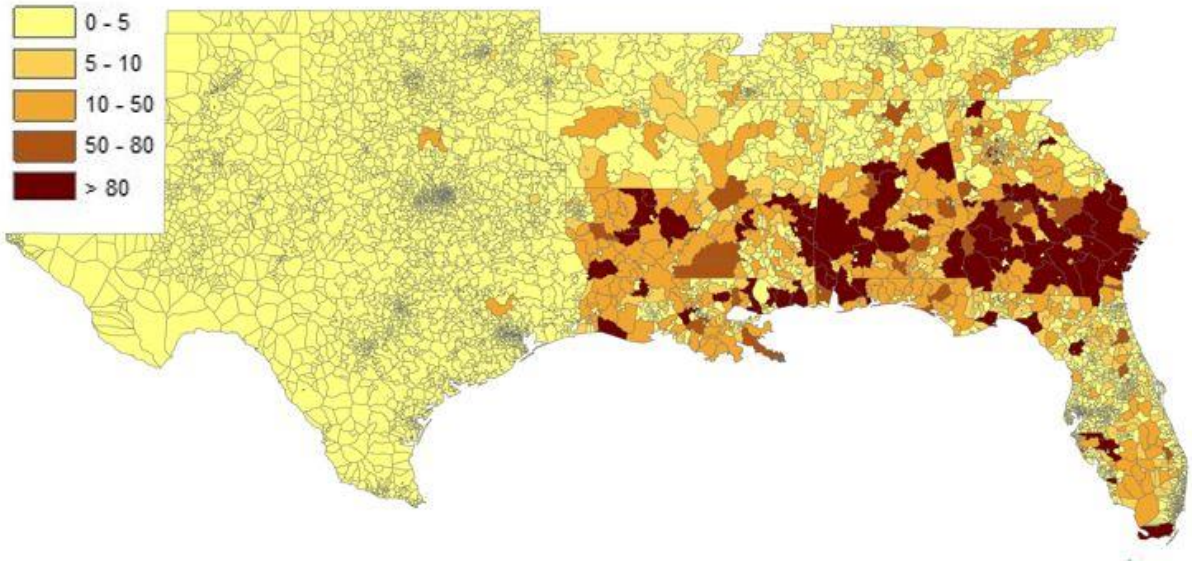

Figure 7.7. Percent Capacity Used during Peak Demand per Substation Service Area, 2011

This result demonstrates the efficiency maximization gains from increased population density discussed in Morikawa (2012) in two ways. The impact of this redistribution on peak load was also that of an increase in efficiency. Figures 7.8 and 7.9 show the differences in average demand vs capacity for each of the two 2030s examples. The first of the two figures shows that by the 2030s it is expected that the population in these states will have decreased significantly. The second shows that redistribution of the service areas as a result minimizes the load on individual substations.

7.3.2 Addition of Increased Demand Due to Storm Motivated Migration

For the decades of both the 2030s and the 2050s, the effects of a 2005-type hurricane season were simulated with the demand model, and results for differences in peak demand for each decade for the year following the hurricane season are shown in Figures 7.10 and 7.11. For 2030

(Figure 7.10) largest increases in demand to capacity percentage are seen in East Baton Rouge Parish for Louisiana and in Mobile, AL and several northeast counties in Alabama. Southeast counties in Georgia also see highest increases. This effect is amplified somewhat for the 2050s (Figure 7.11) as largest increases are larger still and the area of increase has expanded. For the three most popular Texas destinations (Houston, Dallas, San Antonio), there is little impact on the demand to capacity ratio. This is because the Texas ERCOT has built in plenty of extra capacity in all locations to avoid dependence on the continental grid. These results account for the cumulative effects of hurricane events from 2005, 2030 and 2050.

Betweenness and Vulnerability

One service area location that stands out in plots 7.10-7.12 is that of greater Birmingham, AL. In each of the simulations, this area shows the largest increase in demand vs. capacity. This may be due in part to the "betweenness" that is characteristic of this location. In graph theory, betweenness is defined as the number of shortest paths passing through a given node (Demsar et al., 2007). Thus, nodes with the highest betweenness are those that are located on the greatest number of shortest paths passing through that node in a connected network. Transmission and Distribution substations in the northeastern Alabama regions have high betweenness because of the large confluence of transmission lines there (Sulewski, 2013). These substations become particularly vulnerable when overall demand spikes.

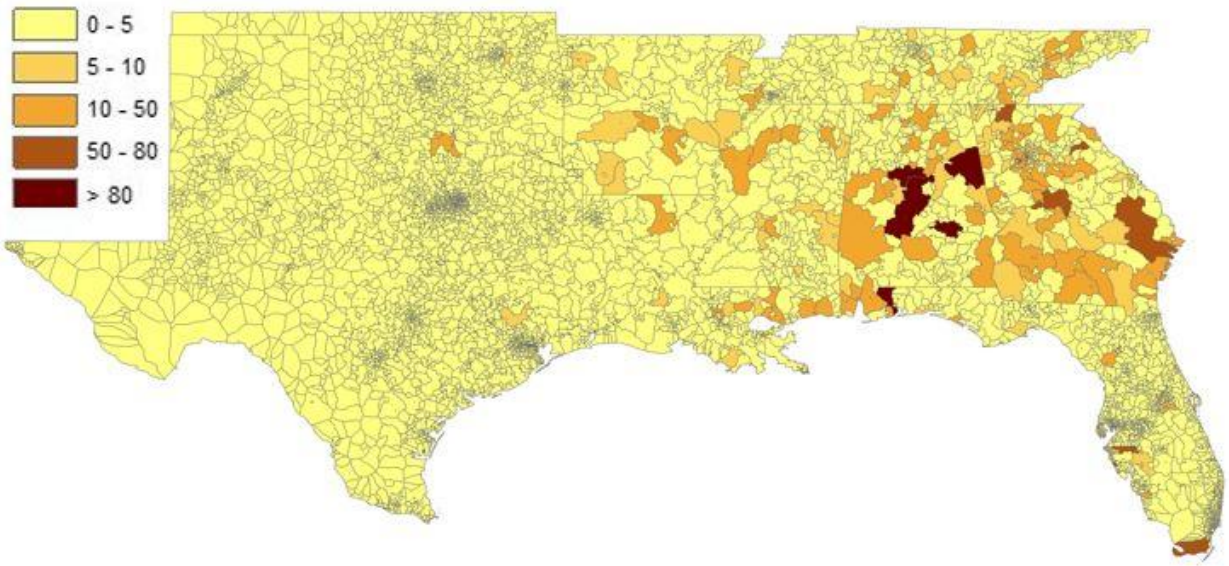

Figure 7.8. Percent Capacity Used per Substation Service Area, 2030 Using 2011 Service Areas

Implications for Distributed Generation

Substations are involved primarily with transmission and distribution of electricity that has been generated elsewhere, so percent demand predictions for the existing substations may not be affected too much by the addition of distributed generation to overall grid processes. However, collector substations will need to be added to the system to place new generation into the existing system, and the electricity generated by distributed sources will need mechanisms for direct

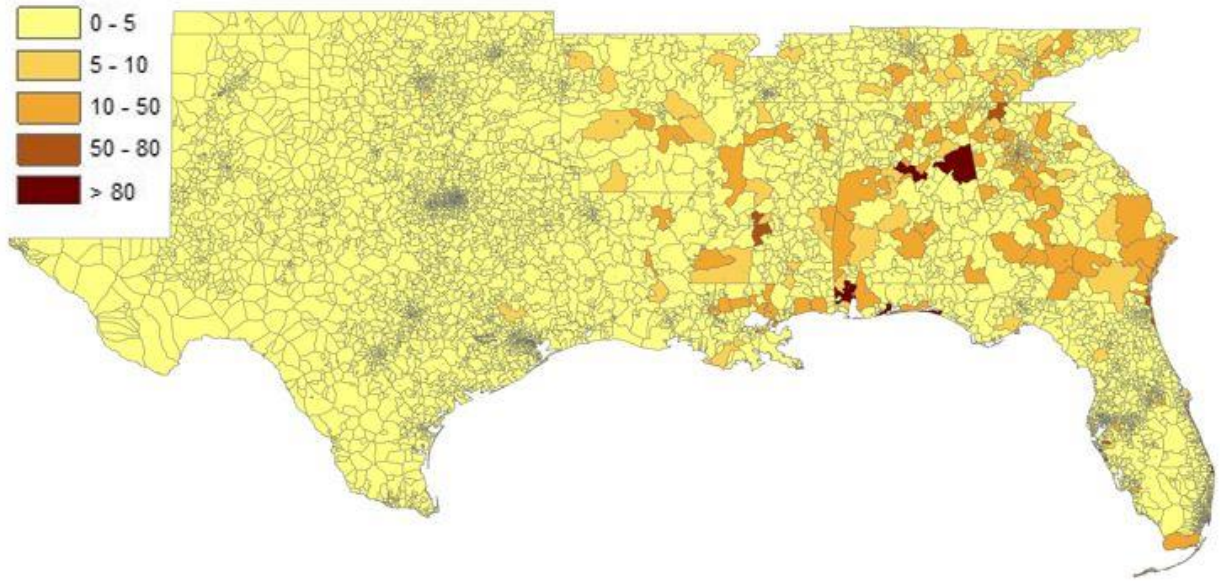

Figure 7.9. Percent Capacity Used per Substation Service Area, 2030 Using Redistributed 2030 Service Areas

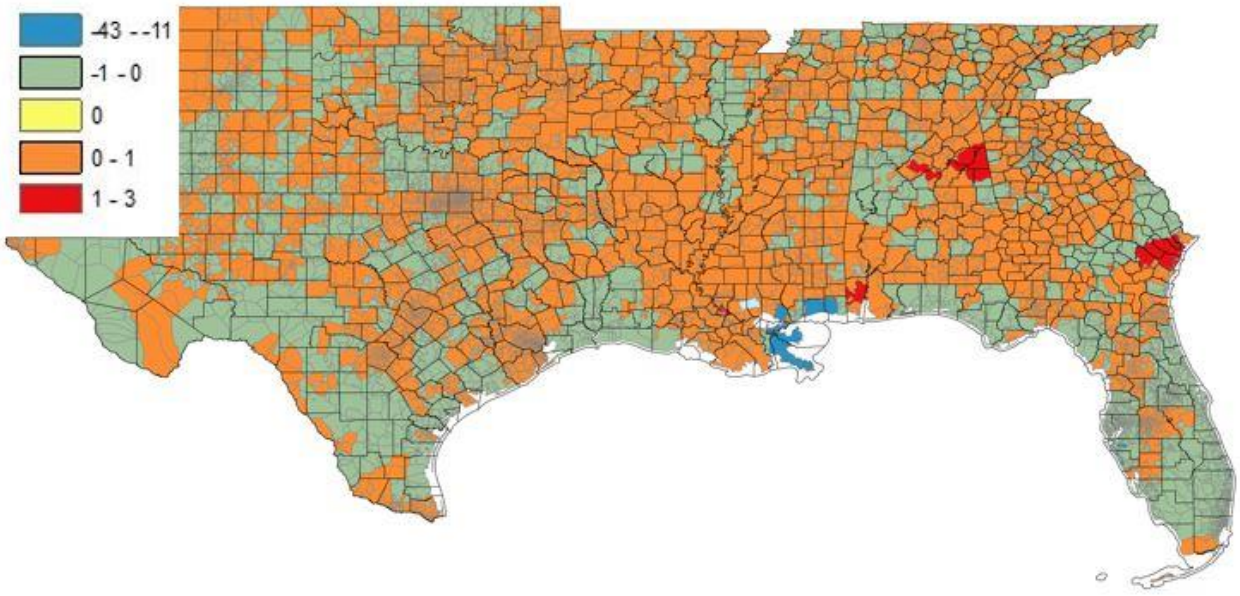

Figure 7.10. Difference in Percent Capacity per Service Area, 2030s Due to Storm Motivated Population Movement

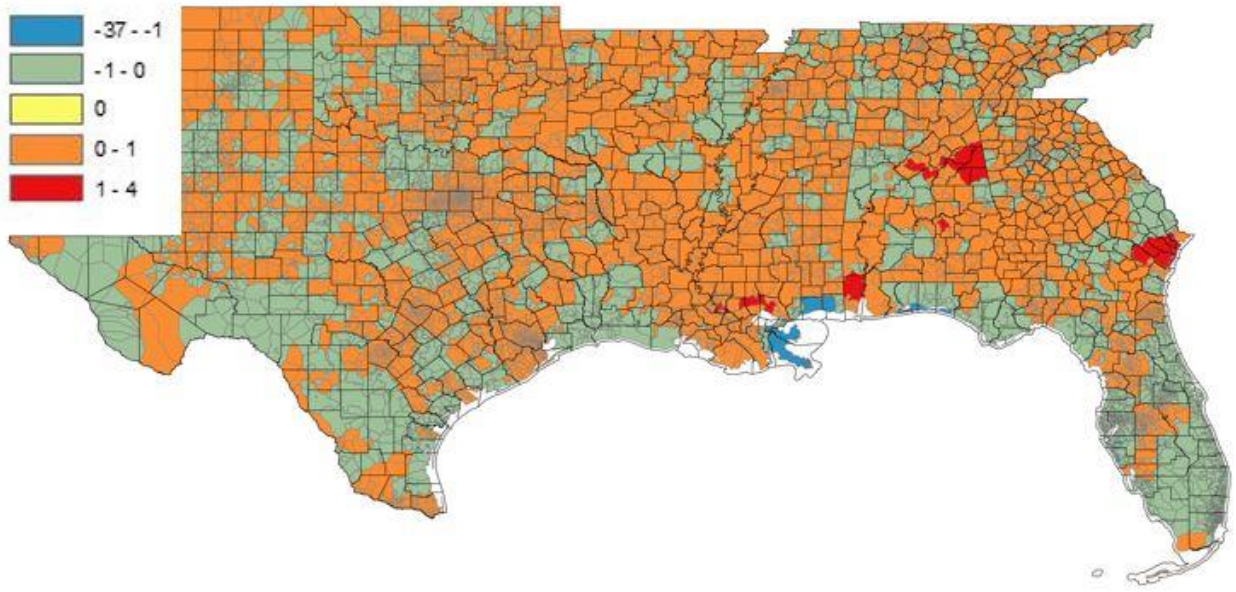

Figure 7.11. Difference in Percent Capacity per Service Area, 2050s Due to 2005-like Population Movement

current (DC) to alternating current (AC) conversion for grid connection. Individual household battery storage for local backup power and ancillary service provision may also be needed (Zipperer, 2013). Much of this power communication depends, however, upon the capacity of the feeder lines rather than on substation capacity. Thus, this new generation may affect betweenness in new ways.

7.3.3 Addition of Increased Demand Due to Rise in Maximum Temperatures

Finally, calculations for increase in demand due to temperature increase predictions from Weather Regional Forecasting (WRF) dynamically downscaled Community Earth System Model (CESM) results were made according to the procedure described in Section 7.2.6. Temperature predictions were at 12 km resolution for the years 2004 and 2057. Temperatures in Fahrenheit from both years were averaged for each service area. For peak demand especially, the difference

in temperature had a large impact on percent demand of available capacity. Figure 7.12 shows the spatial distribution of these differences.

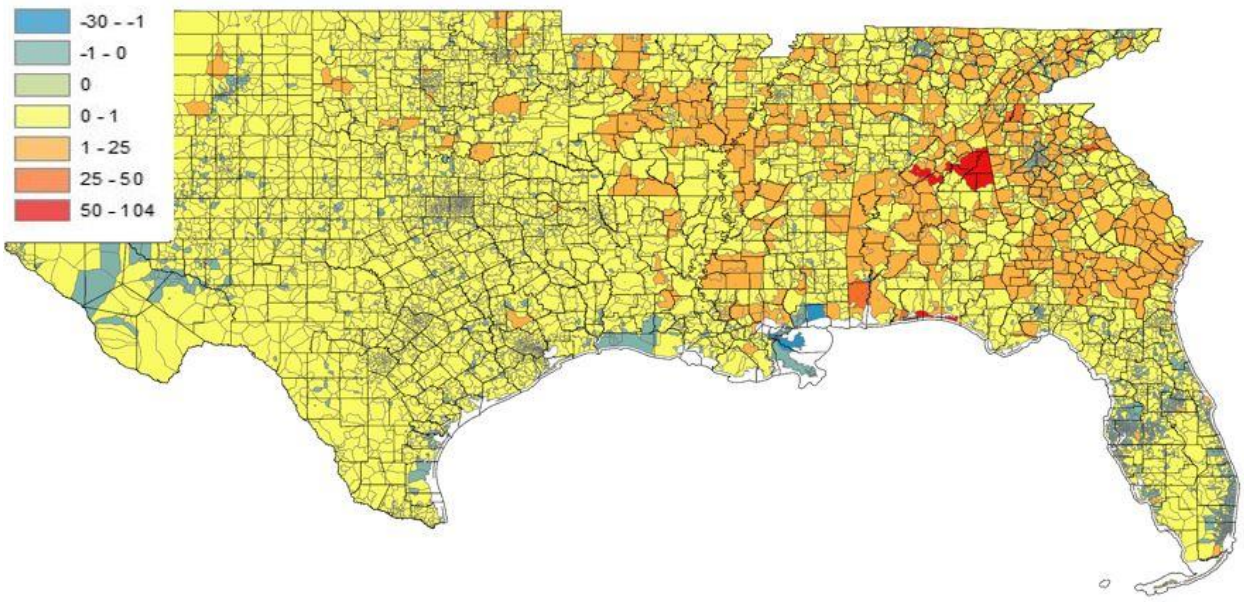

Figure 7.12. Difference in Percent Capacity per Service Area, 2050s Due to Added Changes in Temperature

7.3.4 Error and Accuracy

Because of the sensitivity of the electricity demand data for each utility's customers, it is difficult to measure the accuracy of the predictions given here even for the 2011 base case, but the methodology does lend itself to various checks should the data be available. Root Mean Square (RMS) error measurements between actual and forecast loads and respective load growths for a given area can provide a first check. Additionally, such checks can be performed over various redistributions of service areas associated with the substations in use.

7.4. Conclusions

The use of high-resolution population distribution data and dynamically downscaled climate projections provides an improved method for identifying specific locations of electrical grid vulnerability to increased electricity demand due to regional temperature changes as a result of global climate change, and to population shifts in response to typical (e.g., economic) drivers and to extreme weather events. Results show that compared to the effect of large population influx into a service area, demand increases due to temperature rise have little impact. It is also evident that some sections of the national electrical grid are more adaptable to these population shifts and changing demand than others are; and that detailed projections of changing local electricity demand patterns are important for planning at the urban level. While these projections could be improved with access to customer usage data for validation, they nevertheless can serve to inform planning for regional utilities regarding reorganization of substation service areas, addition of capacity to existing substations or the addition (or removal of) substations to existing service areas, and the evaluation of transmission line capacity and connections to substations for each service area as the 21st century grid begins to evolve in a variety of ways.

7.5. Future Work

Emanuel et al. (2006) have developed a physics-informed statistical wind risk assessment method for determining tracks of future Atlantic hurricanes based on past activity and future climate predictions. A simulation of this type could better inform frequency and intensity of storms (and possibly, direction of population movement response with respect to storm track) for

vulnerable locations. Combined with a reliable agent-based model, population movements and resulting spatial changes in demand may be more accurately predicted.

Additionally, comparison of these results to those obtained using similar inputs to models such as the EIA National Energy Modeling System (NEMS) model and the Eastern Interconnection Planning Collaborative (EIPC) North American Electricity and Environment Model (NEEM) could be combined to serve as a (albeit limited) “model spread” in order to provide a more robust confidence bound for interpretation of results for planning.

7.6. Acknowledgements

This manuscript has been authored by employees of UT-Battelle, LLC, under contract DE-AC05-00OR22725 with the U.S. Department of Energy. The authors would also like to acknowledge the financial support for this research by the Integrated Assessment Research Program of the U.S. Department of Energy¹s Office of Science.

References

Auffhammer, M., Aroonruengsawat, A. (2012). *Hotspots of Climate-Driven Increases in Residential Electricity Demand: A simulation Exercise Based on Household Level Billing Data for California*, prepared for the California Energy Commission by the University of California, Berkeley.

Clarke, K. C., and Leonard J. G. (1998). Loose-coupling a cellular automation model and GIS: long-term urban growth prediction for San Francisco and Washington/Baltimore, *Geographical Information Science*, **12**/ 7, 699-714.

Curtis, K. J. and A. Schneider (2011). Understanding the demographic implications of climate change: estimates of localized population predictions under future scenarios of sea-level rise, Population and Environment, DOI 10.1007/s11111-011-0136-2.

Desmar, U., O. Spatenkova, K. Virrantaus (2007). Identifying critical locations in a spatial network with graph theory, *ISRAM Intelligent Human Computer systems for Crisis Response and Management*, Delft, the Netherlands, 201-209.

Eastern Interconnection Planning Collaborative Steady State Modeling and Load Flow Working Group 2020 Roll-Up Integration Case Report, March, 2011. Retrieved August 26, 2013: http://www.eipconline.com/Resource_Library.html

Emanuel, K. (2005). Increasing destructiveness of tropical cyclones over the past 30 years. *Nature*, **436**, 686–688.

Emanuel, K.A., S. Ravela, E. Vivant, and C. Risi (2006). A statistical deterministic approach to hurricane risk assessment. *Bull. Amer. Meteor. Soc.*, **19**, 299–314.

Emanuel, K.A. (2013). Downscaling CMIP5 climate models shows increased tropical cyclone activity over the 21st century. *Proc. Nat. Acad. Sci*., **110**, doi/10.1073/pnas.1301293110.

Environmental Systems Research Institute (ESRI), http://webhelp.esri.com/arcgisdesktop/9.2/index.cfm?topicname=Understanding_cost_distance_analysis

Garin, R.A. (1966). A Matrix Formulation of the Lowry Model for Intrametropolitan Activity Location, *Journal of the American Institute of Planning*, 32, 361 – 364, 1966.

Gao, Y., J.S. Fu, J.B. Drake, Y. Liu, J-F Lamarque (2012). Projected changes of extreme weather events in the eastern United States based on a high resolution climate modeling system. *Environmental Research Letters*, 7 (4) 044025 DOI: 10.1088/1748-9326/7/4/044025

Hadley, S. W., Erickson III, D. J., & Hernandez, J. L. (2006). Responses of energy use to climate change: A climate modeling study, *Geophysical Research Letters*, **33**, L17703, doi:10.1029/2006GL026652.

Hidalgo, H.G., M.D. Dettinger, and D. R. Cayan (2008). Downscaling with Constructed Analogues: Daily Precipitation and Temperature Fields Over the United States. California Energy Commission, PIER Energy-Related Environmental Research. CEC-500-2007-123.

Integral Analytics (2010). LoadSEER™ Spatial Electric Expansion & Risk, http://www.integralanalytics.com/files/documents/related-documents/LoadSEER.pdf.

Keim, B.D., R.A. Muller and G.W. Stone (2007). Spatiotemporal Patterns and Return Periods of Tropical Storm and Hurricane Strikes from Texas to Maine, *Journal of Climate*, **20**, 3498-3509.

Lariviere, I. and G. Lafrance (1999). Modelling the electricity consumption of cities: effect of urban density. *Energy Economics* **21**, pp. 53-66.

LeClaire, R.J., D. Pasqualini, J.S. Dreicer, G.L. Toole, N.M. Urban, R.W. Bent, T.N. McPherson and N.W. Hengartner (2012). *Infrastructure Modeling: Status and Applications*, LA-UR-12-25481, Los Alamos National Laboratory.

Lowry, I.S. (1964). *A Model of Metropolis,* Santa Monica, The Rand Corporation.

McKee, Jacob J., Rose, Amy N., Bright, Eddie, & Huynh, Timmy (2014, Under Review). A Locally-Adaptive, Spatially-Explicit Projection of U.S. Population for 2030 and 2050. *Proceedings of the National Academy of Sciences,* In Review.

Mays, G.T., R.J. Belles, B.R. Blevins, S.W. Hadley, T.J. Harrison, W.C. Jochem, B.S. Neish, O.A. Omitaomu, A.N. Rose (2012). *Application of Spatial Data Modeling and Geographical Information Systems (GIS) for Identification of Potential Siting Options for Various Electrical Generation Sources.* ORNL Technical Report ORNL/TM-2011/157/R1.

Morikawa, Masayuki, 2012. Population density and efficiency in energy consumption: An empirical analysis of service establishments, *Energy Economics*, vol. **34**(5), pp. 1617-1622.

Omitaomu, Olufemi A., Steven J. Fernandez, and Budhendra L. Bhaduri (2010). Estimating the Spatial Distribution of Population without Power during Extreme Weather Events. *Presented at the 2010 Annual Meeting of the Association of American Geographers*, Washington, DC, April 14 – 18, 2010.

Olufemi A. Omitaomu (2008). A Parallel Disintegrated Model for Uncertainty Analysis in Estimating Electrical Power Outage Areas. *Presented at the 2008 AGU Session on Impacts of Severe Weather on Environment, Economy, and Society* (Abstract #: U41A-02), Fort Lauderdale, FL, May 27 – 30.

Olufemi A. Omitaomu, Leanne Sulewski, Jeffery Kodysh (2012). Power Distribution Model. *Oak Ridge National Laboratory Technical Manual.*

Phase 1 Report: Formation of Stakeholder Process, Regional Plan Integration and Macroeconomic Analysis, DE-OE0000343, December, 2011. Retrieved August 26, 2013: http://www.eipconline.com/Resource_Library.html

Pielke Jr, R. A., Gratz, J., Landsea, C. W., Collins, D., Saunders, M. A., & Musulin, R. (2008). Normalized Hurricane Damage in the United States. *Natural Hazards Review*, 29-42.

Strazzo, S.; Elsner, J.B.; Trepanier, J.C.; Emanuel, K.A. (2013). Frequency, intensity, and sensitivity to sea surface temperature of North Atlantic tropical cyclones in best-track and simulated data, *Journal of Advances in Modeling Earth Systems*, ***5***(3), 500-509, 10.1002/jame.20036.

Sulewski, Leanne, "A Geographic Modeling Framework for Assessing Critical Infrastructure Vulnerability: Energy Infrastructure Case Study" (2013). Theses and Dissertations. Paper 1305.

Toole, G.L., S. Flaim, S.J. Fernandez, J. Bossert, B.W. Bush, B. Neenan (2006). *Effects of Climate Change on California Energy Security*, SSR Conference, LA-UR-06-0984.

Willis, H.L. and J.R. Aguero (2007). *Spatial Electric Load Forecasting Methods for Electric Utilities: A report done for and with participation of the Electric Energy Delivery Planning Consortium*. Quanta Technology Technical Report.

Young, B.S., S.J. Fernandez and O.A. Omitaomu (2009). Dynamic Modeling of Components on the Electric Grid, Oak Ridge National Laboratory Report ORNL/TM-0000/00.

Zipperer, A; Aloise-Young, P.A; Suryanarayanan, S.; Roche, R.; Earle, L.; Christensen, D.; Bauleo, P.; Zimmerle, D. (2013). Electric Energy Management in the Smart Home: Perspectives on Enabling Technologies and Consumer Behavior, *Proceedings of the IEEE* , **101/11**, 2397-2408. doi: 10.1109/JPROC.2013.2270172.

Appendix 7A: Hurricane Intensity and Frequency as a Result of Climate Change

Studies conducted by Emanuel et al. (e.g., 2005, 2013; Strazzo et al., 2013) indicate that increases in both intensity and frequency of hurricanes will characterize the climate of the latter half of the 21st century. His calculation of Power Dissipation Index (PDI) for 2006-2100 shows an increase of 0.5E8 m^3s^{-2} in the Gulf Coast region. This prediction upgrades tropical depressions, tropical storms and hurricanes as outlined in Table 1. In general, damage rises by about a factor of four for every category increase (Pielke et al., 2008); thus, population stresses associated with hurricanes are likely to increase with the increase in hurricane intensity.

Table 7A.1 Increase in Intensity (using PDI ($Vmax^3$ integrated over 2 hours))

Wind Scale (1-min sust)	1900-2005	Classification	2006-2100	Wind Scale	Classification
0-7 Beaufort	59 km/h	Trop Depress	67.9240	8	Trop Storm
7	61 km/h		69.4502	8	
8	63	Trop Storm	71.0090	9-10	
8	69		75.8574	9-10	
9-10	70		76.6877	9-10	
9-10	100		103.4777	11	
11	102		105.3490	11	
11	117		119.5729	12+	Cat 1 Hurricane
12+	119	Cat 1 Hurricane	121.4897		
	153		154.5227		Cat 2 Hurricane
	154	Cat 2 Hurricane	155.5032		
	177		178.1417		Cat 3 Hurricane
	178	Cat 3 Hurricane	179.1290		
	208		208.8288		Cat 4 Hurricane
	209	Cat 4 Hurricane	209.8209		
	251		251.5701		
	252	Cat 5 Hurricane	252.5656		Cat 5 Hurricane

Saffir-Simpson Hurricane Wind Scale (NOAA/NWS/NHC http://www.nhc.noaa.gov/aboutsshws.php)

Calculations for Table 7A.1 are made using the following procedure:

The Emanuel Power Dissipation Index is calculated:

$$PDI = \int_0^{\tau} V_{max}{}^3 \, dt$$

With V_{max} = maximum windspeed given for each storm category for 1900-2005.

1. Integrate each V_{max} over τ = 2h as per the Emanuel definition (2010).
2. Add increase for Gulf region (0.5E8 m^3s^{-2} per Emanuel)
3. Back out calculations to V_{max} to obtain 2006-2100 estimates.

Likewise, Emanuel (2013) shows an increase in the probability of storms occurring in the Gulf Coast region. This added probability is around 0.025. If we adjust the Keim (2007) predictions to reflect this increase we obtain the values in Table 2. Thus, projections into the far future must necessarily include these indicated changes in climate regimes.

Table 7A.2 Increase in Frequency (+0.025 probability more storms per year)

Parish	**1900-2005 Rtn**	**1900-2005 P**	**2006-2100 P**	**2006-2100 Rtn**	**Classification**
Cameron	3	1/3 (0.333)	0.358	2.79	TS + Hurricanes
Terrebonne	3	1/3 (0.333)	0.358	2.79	
Plaquemines	3	1/3 (0.333)	0.358	2.79	
Cameron	15	1/15 (0.067)	0.092	10.9	All Hurricanes
Terrebonne	10	1/10 (0.100)	0.125	8	
Plaquemines	7	1/7 (0.143)	0.168	5.96	
Cameron	52	1/52 (0.019)	0.044	22.6	Cat 3+ Hurricanes
Terrebonne	26	1/26 (0.038)	0.063	15.76	
Plaquemines	26	1/26 (0.038)	0.063	15.76	

Calculations for Table 7A.2 are made using the following procedure:

1. Convert return period (Keim, 2007) to probability (1/T)
2. Add probability difference for Gulf as given By Emanuel (2010)
3. Convert probability back to return period (1/P)

Chapter 8

Conclusions and Recommendations

Using combinations of climate models and critical infrastructure tools, we can develop scenarios for which responsive action is needed. Both dynamical and statistical methods for downscaling global climate model output, along with high resolution satellite observations and high resolution projection methods for population data provide high quality input for modeling and analysis of the impacts of climate change on urban infrastructure.

We showed that Information Complexity Criteria could provide a quantitative analysis of the probability distribution of measured extreme rainfall events, and that the measurements analyzed followed a single parameter exponential distribution. This finding allowed for meaningful multivariate regression of meteorological state variables using an exponential formulation for models that were then scored by these criteria. The results of the exponential regression showed that regional precipitation is affected by both local and remote forces; and that extreme precipitation patterns and their contributing processes differ from region to region. Thus, downscaling methods that incorporate these various processes are necessary to provide appropriate inputs to critical infrastructure models, which deal with planning issues for much smaller spatial and temporal resolution than are resolved by global climate modeling. Robust statistical methods can provide a readily accessible way for field hydrologists and infrastructure developers to evaluate both historical data and climate model predictions, without the requirement of extensive computing power, as they plan for flood mitigation and minimization of urban consequences due to extreme precipitation events.

Next, we created a prototype agent-based population distribution model to anticipate emerging power grid vulnerabilities due to population shifts following natural disasters. Results suggested that the importance of established evacuation routes that move large populations repeatedly through convergence points as an indicator may be under recognized, and that planning for sudden shifts in response to storms can be informed by the direction of these routes in addition to the demographics of the departing population.

We then combined US Census and Internal Revenue Service (IRS) population migration data and dynamically downscaled climate modeling data with Department of Energy (DOE) Connected Infrastructure Dynamics Models (CIDM) to examine electricity demand response to increased temperatures, population migration in response to extreme cyclonic events, consequent net population changes and new regional patterns in electricity demand. Results showed that compared to the effect of large population influx into a service area, demand increases due to temperature rise have little impact and that some sections of the national electrical grid are more adaptable to population shifts and changing demand than others are. The method provided an improved process for identifying specific locations of electrical grid vulnerability to increased electricity demand.

Thus, we showed that analyses using these tools can provide insight for local, regional and national planning for critical infrastructure needs. Accordingly, we find that with these tools, key studies can be designed to examine future states of critical infrastructure resulting from population shifts, both typical and those due to increasing frequency and intensity of extreme events at vulnerable locations, and to changes in global and regional temperature.

Vita

Melissa Allen holds a Master of Science degree in Environmental Engineering from the University of Tennessee, and is currently working on a PhD at UT in Energy Science and Engineering. Her work with scientists at both Oak Ridge National Laboratory and the University of Tennessee has included global modeling and analysis of atmospheric species transport, statistical and dynamical downscaling of various climate model output, analysis of direct and indirect effects of climate change on electricity demand, and consideration of climate change issues that impact the evolution of the electrical grid.